Dissertation

Submitted to the
Combined Faculties of the Natural Sciences and Mathematics
Heidelberg University, Germany
for the degree of
Doctor of Natural Sciences (Dr.rer.nat.)

Presented by

Li Han (韩丽)

Born in: Huining, Gansu/ People's Republic of China

(出生地：中华人民共和国甘肃省会宁县)

Oral examination: December 8th, 2021

INAUGURAL-DISSERTATION

zur
Erlangung der Doktorwürde
der
Naturwissenschaftlich-Mathematischen
Gesamtfakultät
der
Ruprecht-Karls-Universität
Heidelberg

Vorgelegt von

Li Han (韩丽)

aus: Huining, Gansu/ People's Republic of China

(出生地：中华人民共和国甘肃省会宁县)

Tag der mündlichen Prüfung: December 8th, 2021

Hydrological change in response to climate change and permafrost dynamics in southern Siberia

Gutachter: Prof. Dr. Lucas Menzel (Ruprecht-Karls-Universität Heidelberg)
Prof. Dr. Markus Disse (Technische Universität München)

Zusammenfassung

Es ist zu erwarten, dass die durch die globale Erwärmung verursachten Veränderungen in der Kryosphäre den terrestrischen Wasserkreislauf beeinflussen, mit unvermeidlichen Folgen für die Verfügbarkeit von Süßwasser für Menschen und Ökosysteme. In den kalten Regionen der Erde beeinflusst der dort vorhandene Permafrost die Wasserflüsse und -dynamiken im Untergrund. Insgesamt sind die damit verbundenen, hydrologischen Prozesse kompliziert, jedoch ist aufgrund des Fehlens langer und großräumiger Permafrostbeobachtungen noch nicht klar, wie die mit der Erwärmung verbundene Permafrostdegradation die großräumigen hydrologischen Prozesse beeinflussen kann. Mit dieser Arbeit soll diese Forschungslücke geschlossen werden, und zwar indem die hydroklimatische Dynamik im Zeitraum 1954-2013 auf verschiedenen Zeitskalen untersucht wird, d. h. auf der 60-jährigen, 30-jährigen, dekadischen und ereignisbezogenen Skala. Die Untersuchungen fokussieren auf drei südsibirischen Einzugsgebieten mit unterschiedlichen Ökosystemen und Permafrostausbreitungen: Die semiaride Selenga mit sporadischem Permafrost, die boreale Lena mit diskontinuierlichem und die boreale Aldan mit kontinuierlichem Permafrost. Die Untersuchungen dieser Arbeit werden dazu beitragen, Erkenntnisse über die Folgen der Permafrostdegradation auf die terrestrische Wasserverfügbarkeit aus der Perspektive der Hydrologie-Permafrost-Klima-Kopplung zu gewinnen.

Aufgrund der räumlich oszillierenden, großräumigen atmosphärischen Zirkulation über Sibirien wurde festgestellt, dass Niederschlag und Abfluss periodischen natürlichen Veränderungen zwischen trockenen und feuchten Zuständen unterliegen: Während die klimatischen Bedingungen in der Selenga von 1954 bis 2013 in einem Nass-Trocken-Nass-Trocken-Muster oszillieren, schwingen diese im Lena- und Aldan-Gebiet in einem Trocken-Nass-Trocken-Nass-Modus. Neben diesen Oszillationen weist der Niederschlag in allen Einzugsgebieten vernachlässigbare langfristige Trends (60 Jahre) auf. Allerdings werden in diesen Einzugsgebieten signifikante Langzeittrends beim Abfluss beobachtet, die mit der unterschiedlichen Dynamik der Permafrostdegradation in Verbindung gebracht werden können. Im Gebiet der semi-ariden Selenga, die von einer lateralen Permafrostdegradation (d. h. einer abnehmenden Permafrostausdehnung) geprägt ist, kommt es zu einem starken Wasserverlust aufgrund von verstärkter Infiltration und Versickerung, was zu insgesamt trockeneren Bedingungen und letztendlich zu einem geringeren Abfluss führt. Im borealen Lena- und Aldan-Gebiet hingegen, wo vertikale Permafrostdegradation vorherrscht, befindet sich unter der mächtiger werdenden Auftauschicht nach wie vor eine gefrorene, undurchlässige Schicht (Permafrost), die für insgesamt feuchtere Bedingungen und einen erhöhten Abfluss sorgt. Infolgedessen kommt es zu erheblichen Verschiebungen zwischen trockenen und feuchten Bedingungen in den Einzugsgebieten. In der Selenga, wo die klimatischen Bedingungen zwischen 1984 und 2013 von einem eher feuchten hin zu einem eher trockenen Zustand wechselten, hat die laterale Permafrostdegradation die Austrocknungsdynamik weiter verstärkt, was zu einer geringeren Abflusseffizienz und einer lang anhaltenden Trockenperiode führte. In den Gebieten von Lena und Aldan, die im Zeitraum 1984-2013 von einem eher trockenen in einen eher feuchten Zustand wechselten, hat die vertikale Permafrostdegradation zu einem noch feuchteren hydroklimatischen Zustand in der borealen Region geführt. Dieses gegensätzliche Verhalten spiegelt das in früheren Forschungsarbeiten beschriebene Phänomen "trocken wird trockener, feucht wird feuchter" wider. Darüber hinaus wird gezeigt, dass die verstärkten hydraulischen Verbindungen zwischen Oberfläche und Untergrund auch zu einem beispiellosen Anstieg des Grundwasserspiegels in der kalten Jahreszeit geführt haben. Diese Untersuchungen verdeutlichen den überragenden Einfluss der mit der Er-

wärmung verbundenen Permafrostdynamik auf regionale hydrologische Veränderungen. Die Auswirkungen könnten umfassende Konsequenzen für die Bewirtschaftung der terrestrischen Wasserressourcen in von Permafrost betroffenen Regionen nach sich ziehen.

Abstract

Changes in the cryosphere caused by global warming are expected to alter the terrestrial hydrological cycle, with inevitable consequences for freshwater availability to humans and ecosystems. In particular, the presence of permafrost influences water fluxes and dynamics in the subsurface system, thus, complicating the hydrologic processes in the permafrost-affected region. However, due to the absence of long-term, large-scale permafrost observations, a systematic understanding of how the warming-related permafrost dynamics may influence the large-scale hydrological processes is not clear yet. This work aims to address this research gap by investigating the hydro-climatic dynamics during 1954-2013 over multiple temporal scales, i.e., 60-year, 30-year, decadal and event scales. The study area is focused on three southern Siberian catchments with diverse ecosystems and permafrost distributions, namely, the semi-arid Selenga featured with sporadic permafrost, the boreal Lena covered by discontinuous permafrost, and the boreal Aldan is underlain by continuous permafrost. Our investigations will help to gain insights into the consequences of permafrost degradation on the terrestrial water availability from a hydrology-permafrost-climate coupling perspective.

Due to "seesaw-like" large-scale atmospheric circulations over the Siberian region, we found that precipitation and river runoff resemble periodical natural oscillations between dry and wet states: while Selenga oscillates in a wet-dry-wet-dry pattern from 1954 to 2013, Lena and Aldan oscillate in a dry-wet-dry-wet mode. On top of these oscillations, the precipitation in all the catchments shows negligible long-term (60-yr) trends. However, significant but divergent long-term trends are observed in the river runoff among these catchments that can be related to different permafrost degradation dynamics. The semi-arid Selenga, dominated by lateral permafrost degradation (i.e., decreasing permafrost extent), suffers from severe water loss due to enhanced infiltration and percolation, leading to a drier condition and decreasing runoff. However, in the boreal Lena and Aldan where vertical permafrost degradation prevails, the thickened active layer is still underlain by a frozen layer that sustains a more water-rich surface condition and increasing runoff. As a consequence, a significant regime shift exists between the dry and wet states. In Selenga which is oscillating from a wet to dry state during 1984-2013, lateral permafrost degradation has further enhanced the drying dynamics, with a reduced runoff efficiency and a long-lasting dry period. In Lena and Aldan which is shifting from a dry to wet regime during 1984-2013, vertical permafrost degradation has led to an even wetter hydro-climatic condition in the boreal region. These contrast behaviors reflect a "dry gets drier, wet becomes wetter" phenomenon observed by previous researches. Furthermore, we show that the enhanced surface-subsurface connections have also induced an unprecedented increase in the baseflow during cold seasons. These investigations highlight the remarkable imprint of warming-related permafrost dynamics on regional hydrological changes, and could provide profound implications for the management of terrestrial water resources in permafrost-affected regions.

定风波

苏轼*

莫听穿林打叶声，
何妨吟啸且徐行。
竹杖芒鞋轻胜马，
谁怕？
一蓑烟雨任平生。

料峭春风吹酒醒，
微冷，
山头斜照却相迎。
回首向来萧瑟处，
归去，
也无风雨也无晴。

***Su Shi (苏轼; 8 January 1037 – 24 August 1101), Chinese poet of the Song Dynasty.**

Contents

Chapter 1

Introduction

1.1 Background

Terrestrial water cycle, i.e., the movement and storage of water on Earth, is the central component of the coupled land-atmosphere system. It regulates the partitioning of moisture and energy fluxes between land and atmosphere, governs numerous interactions and feedbacks within the system, and further shapes the landscape at the local and regional scales. Meanwhile, atmosphere and landscape properties can also control the water cycle in a specific region. From the atmosphere aspect, precipitation is the primary driver. Its patterns and fluctuations can firmly control the magnitudes and variability in terrestrial water availability. From the landscape perspective, diverse landscape properties (such as topography, ecosystem, and soil types) can filter the climate signal, modulate local hydrological processes, and eventually bring a high degree of spatial heterogeneity and complexity to the terrestrial water availability in a specific region (Brutsaert et al., 2005).

Permafrost, a frozen soil zone at or below 0 °C for two or more years, is a unique landscape in the cryosphere (Dobinski, 2011; Woo, 2012). It extends approximately 22% of the terrestrial surface in the Northern Hemisphere (Brown et al., 1997). Due to its extreme sensitivity to the warming climate (Woo, 2012), the area covered by permafrost serves as an ideal setting for investigating the response of hydrological processes to climate change and associated landscape evolution, which is recognized as one of the major unsolved problems in hydrology study (Blöschl et al., 2019). Especially, given the identified tipping point in permafrost under climate warming (Devoie et al., 2019; Lenton, 2012; Nitzbon et al., 2020), it provides a proper background for detecting whether warming-related hydrological change is irreversible or not.

1.1.1 Permafrost hydrology

The presence of permafrost influences the fluxes, movement, and distribution of surface and subsurface water, thus, complicating the hydrologic dynamics in the permafrost-affected region (Walvoord & Kurylyk, 2016) (Fig. 1.1). Basically, permafrost acts as an aquiclude that suppresses subsurface water movement due to its low hydraulic conductivity (Woo, 2012). During the warm season, the top of the frozen layer melts and becomes active (i.e., a seasonally thawed layer exists above the permafrost table). Nevertheless, the frozen layer beneath the active layer still serves as an effective barrier that prevents water from percolating deeply. As a result, the active layer can sustain a wet

surface or near-surface conditions (Iijima et al., 2014), which can increase the surface runoff but limit the subsurface drainage.

Continued climate warming is expected to alter the thermal state and hydrogeologic structure of permafrost (Biskaborn et al., 2019; Kurylyk et al., 2014), causing diverse degrading patterns (Evans et al., 2020; Muskett & Romanovsky, 2009; Walvoord & Kurylyk, 2016). According to spatial cover of frozen soil, permafrost regions are normally divided into: (i) Continuous (90-100%), (ii) discontinuous (50-90%), (iii) sporadic (10-50%), and (iv) isolated (<10%). In the ice-rich continuous permafrost region, where more than 90% of the landscape is underlain by permafrost, a warming environment leads primarily to a vertical degradation that increases the thickness of the active layer during the warm season (Muskett & Romanovsky, 2009; V. E. Romanovsky et al., 2010). In regions with less extensive permafrost (i.e., discontinuous, sporadic, and isolated permafrost), thawing is likely to reach the bottom of the frozen layer, thus reduces the lateral extent of the permafrost (Woo, 2012). Such lateral degradation may lead to the formation and expansion of open taliks (i.e., unfrozen bodies of soil beneath the active layer and within the permafrost) or widespread permafrost loss (Muskett & Romanovsky, 2009; Walvoord & Kurylyk, 2016). In both cases, permafrost degradation enhances the pathways connecting the surface and subsurface water systems (Lamontagne-Hallé et al., 2018; Muskett & Romanovsky, 2009; Rowland et al., 2010; Walvoord & Kurylyk, 2016). It also increases the water storage and the movement of water in subsurface and groundwater system (Evans et al., 2020; L. C. Smith et al., 2007; St. Jacques & Sauchyn, 2009; Walvoord & Striegl, 2007).

However, different states of permafrost degradation are also likely to result in diver-

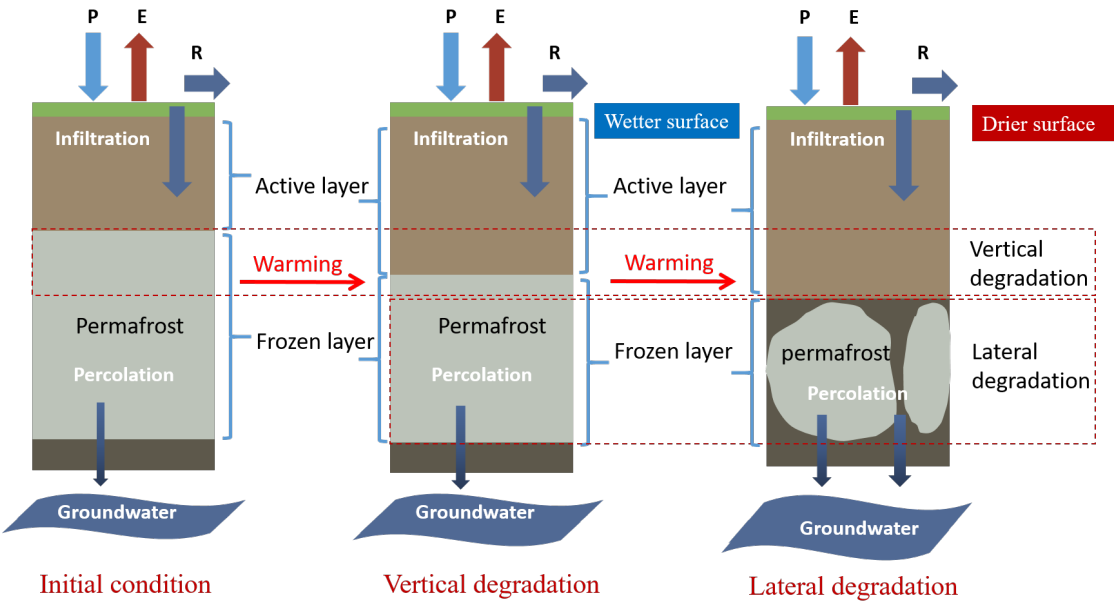

Figure 1.1: Subsurface conditions under a warming climate and permafrost degradation. In the case of vertical degradation, a deeply thawed active layer represents a thicker aquifer in the soil layer for water storage, and thus a wetter surface or upper soil layer. As to the lateral degradation, the increased permafrost-free area in the subsurface could accelerate the infiltration and percolation, resulting in a drier surface and soil moisture condition.

gent surface moisture conditions (Ford & Frauenfeld, 2016; Vecellio et al., 2019). In the case of vertical degradation, a relatively wetter surface condition favors because the thicker active layer is still underlain by a frozen layer with lower permeability (Vecellio et al., 2019). In the case of exacerbated lateral degradation, increased infiltration and percolation into the groundwater system through a larger permafrost-free area are triggered. This results in drier surface and soil moisture conditions during the thawing season (Ford & Frauenfeld, 2016; Ishikawa et al., 2005). These potential hydrological consequences of drying and wetting conditions caused by different permafrost degradations can further affect the atmospheric dynamics through land-atmosphere interactions and feedbacks.

Depending on whether it is in a dry or wet condition, as shown in Fig. 1.2, there are two different dominant feedback loops between the land surface and lower-level atmosphere (Seneviratne et al., 2010, 2006). In a wet surface condition induced by vertical permafrost degradation (Fig. 1.2, left panel), the moisture content is sufficient to sustain the increasing demand for evapotranspiration (ET) under rising temperature. The increased ET from the land surface can lead to the higher moisture content in the atmosphere and contribute more clouds for possible precipitation. This feedback, in turn,

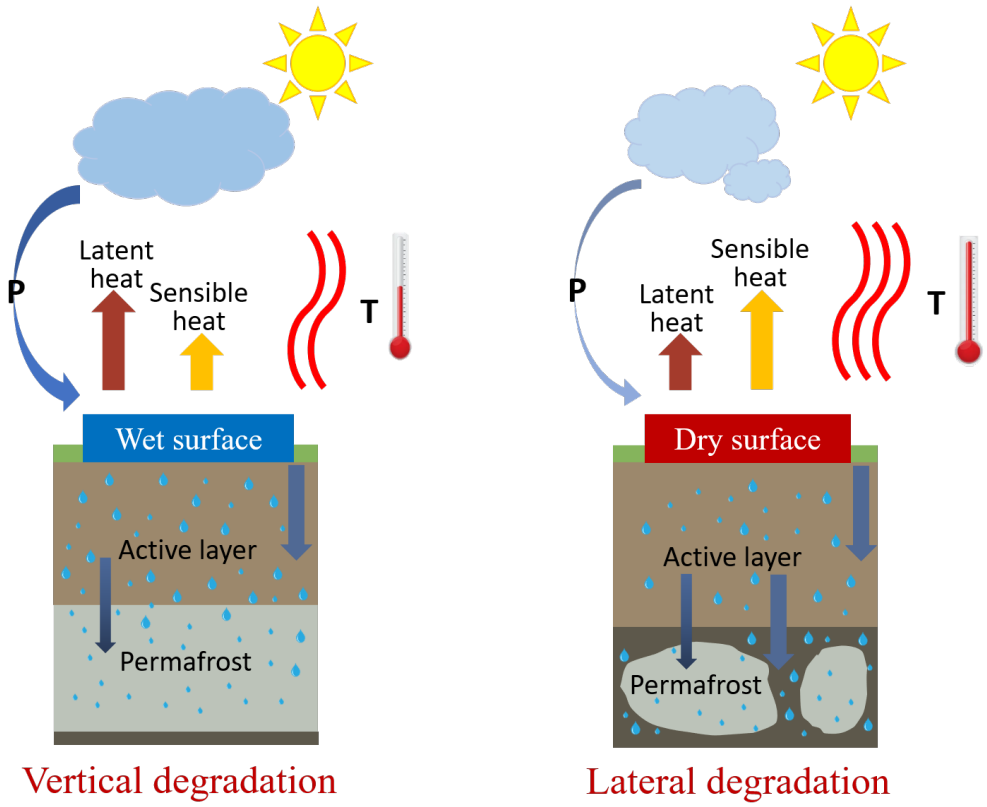

Figure 1.2: Land-atmosphere feedback loops under different permafrost degradations. Left: vertical permafrost degradation induces a wet surface condition. It leads to larger evapotranspiration (latent heat) that favors more clouds and precipitation, which in turn enhances the wet condition on landsurface. Right: lateral permafrost degradation promotes a relatively dry surface condition, which releases higher sensible heat. This results in hotter air temperature that further reinforces the dry surface condition.

results in a high moisture condition in the land surface and soil layer (Seneviratne et al., 2010), enabling a persistent wet surface condition. Meanwhile, the increased ET represents higher latent heat than sensible heat, thus depressing the potential rise in air temperature.

On the contrary, in a dry condition due to enhanced lateral degradation in permafrost (Fig. 1.2, right panel), moisture deficits in land surface can lead to higher sensible heat than latent heat, inducing a potentially reduced cooling effect from ET. As a result, the temperature in the overlying lower-level atmosphere could be greatly elevated (Ford & Frauenfeld, 2016; Seneviratne et al., 2006). At the same time, this dry-induced dynamic is accompanied by a high chance of clear sky and eventually a decline in precipitation, resulting in a continued dry state in the landsurface (Seneviratne et al., 2010).

1.1.2 Challenges and open questions

Despite these severe impacts of permafrost degradation on the terrestrial water availability and land-atmosphere dynamics, the corresponding findings on the drying and wetting dynamics of different permafrost states are mainly investigated by field observations (Disher et al., 2021; Hinzman et al., 2006; Iijima et al., 2014; Ishikawa et al., 2005; Kopp et al., 2014; O'Donnell et al., 2012; Walvoord et al., 2019). Yet, the underlying mechanisms of hydrological response to changing climate and thawing permafrost have not been fully studied at a large scale (Walvoord & Kurylyk, 2016; Yang & Kane, 2020). This is because in a large drainage basin with diverse ecosystems and permafrost types, land-atmosphere interactions and feedbacks often exhibit a high degree of heterogeneity across space. This can thus induce much more complex hydrological processes in the system. Consequently, the well-observed findings at field (or small) scale are not sufficient to represent the full range of behaviors and variabilities of the tightly coupled hydrology-climate-landscape system at a large scale (Wagener et al., 2010).

Furthermore, the time span of direct observations of permafrost is very short, and is only available in recent decades due to limitations of the monitoring ability in permafrost (V. E. Romanovsky et al., 2010). It is therefore still a big challenge to detect the evolution in permafrost from a long-term perspective (Brutsaert & Hiyama, 2012; Frampton et al., 2011). In order to solve this issue, sort of solutions have been suggested by different studies (Brutsaert & Hiyama, 2012; Frauenfeld et al., 2007; S. Lyon et al., 2009; Walvoord & Kurylyk, 2016). Firstly, given the direct thermal response of the land surface to the atmosphere, indices based on the linear relationship between air temperature and permafrost condition are proposed (Frauenfeld & Zhang, 2011; Frauenfeld et al., 2007; Nelson & Outcalt, 1987; Peng et al., 2018; Stefan, 1891; T. Zhang et al., 2005). Since the air temperature data is often available at long-term and large (or global) scale, these indices, such as annual freezing index (FI) and thawing index (TI), can provide a first-order estimation of the long-term permafrost evolution in a large spatial scale (Frauenfeld & Zhang, 2011; Frauenfeld et al., 2007; Peng et al., 2018). In addition, some researchers also used the long-term base flow (river flow sustained by groundwater) records to reflect the historical evolution of permafrost (Brutsaert & Hiyama, 2012; S. Lyon et al., 2009; S. W. Lyon & Destouni, 2010). This method has been widely applied to the permafrost detection in Siberia (Brutsaert & Hiyama, 2012), North America (S. W. Lyon & Destouni, 2010) and Scandinavian region (S. Lyon et al., 2009). However, the base flow is derived from daily streamflow, which often suffers from

high uncertainties in cold region (Shiklomanov et al., 2006). This consequently brings a high degree of biases to the estimation of permafrost degradation. Thirdly, modeling studies based on numerical methods have also been applied to simulate the permafrost thawing and freezing processes (Frampton et al., 2011; Gouttevin et al., 2012; Y. Zhang et al., 2013). It can help to describe the complex dynamics of water and heat in subsurface (Walvoord & Kurylyk, 2016). However, better performance of models needs a vast of parameters to represent physical processes, which are generally available from direct field observations (Riseborough et al., 2008). Since not all the relevant parameters are accurate, the reliability of model projections is under debate (Kurylyk et al., 2014; Walvoord & Kurylyk, 2016).

1.1.3 Research scope of this study

Siberia is widely covered by permafrost, making it extremely sensitive to the ongoing global change (Groisman & Gutman, 2012; Ohta et al., 2019). According to the temperature record during 1950-2010, Siberia is one of the hot spots with dramatically increased temperature throughout the globe (Fig. 1.3). This unprecedented warming trend is expected to continue under current climate change scenarios (Bindoff et al., 2019). During recent decades, in particular, Siberia has seen several record-breaking heatwaves (Ciavarella et al., 2021; Overland & Wang, 2021) and associated wildfires (Grosse et al., 2020; Kim et al., 2020; Yasunari et al., 2021). All these warming effects are accelerating the degradation of permafrost underlain in this region (Biskaborn et al., 2019; V. Romanovsky et al., 2007; V. E. Romanovsky et al., 2010; Streletskiy et al., 2015). While the permafrost degradation will release the stored carbon that may fur-

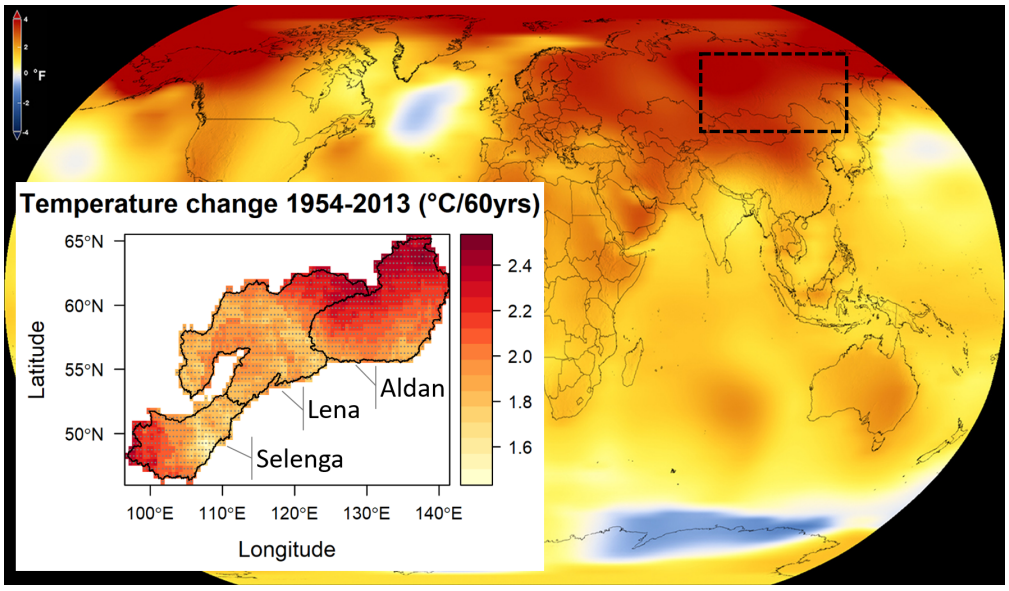

Figure 1.3: Warming throughout Globe and Siberia. Background figure from NASA Scientific Visualization Studio shows the anomalies of global average temperature from 2013 to 2017, in comparison to a baseline average from 1951 to 1980. Figure in front (on the left side) is the warming rate during 1954-2013, based on the temperature data from CRU dataset, for the three southern Siberian catchments: Selenga, Lena, and Aldan.

ther enhance the warming condition (MacDougall et al., 2012; Schuur et al., 2015), the associated alteration in the structure of the subsurface can also modulate the terrestrial water cycle (Kurylyk et al., 2014; Walvoord & Kurylyk, 2016; Woo, 2012).

In this thesis, we focus on the hydrological processes of three southern Siberian catchments (Fig. 1.3, left below) with diverse landscape characteristics: (1) the Selenga in the transition belt from semi-arid land to the boreal ecosystem, characterized by mixed permafrost (ranges from discontinuous, sporadic, and isolated permafrost); (2) the Lena belongs to boreal ecotone, which is mainly underlain by discontinuous permafrost; and (3) the Aldan is also a boreal catchment but is dominated by continuous permafrost that is different from the Lena catchment. These three catchments have been selected as our study area because they are geographically close to each other, but each represents one permafrost type, as we mentioned above.

Furthermore, according to field observations during the past few decades, the permafrost in these three catchments have experienced enhanced but different degradations (Iijima et al., 2014; Ishikawa et al., 2005; Kopp et al., 2014; Ohta et al., 2008; V. Romanovsky et al., 2007; V. E. Romanovsky et al., 2010; Streletskiy et al., 2015). Selenga is undergoing a lateral degradation with the permafrost below flat pasture plains suffering from complete thawing (Ishikawa et al., 2005). The formation of talik and northward migration of the southern boundaries is also documented in this catchment (Davaa & Jambaljav, 2014). As to the continuous and discontinuous permafrost environment in Aldan and Lena, observation studies have recorded increased permafrost temperature and thickened active layer (V. Romanovsky et al., 2007; V. E. Romanovsky et al., 2010; Streletskiy et al., 2015), suggesting a vertical degradation in these two catchments. In addition, the discontinuous permafrost in Lena is also likely to experience a lateral degradation and formation of open taliks (Hiyama et al., 2013).

The different landscape characteristics and evolutions among these three catchments would underpin the different mechanisms of hydrological response to climate change under different permafrost degradations. These detailed investigations can further our understanding of permafrost-affected dynamics and processes in the land-atmosphere system, improve our assessments and predictions on the magnitude and variability in terrestrial water availability, and benefit the management of water resources and water quality in a permafrost-affected region.

1.2 Hydro-climatic change in Siberia

Before we give a detailed description of the objective and structure of this thesis, in this section, we would like to review the current research status on hydro-climatic change across Siberia. We will first introduce the historical characteristics and variations in precipitation and its connection to large-scale atmospheric circulations. After that, we review the current understanding of the hydrological processes related to precipitation variations and thawing permafrost. This mainly includes the research on the periodical oscillations, long-term trends, and regime shifts in runoff of large Siberian rivers and the studies on terrestrial water fluxes and storage based on remote sensing.

1.2.1 Periodical oscillations of precipitation

Precipitation is the major flux to the terrestrial water system (Bring et al., 2016; Brutsaert et al., 2005). Changes in its magnitudes and timing will directly affect the processes in the surface and subsurface hydrological system. Although studies based on short-period (or decadal) records reported increased trends in precipitation in the Siberian continents (Fujinami et al., 2016; Iijima et al., 2010), the precipitation over a long-term period, however, is found to have no apparent trend (Adam & Lettenmaier, 2008; Berezovskaya et al., 2004; Pavelsky & Smith, 2006; Serreze & Etringer, 2003; Troy et al., 2012). One of the reasons might be from the offset of seasonal precipitation, such as increasing snowfall during winter but reduced rainfall in the warm season that results in a weak trend in annual precipitation (Rawlins et al., 2009). However, many studies have suggested that the long-term trend in precipitation is greatly affected by the decadal (or multi-decadal) oscillations of the large-scale atmospheric circulation (Z. Chen & Grasby, 2009; Hannaford et al., 2013; Pekárová et al., 2003).

As a majority of annual precipitation (more than 60%) occurs during the warm season from May to September in Siberia, the connections between precipitation and large-scale atmospheric circulation in this region are mainly dominated in summer (Groisman & Gutman, 2012; C. Sun et al., 2015). The first study on such connection is conducted by Fukutomi et al. (2003), who found a seesaw oscillation pattern between eastern and western Siberia in both summer precipitation and atmospheric 500-hPa geopotential height. After that, a similar seesaw pattern between northern Mongolia and eastern Siberia is found by Iwao and Takahashi (2006). Further investigations suggest that the corresponding oscillation is strongly related to the eastward propagation of quasi-stationary Rossby waves, which is probably affected by the teleconnections between Siberia and the Arctic region (Nicolì et al., 2020; C. Sun et al., 2015).

1.2.2 Historical variations in terrestrial water availability

Driven by the aforementioned quasi-stationary atmospheric circulation, precipitation in Siberia shows periodical oscillations with timescales ranging from several years to several decades (Fukutomi et al., 2003; Iwao & Takahashi, 2006; C. Sun et al., 2015). Such variability is also found to be manifested in river runoff over large Siberian River basins (Fukutomi et al., 2003; Oshima et al., 2018, 2015). Nevertheless, these studies are mainly focused on the climatology and historical variations of the moisture fluxes in the atmosphere and hydrological system (e.g., precipitation and runoff). They have not considered the landscape dynamics, such as permafrost degradation. The latter may further modulate the corresponding oscillation patterns in local hydrological processes.

Different from the negligible long-term trend in precipitation, a wealth of studies have found significant long-term trends in river runoff in the Siberian region (McClelland et al., 2004; Peterson et al., 2002; Rawlins et al., 2009; Tananaev et al., 2016; Yang et al., 2002). For instance, in the Lena River basin, upward trends have been reported for both annual and seasonal runoff during the period of 1936-1999 (Rawlins et al., 2009; Yang et al., 2002; Ye et al., 2003) and the period of 1925-2013 (Tananaev et al., 2016). The authors suggest that thawing of permafrost is likely to be one of the possible reasons inducing such increase (Evans et al., 2020; L. C. Smith et al., 2007; Yang et

al., 2002; Ye et al., 2003). On the other hand, a reduced runoff is also found in the Selenga River (a transboundary river between northern Mongolia and southern Siberia) from 1938 to 2009 (Törnqvist et al., 2014). This historical decline in river runoff is also suggested to be related to the enhanced degradation of permafrost. As another example, the maximum flow (peaks) in the Lena River basin during 1936-1999 shows a weak trend (Shiklomanov et al., 2007), while the lowflow (minimum flow) during the same period shows a substantial increase with an abrupt rise since the late 1980s (L. C. Smith et al., 2007). As lowflow is more dependent on the subsurface conditions, it indicates that the change of lowflow is probably caused by the ongoing permafrost degradation (Evans et al., 2020; L. C. Smith et al., 2007). These historical changes in river runoff extremes also signal a shift toward lower summer runoff and higher winter runoff of the Lena River and its tributary (L. C. Smith et al., 2007; Yang et al., 2002; Ye et al., 2003, 2009). This shift in runoff regime suggests an increased seasonality induced by enhanced permafrost degradation under a warming climate (Walvoord & Kurylyk, 2016; Yang & Kane, 2020).

In addition to these detections on river runoff, studies based on the remote sensing approach also focus on the terrestrial water flux and storage. By comparing the historical satellite images, L. Smith et al. (2005) documented the disappearance of lakes in the southern boundaries of the permafrost domain in Siberia and suggested that the loss of lakes are primarily driven by the enhanced water drainage due to the thawing of permafrost. On the contrary, Boike et al. (2016) observed expanding lakes in eastern Siberia underlain by continuous permafrost from 2002 through 2009, which is also attributed to the permafrost degradation in this region. These divergent patterns of lake dynamics are coincident with the wetting and drying states under different permafrost degradations as we discussed in Sec. 1.1.1. Additionally, remote satellite data has also been used to identify groundwater storage in Siberia, where Muskett and Romanovsky (2009) and Velicogna et al. (2012) have identified an increase in groundwater storage in the Lena River basin during the 2000s. Both of these studies indicate that permafrost degradation has critical consequences on terrestrial water storage in the Siberian region.

Altogether, these studies reveal the importance of permafrost dynamics on hydrological change under a changing climate. However, due to the absence of long-term permafrost observations in Siberia (the monitoring system of permafrost conditions in the Siberian region is available only since the 1980s) (Biskaborn et al., 2019), the profound evidence of the direct relationship between permafrost degradation and variations in terrestrial water availability is still missing. Furthermore, the divergent wet and dry dynamics along with different permafrost conditions indicate that one should treat different types of permafrost and their degradations separately. Also, the studies focused on the long-term historical changes usually did not consider the periodical oscillations mentioned above, making it difficult to disentangle the hydrological consequences of permafrost degradation from that induced by precipitation variations (McClelland et al., 2004). Thus, a comprehensive understanding of the complex land-atmosphere interactions and feedbacks requires multiple-temporal-scale analysis and comparative investigations over varying landscape (permafrost) characteristics.

1.3 Objective and structure of this thesis

1.3.1 Objective and research questions

As we mentioned in Sec. 1.1.1, the permafrost dynamics based on field observations are well understood. However, how such knowledge can improve our understanding of basin-scale hydrological consequences of permafrost degradation is still not fully investigated. Therefore, the broad objective of this thesis is to explore the hydro-climatic processes and dynamics over basin-scale in southern Siberia with varying permafrost properties. This will allow us to better understand the hydrological response to climate change under different permafrost degradations at multiple-temporal scales and enable us to gain insight into the permafrost-degradation-driven consequences and implications for regional water availability. More specifically, we will address the following research questions:

(1) identify hydrological change over multiple timescales and their relationship to climate change.

(2) gain insight into hydrological consequences of permafrost degradation from a land-atmosphere coupling perspective.

(3) examine whether the identified hydrological transformation driven by climate change and permafrost degradation is irreversible.

(4) explore the historical dynamics of hydrological extremes in response to a warming climate and associated permafrost degradation.

With growing archives of freely accessible hydro-climatic observation data as well as improved knowledge in the field-scale permafrost dynamics, we now have the potential possibility to observe and identify the hydro-climatic changes in response to changing climate and associated permafrost degradation at multi-temporal scales. By using a diverse array of modeling, observational and gridded data sets, and a suite of quantitative diagnostic approaches, we are able to gain a mechanistic understanding of key hydrological processes in the hydrology-permafrost-climate system in southern Siberia, and thereby fill the current gap in basin-scale hydrological implications of permafrost degradation under a changing climate.

1.3.2 Thesis structure

This thesis consists of eight chapters, as illustrated in Fig. 1.4. In Chapter 2, we will present the description of the study area, data sets, and methods used throughout this thesis. After that, Chapter 3 concentrates on the identification, description, and interpretation of spatial-temporal change in climatic variables and associated indicators on permafrost conditions. The hydrological response to climate change and permafrost degradation are the main theme of this research, which are presented in Chapters 4-7.

Given the corresponding changes in the hydro-climatic variables across the larger Siberian continent, in Chapter 4, we will discuss the long-term trends, decadal (periodical) oscillations, and inter-annual anomalies in three catchments (Selenga, Lena, and

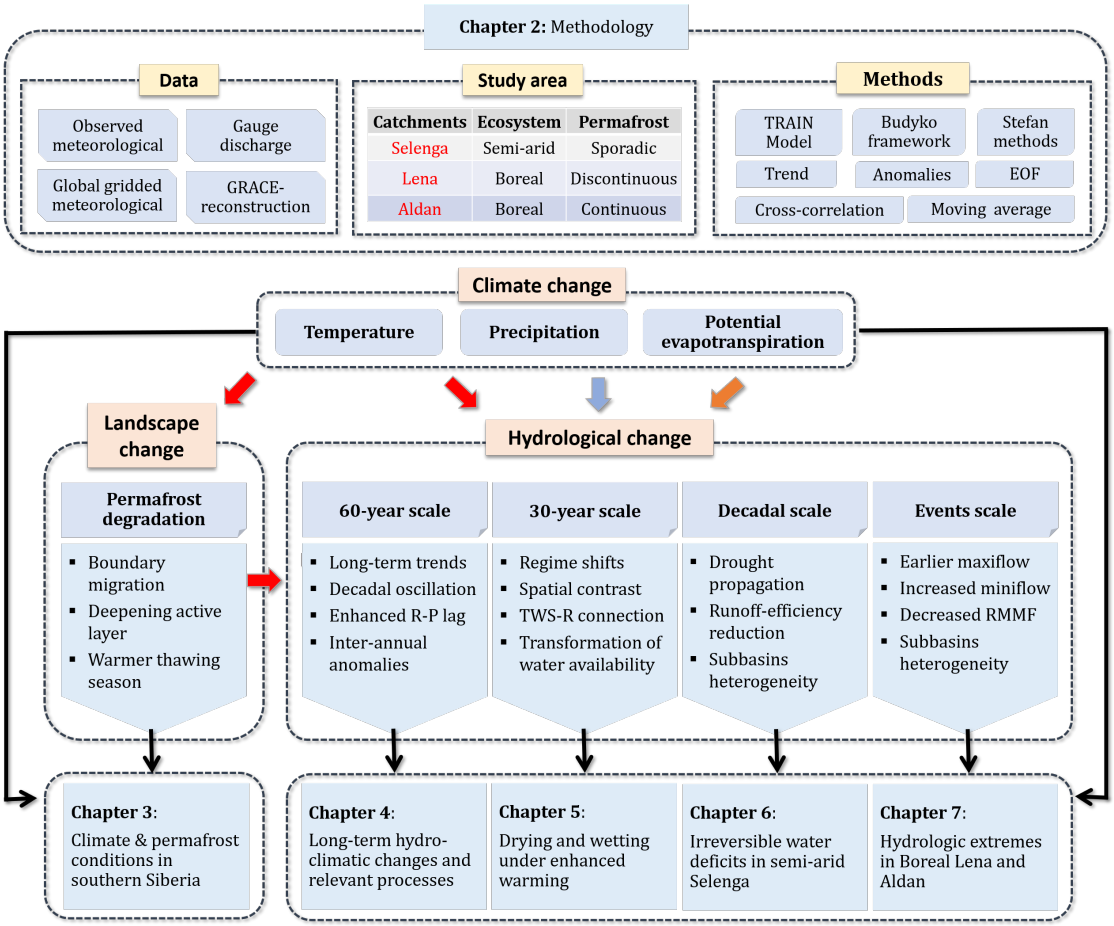

Figure 1.4: A short overview of the research focus and structures of this thesis.

Aldan) over both annual and seasonal scales. Based on the lagged consistency between seasonal runoff and precipitation, we will further employ cross-correlation analysis between runoff and precipitation to verify the potential role of permafrost degradation on runoff generation processes under warming conditions.

In Chapter 5, we will focus on one single cycle of the periodical oscillation and divide this span into dry and wet states. Based on such classification, we present the evolution of the dry and wet states in the context of the intra-annual regime of hydro-climatic dynamics and investigate the potential role of permafrost degradation on the shift in the hydrological regime. We also examine the spatial-temporal patterns of water availability by using the reconstructed terrestrial water storage (TWS) data, which enables us to unravel the spatial relevance of subsurface water conditions to the runoff generation process. Furthermore, we identify the historical evolution of regional water availability to provide insights into the hydrological consequence of climate change and permafrost degradation in southern Siberia.

The analysis in Chapter 5 will also identify an unprecedented drying condition during 1996-2012 in the semi-arid Selenga River basin. Therefore, in Chapter 6, we will try to assess whether this identified hydrological transformation is irreversible under a warming climate and associated permafrost degradation. The characteristics and propagation of

the hydrological droughts during this dry spell during 1996-2012 and their relevance to the atmospheric circulation and permafrost degradation will be investigated.

In Chapter 7, we further explore the hydrological extremes in Aldan and Lena under the changes in climate and permafrost. This is done mainly via the examination of the magnitude and timing in the maxiflow and miniflow and via the potential shifts in the intra-annual regime of runoff. This would allow us to reveal the potential relationship between hydrological extreme and thawing-freezing dynamics of permafrost.

Finally, a summary of this thesis is presented in Chapter 8.

Chapter 2

Methodology

In this chapter, a detail introduction of the study area, the data source, as well as the details of the empirical methods, modeling, and statistical methods are presented.

2.1 Study area

2.1.1 Environmental conditions in southern Siberia

The study area is located in the northeastern part of the Eurasian continent, spanning from 46 °N to 65 °N, and from 95 °E to 140 °E (Fig. 2.1). It features a broad range of

Figure 2.1: Location of selected river basins, i.e., Selenga, Lena and Aldan in northern Mongolia and southern Siberia.

permafrost, climate, topographic, and geo-ecological zones. In order to identify suitable case studies for our investigations on permafrost hydrology, we define two main selection criteria. First, the selected river basins should show the full range of permafrost distribution, including continuous, discontinuous, and sporadic. Second, the flow regimes of the rivers should not be interrupted by dams or any other forms of human intervention. After a thorough examination, we identified the Aldan, Lena, and Selenga basins as suitable candidates (Fig. 2.1). The Aldan and Lena River basins are completely underlain by continuous, and discontinuous permafrost, respectively. Both basins are characterized by boreal forest as the dominant landcover. The Selenga River basin, in contrast, represents the transition between discontinuous, sporadic, and isolated permafrost. This transition is also reflected by a gradual change in landcover from boreal forest to dry steppe.

2.1.1.1 Climate zone and climatology

According to the Koppen-Geiger climate classification (Rubel & Kottek, 2010), the study area we selected is mainly characterized by the subarctic climate (also called boreal climate, Fig. 2.2). It includes Dwc (snow, dry winter, and cold winter) for much of the Selenga basin, half of the Lena basin and part of the Aldan basin, Dfc (snow, humid and cool summer) for the large region of the Lena basin, and part of the Aldan basin, as well as Dfd (snow, humid and extremely continental), Dwd (snow, dry winter, and extremely continental) and ET (polar tundra) in the small parts of the Aldan basin. In

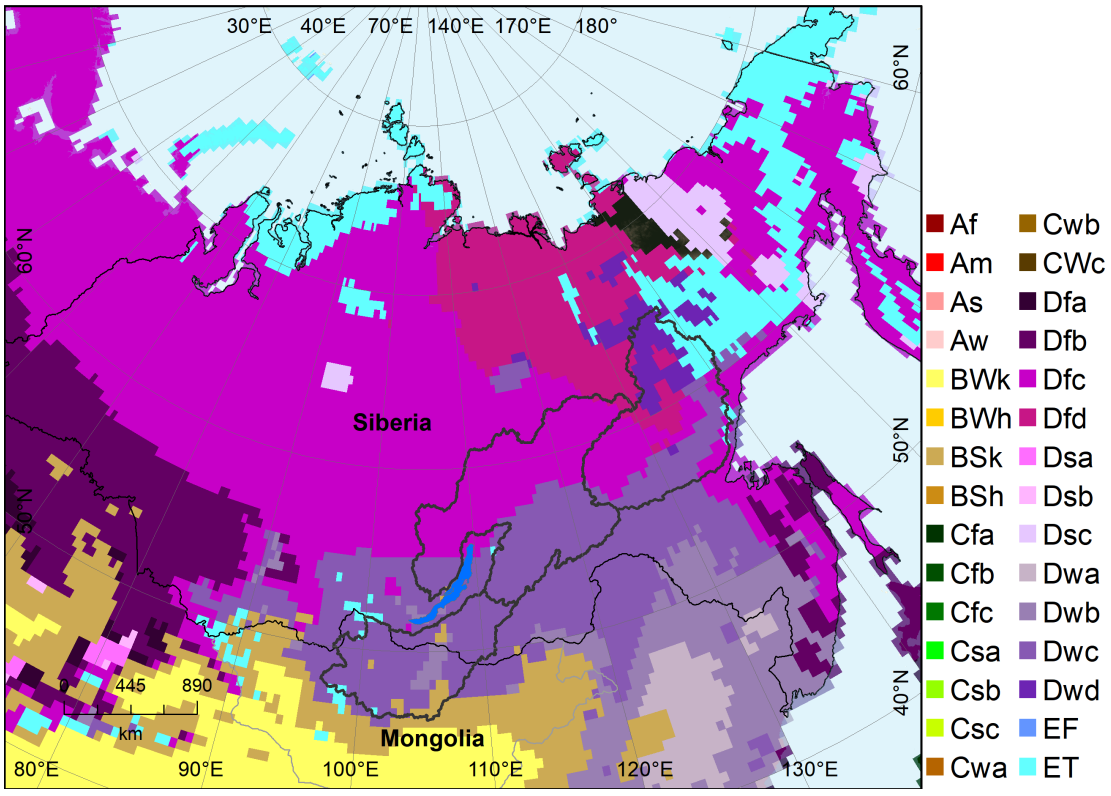

Figure 2.2: Koppen-Geiger climate classification in Siberia (Rubel & Kottek, 2010).

addition, the Bsk (cold semi-arid climate) is found in the southern region of the Selenga basin.

Generally, the study area has long, cold winters and short, cool summers. The spatial distribution of mean annual air temperature (MAAT) and potential evapotranspiration (PET) vary significantly from south to north, exhibiting notable spatial contrast in response to the latitudinal and altitudinal distribution (Fig. 2.3). This can be evident from the comparison between the northern and southern regions, and between regions with lower and higher elevations. For example, the valley region in the Selenga basin is located in the southern boundary region with lower elevation. It has a relatively higher MAAT and PET as compared to the northern Aldan region and the south-western mountainous region in Selenga. The total annual precipitation shows much more complex spatial differences than the MAAT and PET. In general, there is higher precipitation in the domain from 55 °N to 60 °N as compared to the other southern Siberian region. Additionally, there is also extremely higher precipitation in the northern Selenga region, which is close to the boundary of Lake Baikal. This abnormal value in annual precipitation might be induced by the regional modulation of the Lake Baikal.

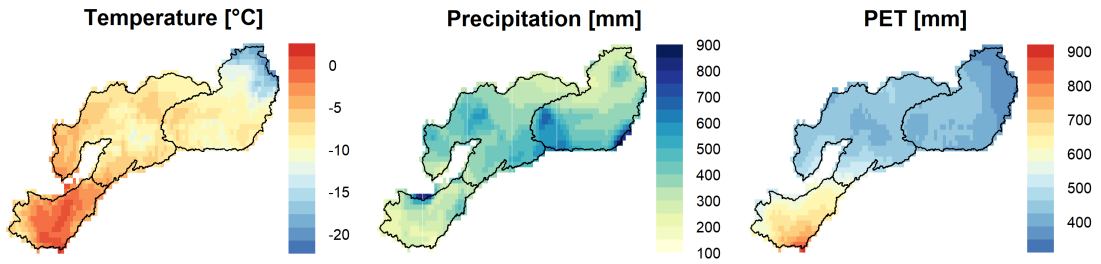

Figure 2.3: Long-term mean annual (reference period is during 1954-2013) of air temperature (T), precipitation (P) and potential evapotranspiration (PET) in southern Siberia, based on the gridded data extracted from CRU dataset (T and PET), and GPCC dataset (P).

2.1.1.2 Characteristics of permafrost and landcover

Due to cold and harsh climate, this region is widely underlain by the permanently frozen ground, including continuous, discontinuous, sporadic, and isolated permafrost (Fig. 2.4). The thickness of continuous permafrost is around 200 m, and even reaches 1000 m in the northeastern region (Dobinski, 2011). Under the extremely cold and harsh environmental conditions, boreal forest prevails in the Aldan and Lena River basin, as well as part of the northeastern region in Selenga. In addition to the boreal forest, a large part of the southern region in the Selenga basin is also covered by the grassland ecosystem (Fig. 2.4). The detailed information of permafrost and ecosystem will be presented in the following subsection for each catchment.

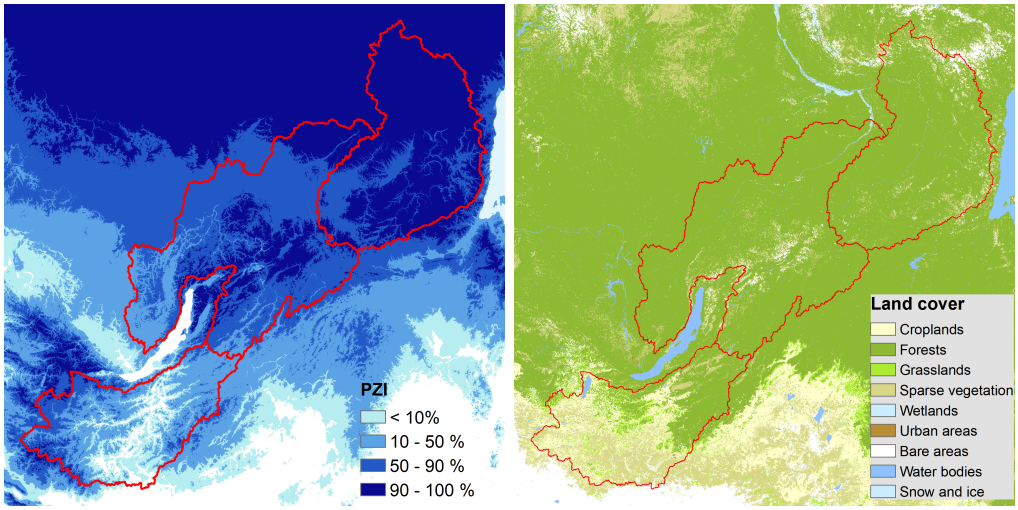

Figure 2.4: Permafrost distribution and land cover. The left figure is the Permafrost Zonation Index (PZI (Gruber, 2012)) represents the permafrost distribution, such that 90-100% is continuous permafrost, 50-90% is discontinuous, 10-50% is sporadic, and $< 10\%$ represents isolated permafrost. The figure on the right side is the land cover, which is derived from the Globcover products based on the ESA Globcover project.

2.1.2 Three selected catchments

2.1.2.1 Selenga River Basin

The Selenga River basin is situated in the central Siberian plateau (Fig. 2.1) and encompasses an area of about 440,000 km^2, the majority of which lies in Mongolia. It is characterized by a number of basins and ranges, with the Khangai and Khentii Mountains peaking at or above 2800 m a.s.l. The Selenga River has a flow length of 943 km and discharges into Lake Baikal in southern Siberia. This region is characterized by a harsh continental climate, with long cold winters and moderately warm summers. The average monthly temperature is close to +15 °C in July and about -23 °C in January (reference period 1954-2013, CRU, Fig. 2.5). The total annual precipitation is about 310 mm, approximately 2/3 of which is concentrated in the summer months (Munkhjargal et al., 2020). The remainder occurs as snowfall between mid-October and mid-April (Fig. 2.5). Precipitation and air temperature show a strong spatial disparity between the mountains and the basins (1954-2013, GPCC, Fig. 2.3). Generally, the mountainous areas in the southwest are characterized by extremely cold and dry conditions, whereas the valley regions close to Lake Baikal are somewhat milder and moister. The Selenga River is fed by both snowmelt and precipitation, as evinced by two runoff peaks over a hydrological year (Törnros & Menzel, 2010) (Fig. 2.5). The first peak occurs around May, which is triggered by the snowmelt freshet. The other peak occurs mainly in August and is due to strong summer precipitation. The dry season is from November to March and is characterized by relatively low runoff (ranging from 1 to 5 L/s*km^2) compared to the wet season (April to September, ranging from 8 to 29 L/s*km^2).

The geology of the Selenga basin is very complex, with a predominance of magmatic rocks, as well as metamorphic and volcanogenic formations (Kasimov et al., 2020). The upstream region of the basin is dominated by a forest-steppe mosaic (Kopp et al., 2014),

while the downstream region is primarily covered by boreal forest but includes some agricultural areas (Klinge et al., 2018). The Selenga River basin is characterized by a mixture of permafrost types, with discontinuous permafrost underlying the mountainous regions and sporadic/isolated permafrost occurring toward the center of the basin (Törnqvist et al., 2014).

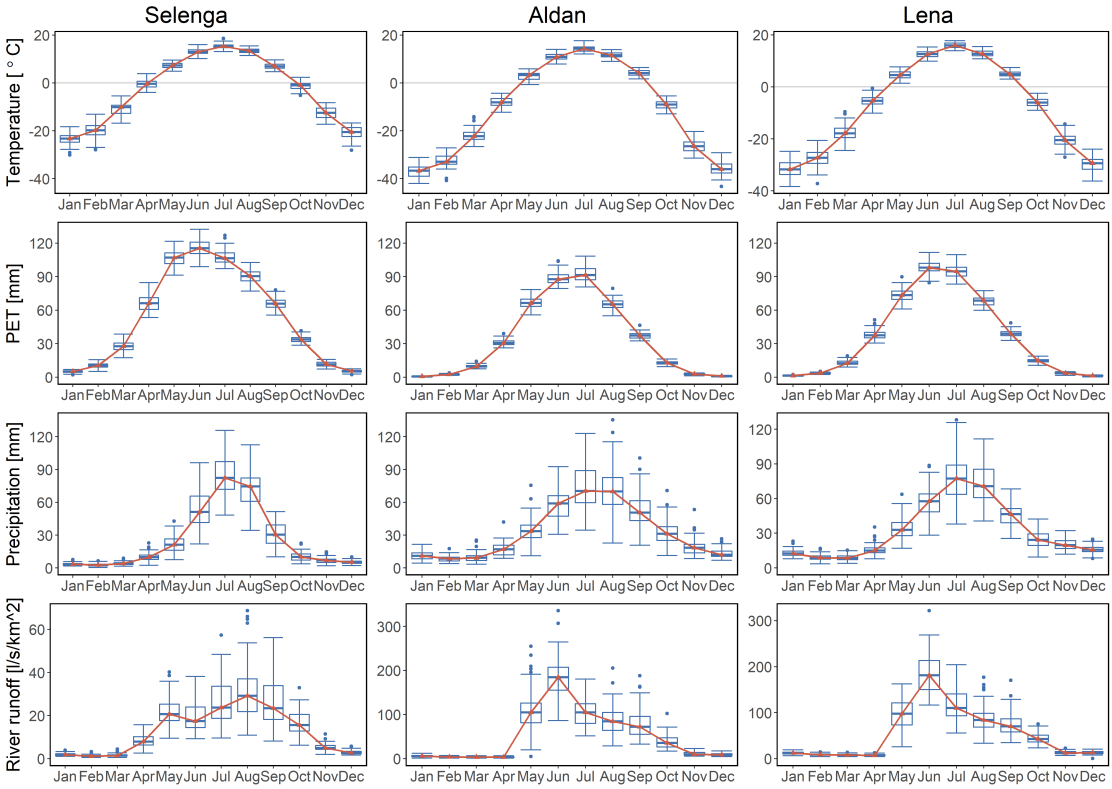

Figure 2.5: Intra-annual distribution of monthly mean air temperature (T), potential evapotranspiration (PET), precipitation (P), and river runoff (R) based on the reference period during 1954-2013 over Selenga, Aldan and Lena river basins. The basin-wide monthly series of T and PET are extracted from CRU dataset, and P is from GPCC dataset. The R data is from GRDC dataset.

2.1.2.2 Lena River Basin

The Lena Basin (gauged at Tabaga) (61.83 °N, 129.6 °E) is selected as the second representative for the Southern Siberian catchment. It drains a 897,000 km^2 basin and contributes 223 km^3 of water per year to the Lena River. This Lena basin also has an extreme continental climate with a long period of cold winters and relatively short summers. In the observation period of 1954-2013, mean annual air temperature of this region was -7 °C (CRU), Fig. 2.5), with mean monthly temperature ranging from -37 °C in January to 15 °C in July. The average annual precipitation is around 389 mm, and most precipitation (79%) emerges in the warm season (May to October). In the cold season, continuous snow cover exists from early October until the end of April. From a spatial perspective, the southwestern region typically experiences a warmer and wetter climate as compared to the northeastern region (Fig. 2.3). The runoff peak of the Lena River (gauged at Tabaga) occurs in June (183 L/s*km^2), which is a typical snowmelt-fed

regime. Similar to the precipitation, most of the river runoff (91%) is concentrated in the warm season compared to the cold, dry season (November to April).

Surrounded by the Transbaikal Mountain and the Lena Plateau (also called Prilensky Plateau), the Lena River receives river discharge from two large tributaries, the Vitim River and Olekma River (Fig. 2.1). The primary rock formation in this region is the gypsum-bearing and saline limestone (Rachold et al., 1996). Land cover types of this region are mainly Taiga forest, shrubland, and grasslands (Boike et al., 2016). 70% of the Lena region is underlain by ice-rich permafrost. As thus, permafrost in this region primarily belongs to the type of discontinuous permafrost (Velicogna et al., 2012).

2.1.2.3 Aldan River Basin

Aldan River is the second-longest tributary of the Lena River. It is 2,273 km long and drains an area of approximately 696,000 km^2, providing nearly 30% of the discharge of the Lena River (Fig. 2.5). The climate in the Aldan basin is characterized by long, cold winters with minimum temperatures of -37 °C in January and short, moderately warm summers with maximum temperatures of up to +14 °C in July (reference period 1954-2013, CRU). The average annual precipitation is around 390 mm (1954-2013, GPCC), with almost 70% occurring between May and September. The area is snow-covered from early October until the end of April. Spatially, the southern region is dominated by relatively mild and wet climatic conditions, whereas the north is cold and dry (Fig. 2.3). As a snowmelt-fed river basin, the Aldan River experiences peak runoff in June (185 L/s*km^2). Due to the low temperatures (continuously below 0 °C from November to April), runoff is very limited (3-10 L/s*km^2) during the cold season as compared to the flood season (May to October, 36-185 L/s*km^2).

Geographically, the Aldan basin is located on the Prilenskoe Plateau and is composed mainly of limestone and limestone-terrigenic sediments (Rachold et al., 1996). Taiga (or boreal) forest is the dominant landcover type in the basin (Bartsch et al., 2009). More than 90% of the Aldan River basin is dominated by deep and ice-rich continuous permafrost (Ye et al., 2009). In addition, the population density is relatively low, and human influence in the basin is limited.

2.2 Data source

2.2.1 Data introduction

Observational data with continuous measurement and high quality is essential for the hydro-climatic study. However, in some remote regions characterized by harsh climate conditions, hydro-climatic monitoring is often very limited, and some variables are not even monitored. Our study area in southern Siberia, for instance, has a lack of sufficient observations for multiple hydro-climatic variables. Thus, the gridded reanalysis data could be used to overcome this difficulty. In this section, a detailed introduction for the hydrological and meteorological data used for our study is presented.

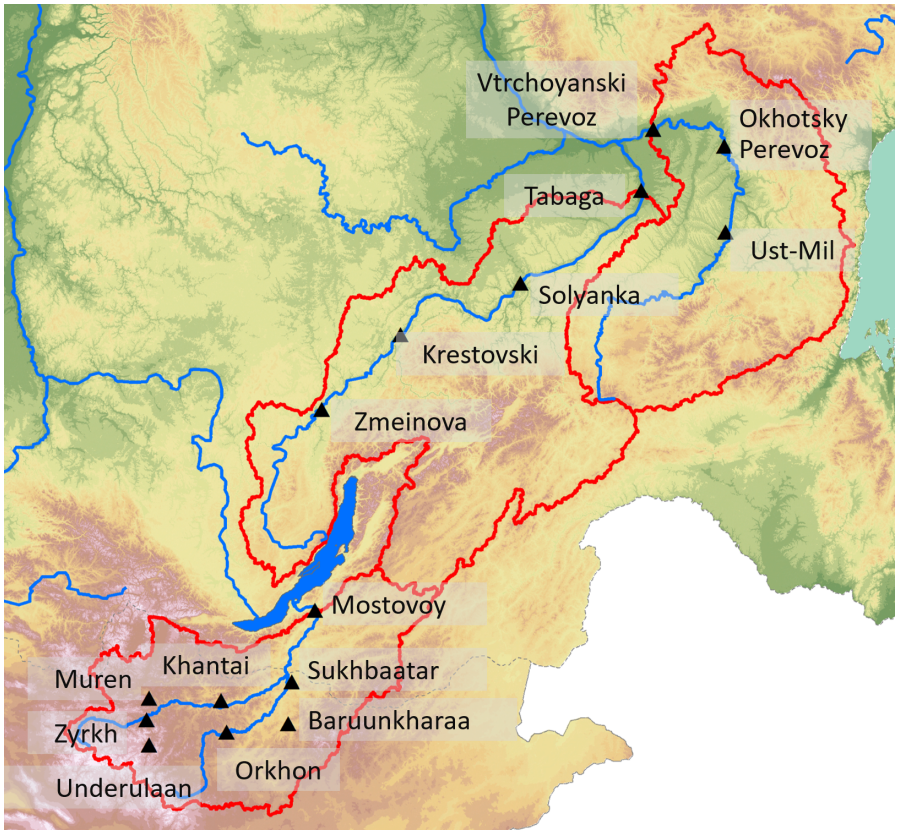

Figure 2.6: River runoff gauges in the study area. There are eight, four and three gauges for Selenga, Lena and Aldan, respectively.

2.2.1.1 Gauge discharge observation

Long-term (1954-2013) mean monthly river runoff records, measured at the gauging stations located at the river mouths (Selenga: Mostovoy; Aldan: Verkhoyanskiy Perevoz; Lena: Tabaga, Fig. 2.6), is available from the Global River Runoff Center (GRDC, 2019), Table. 2.1). In addition to these monthly river runoff data at the outlets of these three basins, we also use other runoff observations for some specific studies in different chapters. In Chap. 6, daily runoff records from 1982 to 2010 gauged at seven stations in the subbasin of the Selenga River are used. In Chap. 7, studies of extreme events is done by using the daily runoff observation from seven gauges in the Lena and Aldan River basin during 1950-2011. The location of all the gauges is shown in Fig. 2.6.

2.2.1.2 Global gridded meteorological data

Because the meteorological station network in southern Siberia is sparse and records are irregular (Bring et al., 2016; Rawlins et al., 2010), we use multiple global gridded datasets to overcome this issue in our study. Precipitation data were obtained from the Global Precipitation Climatology Center (GPCC), air temperature and potential evapotranspiration (PET) data were downloaded from the Climate Research Unit (CRU), and evapotranspiration (ET) and global radiation data were derived from ERA-Interim.

Basic information, such as spatial resolution, time step, and access details, are provided in Table. 2.1. The monthly time series of these datasets were extracted at the basin scale, and the basin-wide averaged monthly series was further used to aggregate to seasonal and annual series. These series are further applied for statistical time-series analysis for the same time period as the river runoff data (1954-2013), except for ERA-Interim, which starts in 1984.

GPCC precipitation

The precipitation data used in this study is obtained from the Global Precipitation Climatology Center (GPCC) (Schneider et al., 2018). The GPCC is a gauge-based dataset that obtained observations from more than 80,000 stations worldwide and is one of the most commonly used global precipitation product (Q. Sun et al., 2018). Both daily (1984-2013) and monthly (1954-2013) GPCC products (GPCC Full Data Monthly Product Version 2018) were used in our study.

CRU temperature and PET data

Monthly temperature and PET data (the CRUTS 3.10 dataset: 1954-2013) were obtained from the Climate Research Unit (CRU (Harris et al., 2014)) at East Anglia. The CRU dataset has a relatively long history and high spatial resolution with measurements obtained from national meteorological agencies (NMAs), the WMO, the CRU, the Centro Internacional de Agricultura Tropical, the Food and Agriculture Organization (FAO), and others. The PET equation used by the CRU is a variant of the Penman-Monteith equation: the FAO (Food and Agricultural Organization) grass reference evapotranspiration (Monteith, 1965; Sheffield et al., 2012). It is derived from the absolute values of the meteorological variables such as monthly mean temperature, monthly mean minimum temperature, monthly mean maximum temperature, monthly mean vapor pressure, and monthly mean cloud cover.

ERA-Interim dataset

ERA-Interim is a global atmospheric reanalysis data generated by the European Centre for Medium-Range Weather Forecasts (ECMWF) (Dee et al., 2011). It consists of 3-hour to daily data since 1979. Specifically, the daily global radiation data during 1984-2013 in this dataset is used as the radiation input of the hydrological TRAIN model for the evapotranspiration (ETa) simulation. Since this dataset contains its own ETa data, we also use the ERA-Interim ETa data to verify our simulated ETa data generated from the TRAIN model.

NCEP-NCAR reanalysis dataset

Large-scale circulation is characterized by using the geopotential height data from National Centers for Environmental Prediction-National Center for Atmospheric Research (NCEP-NCAR) reanalysis (Kalnay et al., 1996). This includes gridded (2.5×2.5 degree latitude-longitude) monthly means of geopotential height patterns at different atmospheric levels, such as 1000-hPa, 850-hPa, 500-hPa, 250-hPa, ..., 10-hPa geopotential height.

GRACE-REC dataset

NASA's Gravity Recovery and Climate Experiment (GRACE) joint U.S.-German satellite mission (Tapley et al., 2004) was launched in 2002, which provides integrated information on the water storage variations at monthly temporal resolution for all the components of the surface and subsurface water reservoirs, including soil moisture, groundwater, surface water such as rivers, lakes, and wetlands, as well as cryospheric components like snow and land ice. It also reflects the integrated influences of the natural climate variability, global climate change, and human water extraction on hydrological variations, including groundwater that is hard to monitor in many parts of the world.

The GRACE-REC dataset (Humphrey & Gudmundsson, 2019) used in this study is constructed based on two different GRACE products and three different meteorological forcings, producing six reconstructed datasets (i.e., JPL-MSWEP, JPL-GSWP3, JPL-ERA5, GSFC-MSWEP, GSFC-GSWP3, and GSFC-ERA5), and each of which has 100 ensemble members. These TWS reconstructions perform well as compared to the global hydrological models. In this study, the average of the ensembles of six TWS reconstructions, with a spatial resolution being 0.5×0.5 degree, is applied for the southern Siberian region.

Table 2.1: Datasets description

Data set	Data category	Dataset	Resolution	Frequency	Period
Runoff data	Runoff (R)	GRDC	Station	Monthly	1954-2013
Meteorological station data	Temperature (T) Precipitation (P) Wind speed (u) Dewpoint temperature (Tdew)	GSOD	Station	Daily	1954-2013
	Radiation (Rd)	GEBA	Station	Monthly	1984-2005
Global gridded data	Temperature(T) Potential evapotranspiration (PET)	CRU	0.5°× 0.5°	Monthly	1954-2013
	Precipitation (P)	GPCC	0.5°× 0.5°	Monthly	1954- 2013
			1.0°× 1.0°	Daily	1984- 2013
	Global radiation (Rd) Evaporation (E)	ERA-interim	0.7°× 0.7°	Daily	1984-2013

2.2.2 Study period and data availability

There are several sets of reference periods for assessing the historical hydroclimatic change in this study. The 1954-2013 reference period is particularly used for detecting the long-term changes in hydroclimate conditions. The choice of the beginning and ending year is based on the availability of the hydroclimatic datasets. For instance, the period since the starting date of 1954 generally cover a complete observation in the GRDC river discharge datasets. The year 2013 is chosen as the end date because the cover period of GPCC precipitation datasets is from 1901 to 2013. Further, in order to account for the historical changes under changing climate, we split the 60-yr period into two 30-yr periods, i.e., 1954-1983 and 1984-2013. These two periods can be used to reflect the changes in the average and extreme hydroclimate conditions in a non-stationary earth system. The choice of a 30-yr period is also suggested by the World Meteorological Organization's recommendation for hydroclimatic statistics.

2.2.3 Assessment of datasets

In this study, both the gauge-based observation data and gridded-based data are used. Each of them contains uncertainties. Observational uncertainties are primarily related to imperfect gauging techniques and spatial heterogeneity in hydro-climatic conditions. Most of these uncertainties are existing in the precipitation and river runoff data. Firstly, the uncertainties in precipitation have been recognized as one of the most dominant reasons that induce biases into hydro-climatic analysis in cold regions (McClelland et al., 2004). The uncertainty in the observation of precipitation is dominated by: (1) point scale measurement error, especially the gauge undercatch of the solid precipitation in winter (Goodison et al., 1998), and (2) systematic biases induced by complex topography, which is especially large in the region with large elevation gradients (Barstad et al., 2007).

River discharge is estimated using the open channel rating curve method in the Sibeia (Shiklomanov et al., 2006). The accuracy of this method is substantially affected by thicker ice, cold temperature, and low river flow velocity below the ice (McClelland et al., 2004). In addition, uncertainties also exist in the management of river discharge data, storage, or post-processing, including malfunctioning measurement equipment and human-induced measurement errors. These uncertainties mentioned above are more considerable with respect to the observations with lower density (Rawlins et al., 2009; Serreze & Etringer, 2003). Last but not least, the number of the monitoring system for river discharge has been in decline during the recent decades (Shiklomanov et al., 2002). This decline in observation number might involve more considerable uncertainties in the estimation of hydrological change in Siberia (Bring et al., 2016).

The gridded-based data has enabled improvements in estimating hydro-climatic changes across the data scarcity region (Hrachowitz et al., 2013). They are homogeneously processed using the same consistent standards and methodology over both time and space scales. As thus, they can enable an evenly distributed estimation over regional scale and with complete temporal coverage. Besides, most of the remote sensing datasets are publicly accessible. Thus, the globally gridded-based datasets such as GPCC, CRU, ERA-Interim, and GRACE data are particularly advantageous for the region that suffers from data scarcity like southern Siberia.

2.3 Methods

2.3.1 Modeling and empirical methods

2.3.1.1 TRAIN model

Because there is no ET observation network in the Selenga and Aldan basins (or anywhere close) (Bring et al., 2016), we used the distributed hydrological model TRAIN (Menzel, 1996b) to simulate ET. This is regarded as an additional source of information and complements data gathered from the gridded ERA-Interim dataset. Details in the analysis of ET are presented in Chap. 5.

Forcing data

TRAIN is driven by multi-source-based data (i.e., station observations, reanalysis estimates), including air temperature, precipitation, wind speed, relative humidity, and global radiation. The model considers the vertical water fluxes in the soil-plant-atmosphere system and their drivers. For the simulation of transpiration, the model uses the Penman-Monteith equation. The determination of canopy resistances follows an approach described in Menzel (1996b) that considers current meteorological conditions, soil water status, and the stage of vegetation development. When precipitation occurs, the model also considers the processes of interception and interception evaporation (Menzel, 1996a). The calculation of the soil moisture content and of percolation is based on the conceptual approach from the HBV model (Bergström et al., 1995). Further information on model development based on field experiments, as well as on model applications, can be found in Stork and Menzel (2016); Tijdeman and Menzel (2021); Törnros and Menzel (2014).

Information regarding soil depth and soil water-holding capacity, leaf area index (LAI), and vegetation/crop height is also essential for running the model. Information about LAI and vegetation/crop height can be provided directly to the model or estimated within the model from typical values. For example, the seasonal development of LAI depends on the specific crop or vegetation type. The station-based daily meteorological data for the application of TRAIN comes from the GSOD dataset (NESDIS, 2019). For the calculation of ET, 17 stations in the Aldan basin and 10 stations in the Selenga basin were selected. The GSOD daily precipitation dataset suffers from large gaps during the late 1990s and early 2000s (Fig. A.1). Gridded daily precipitation data from the GPCC dataset at the corresponding stations have been used to fill those gaps. The validation of the GPCC daily data is provided in the supplementary materials (Fig. A.2).

Data regarding incoming short-wave radiation can be obtained from a new version of the Global Energy Balance Archive (GEBA) developed and maintained at ETH Zurich (Switzerland) (Wild et al., 2017). However, the GEBA-based observations are very limited in our study region, with only five stations located in or within the vicinity of the Selenga basin. Thus, the long-term global radiation forcing data from the ERA-Interim reanalysis dataset has been used as a substitute. Additionally, the five GEBA radiation observations have been applied to validate the gridded ERA-Interim radiation data (see Fig. A.3 in the supplementary material). The entire input datasets, especially wind speed, relative humidity, and global radiation, are only available after the year

1979. As a consequence, the corresponding ET analysis is limited to the second period of this study, 1984-2013. Note that for the calculation of daily ET at each station, we assumed short-grass as the vegetation. Also, for comparability, identical soil physical parameters were assumed at all stations.

Validation of ET data

We used water balance closure to validate both the remote-sensing (ERA-Interim) and model-based (TRAIN) ET data. We found that the gridded ERA-Interim evaporation data, extracted based on the geographic extents of the Selenga and Aldan watersheds, always produce large deviations in the annual water balance [(P-ET-R)/P = -46% and -35% for Selenga and Aldan, respectively] Table. A.1. With the TRAIN-simulated ET, this deviation in the annual water balance is reduced to 3.8% in Selenga but remains high at -40% for the Aldan basin.

The negative deviation in the water balance in the Aldan basin, i.e., P-ET-R < 0, is in agreement with previous water balance evaluations for Siberian regions with continuous permafrost (Serreze et al., 2006). The change in groundwater storage induced by permafrost degradation may play an important role in the imbalances observed in the water cycle in eastern Siberia (Muskett & Romanovsky, 2009; Velicogna et al., 2012). We used the reconstructed GRACE terrestrial water storage (TWS) data (Humphrey & Gudmundsson, 2019) to account for the increased groundwater storage and found that it accounts for 10% of the precipitation in the Aldan basin (Table S2). This indicates enhanced subsurface connectivity in a warmer climate (Walvoord & Kurylyk, 2016).

We also compared both the TRAIN simulation and the ERA-Interim reanalysis with the ET data measured by Ohta et al. (2008) at an observation site that is geographically close (approximately 190 km) to one of the meteorological stations (Curapca) in the Aldan basin. The annual average ET values of the TRAIN simulation and the ERA-Interim reanalysis differ from the observed average ET by 12.8% and 33%, respectively (Table. A.2). Because the ET data simulated by the TRAIN model are more consistent with the observation data, we use them to evaluate the historical ET variations in the following analysis.

2.3.1.2 Budyko framework

The Budyko framework (Budyko, 1974) is a simple and widely-used tool for estimating shifts in basin water availability in response to climate change and landscape disturbances at mean annual scales (Berghuijs et al., 2014; Greve et al., 2014; Teuling et al., 2019). It first defines a dryness index

$$\mathrm{DI} = \frac{\mathrm{PET}}{\mathrm{P}} \tag{2.1}$$

to capture the ratio between the atmospheric water demand (PET) and the atmospheric water supply (P). This equation can be used to determine climate classifications for different basins: humid or energy-limited ($\mathrm{DI} \leq 1.5$), dry sub-humid or transition ($1.5 < \mathrm{DI} \leq 2$) and semi-arid or water-limited ($2 < \mathrm{DI} \leq 5$) (UNEP & Thomas, 1992). Then,

the framework defines an evaporative index

$$\mathrm{EI} = \frac{\mathrm{ETa}}{\mathrm{P}} \tag{2.2}$$

to reflect the water consumed by the actual evapotranspiration process. Since actual evapotranspiration (ET) can neither exceed the potential evapotranspiration (PET) nor exceed the water supply (P), EI satisfies $\mathrm{EI} \leq \min(\mathrm{DI}, 1)$. Here, we assume that precipitation is the only water source. However, depending on the region, other sources such as lakes, wetlands, and glaciers may contribute water to the evapotranspiration process, making $\mathrm{EI} > 1$. For water-limited basins, EI is constrained by the available water supply. In energy-limited basins, the magnitude of EI is controlled by the available evaporative energy.

In this study, we used GPCC precipitation, CRU potential evapotranspiration, and ET data to compute station-based DI and EI combinations for the Selenga (17 stations) and Aldan (10 stations) basins over the 30-year period from 1984 to 2013. The average of these station-based combinations in each basin is aggregated to represent the hydroclimatic characteristics at the basin scale. The shift in the water availability is reflected by the average change in DI and EI between the earlier and later 15-year periods. See the analysis results of the Budyko framework in Chap. 5.

2.3.1.3 Stefan methods

Here the Stefan methods, which is introduced by (Stefan, 1891) and modified by (Frauenfeld et al., 2007; Nelson & Outcalt, 1987; Peng et al., 2018; T. Zhang et al., 2005), is applied to calculate freezing index (FI), Thawing index (TI), and active layer thickness (ALT). Further, we estimate both the long-term average and trends of these three indicators of changes in ground thermal regime at each gridded cell for the three southern Siberian catchments over the period 1954-2013. The detail of the analysis is shown in Sec. 3.2.

Empirically, FI is the absolute value of the summation of the daily air temperatures when temperature is below freezing, i.e., for $i = 1, 2, \ldots N_F$:

$$\mathrm{FI} = \sum_{i=1}^{N_F} |T_i|, \quad T_i < 0\ ^\circ\mathrm{C}. \tag{2.3}$$

TI is the summation of the daily air temperatures when temperature is above freezing, i.e. for $i = 1, 2, \ldots N_T$:

$$\mathrm{TI} = \sum_{i=1}^{N_T} |T_i|, \quad T_i \geq 0\ ^\circ\mathrm{C}. \tag{2.4}$$

Since the long-term continuous daily observed temperature data is not available in our study area, here, we apply the monthly air temperature data (CRU dataset) in the Stefan method. This method is promoted and validated by Frauenfeld et al. (2007).

FI is the absolute value of the summation of the monthly air temperatures, when

temperature is below freezing, i.e., for $i = 1, 2, \ldots M_F$:

$$\mathrm{FI} = \sum_{i=1}^{M_F} |T_i| * D_i, \quad T_i < 0\ ^\circ\mathrm{C}. \tag{2.5}$$

TI is the summation of the monthly air temperatures, when temperature is above freezing, i.e. for $i = 1, 2, \ldots M_T$:

$$\mathrm{TI} = \sum_{i=1}^{M_T} |T_i| * D_i, \quad T_i \geq 0\ ^\circ\mathrm{C}, \tag{2.6}$$

where the T_i is the mean monthly air temperature, D_i is the number of days in that month.

Furthermore, TI can be used to calculate ALT by using the method (T. Zhang et al., 2005):

$$\mathrm{ALT} = E * \sqrt{\mathrm{TI}}, \tag{2.7}$$

where TI is the thawing index; E is a parameter that can be referred to as the empirical term (Nelson & Outcalt, 1987). In this study, the E factor equals 4, which is determined from the spatial map of E factor in the Northern Hemisphere (Peng et al., 2018).

2.3.2 Statistical methods

2.3.2.1 Trend detection

In this study, trend detection for the hydro-climatic series is performed in two steps. First, the determination of trend magnitude is calculated using both ordinary linear regression and Sen's slope (Sen, 1968). Second, the statistical significance of the trend is computed using the nonparametric Mann-Kendall (MK) test (Kendall & Gibbons, 1975; H. B. Mann, 1945). The trend is defined to be statistically significant when the p-value is smaller than 0.05. The MK test is one of the most commonly used and robust methods for detecting statistical significance of long-term trends in hydro-climatic time series (Déry & Wood, 2005; Shiklomanov et al., 2006; St. Jacques & Sauchyn, 2009; Yue & Wang, 2002). Its performance can be relied on only when the data have no serial correlation. The hydro-climatic regimes of the Aldan and Selenga River basins show strong seasonality (Fig. 2.5); the time series of hydro-climatic variables are therefore assumed to be serially independent.

2.3.2.2 Moving window average approach

Although trend detection can reveal the long-term rate of hydrological change, its magnitude and significance are sensitive to the selected time period (Hannaford & Buys, 2012; Kundzewicz & Robson, 2004). We, therefore, apply a 10-year moving window approach to analyze the long-term time series. This approach reduces the bias caused by year-to-year variations and possible extreme conditions in individual years. As such,

it can robustly illustrate the oscillation patterns in the hydro-climatic series, which can be used to detect the potential connections between hydro-climatic variables.

2.3.2.3 Anomaly analysis

Anomaly analysis enables us to distinguish the condition of the individual year in comparison to the general condition during the long-term period (1954-2013) on hydro-climatic variables. For example, the negative anomalies of the precipitation, river runoff, and terrestrial water storage (TWS) refer to water deficits in these water-related variables. By removing the long-term mean of the time series, one can get the anomalies. Based on these anomalies, one can further calculate the percentiles ranking, which can be used for detecting extreme events such as droughts, heatwaves, or floods.

2.3.2.4 Percentiles ranking analysis

In order to place the hydro-climatic timeseries into historical perspective, the timeseries are sorted from lowest to highest, with ranks assigned to each value. The numeric rank represents the position of that specific value throughout the historical record. For our analysis during the period of interest from 1954 to 2013, depending on the magnitude of the corresponding variable, they are ordered from 1 to 60, with the value of 1 refers to the record lowest, and the value of 60 refers to the highest (Tijdeman et al., 2020).

In this study, three percentiles (20%, 50%, and 80%), representing the percent of distribution equal to or below it, are used as the threshold for dry and wet (cold and warm) conditions. Specifically, 50% is used as a threshold for dividing the dry and wet (cold and warm) period. For instance, all the values below 50% belong to dry (cold) conditions, while the value above 50% refers to wet (warm) conditions. The two classifications 20% and 80% represent the very dry (cold) and very wet (warm) conditions, respectively. Based on these thresholds, four types of dry and wet (cold and warm) conditions (i.e., 20%, 20-50%, 50-80%, and 80%) are divided for each hydro-climatic timeseries.

2.3.2.5 Cross-correlation analysis

Although cross-correlation does not always imply causality, it can nonetheless be used to express the strength of the relationship between runoff and its drivers (Seneviratne et al., 2010). It can also provide valuable information about the mechanisms driving the hydrological change in a specific basin. Spearman's correlation is a rank-based parametric measure of correlation that has been successfully applied to analyze the relationship between climatic components and river runoff (Pavelsky & Smith, 2006; Seneviratne et al., 2010). The Spearman's rank correlation coefficient ($\tau(X, Y)$) between two sets of subseries, X(t) and Y(t), is defined as

$$\rho(X(t), Y(t)) = \frac{\overline{X(t) \cdot Y(t)} - \overline{X(t)} \cdot \overline{Y(t)}}{\sqrt{\overline{X^2(t)} - \overline{X(t)}^2}\sqrt{\overline{Y^2(t)} - \overline{Y(t)}^2}}, \tag{2.8}$$

where $\overline{X(t)}$ and $\overline{Y(t)}$ are the mean of $X(t)$ and $Y(t)$, respectively. The relationship between $X(t)$ and $Y(t)$ is quantified by the correlation coefficients $\rho(X, Y)$ and is treated as statistically significant when $p \leq 0.05$.

River runoff conveys integrated characteristics of climatic change over a given basin. It is naturally lagged and smoothed from precipitation through surface and subsurface hydrological processes (Brutsaert & Hiyama, 2012). Therefore, to further examine the lag relationship between seasonal runoff and precipitation, we generalize the Spearman's rank correlation by introducing a time lag τ into the variable $X(t+\tau)$ (Djebou et al., 2015; Keener et al., 2010). This lagged correlation coefficient between the two sets of subseries, $X(t+\tau)$ and $Y(t)$, is defined as

$$\rho(X(t+\tau), Y(t)) = \frac{\overline{X(t+\tau) \cdot Y(t)} - \overline{X(t+\tau)} \cdot \overline{Y(t)}}{\sqrt{\overline{X^2(t+\tau)} - \overline{X(t+\tau)}^2}\sqrt{\overline{Y^2(t)} - \overline{Y(t)}^2}}, \tag{2.9}$$

In our study, the major application of cross-correlation analysis is for detecting the lagged runoff-precipitation response. As thus, $X(t+\tau)$ and $Y(t)$ are the seasonal river runoff and precipitation in season τ, respectively. $\tau = 0, 1, 2, 3$ represents the number of seasons lagged between river runoff and precipitation. For example, with regard to summer precipitation, $\tau = 0$ means runoff in summer, while $\tau = 1$ denotes runoff in autumn, and so on. The detailed description of cross-correlation is displayed in Sec. 4.2.

2.3.2.6 Empirical Orthogonal Function (EOF) analysis

The Empirical Orthogonal Function analysis (EOF analysis), also called as Principal Components analysis (PC analysis). It can be used to identify the modes of variability in hydro-climatic factors (Bonfils et al., 2020; Korres et al., 2010; Wouters & Schrama, 2007). Each EOF mode denotes a certain proportion of the total variations in the hydro-climatic factors. Among which, the first few modes with a more significant percentage represent the most prevalent pattern in the variables. In this study, EOF analysis is used to interpret the spatial patterns of the terrestrial water storage (TWS) (See results in Chap. 5).

For the continuous variable $Z(t, s)$, t and s denote temporal and spatial position, respectively. The formula of EOF is

$$Z(t, s) = \sum_{k=1}^{K} c_k(t) u_k(s), \tag{2.10}$$

where K is the total number of modes included in the variable. $u_k(s)$ represents the basis functions of space and $c_k(t)$ is the basis functions of time, the most optimal set of $u_k(s)$) and $c_k(t)$ will be showing in the EOF_1, and so on. The EOF analysis provides a set of orthogonal spatial patterns (EOF_k) together with a set of associated principal components (PC_k) (e.g., PC_1 corresponds to EOF_1). This method also denotes the explanation of the variance, which indicates how much variability of variable Z is explained by each modes (i.e., EOF_k or PC_k).

Chapter 3

Climate and permafrost conditions in southern Siberia

Before we start the detailed investigation of the hydrological processes, in this chapter, we first examine the spatial distribution of the 60-year mean value and trends (based on reference period during 1954-2013) in the climate components, such as precipitation (P), air temperature (T), and potential evapotranspiration (PET). This can enable us to assess the long-term climatology and spatial-temporal change in climate variables, which can provide a basis for the hydrological studies in the subsequent chapters.

Since the observations of permafrost are only available at field scale and with a short period (Brutsaert & Hiyama, 2012; Frampton et al., 2011; Walvoord & Kurylyk, 2016), it is therefore a big challenge to detect the changing pattern in permafrost at a large spatial scale and long-term temporal scale. To resolve this issue, in the second part of this chapter, we apply permafrost indices, namely annual freezing index (FI), thawing index (TI), and active layer thickness (ALT), to detect the historical changes in permafrost distributions and dynamics. Such indices are derived based on a linear relationship between the air temperature and ALT of permafrost and can provide a first estimation of the long-term permafrost evolution over a large spatial scale (Frauenfeld et al., 2007; Peng et al., 2018; T. Zhang et al., 2005).

3.1 Spatial-temporal distribution and variability of climate variables

3.1.1 Air temperature

The first two columns of Fig. 3.1 present the spatial distribution of mean annual air temperature (MAAT) and mean seasonal air temperature (MSAT), and their long-term trends, respectively. The last two columns of Fig. 3.1 are the probability density functions (PDFs) of the mean value and trends over each catchment, respectively. In general, the climatology of both the MAAT and MSAT shows similar spatial patterns which decline from the low latitudes to the high latitudes. In addition to this latitudinal dependence, the distribution of the MAAT and MSAT is also governed by the altitude. For example, the mountainous area located in the southwestern region of the Selenga basin is relatively colder as compared to the flat region at the same latitudes. This difference is pronounced during summer when the air temperature is generally high. Throughout the four seasons, the most significant spatial difference is observed in winter, with a >30 °C

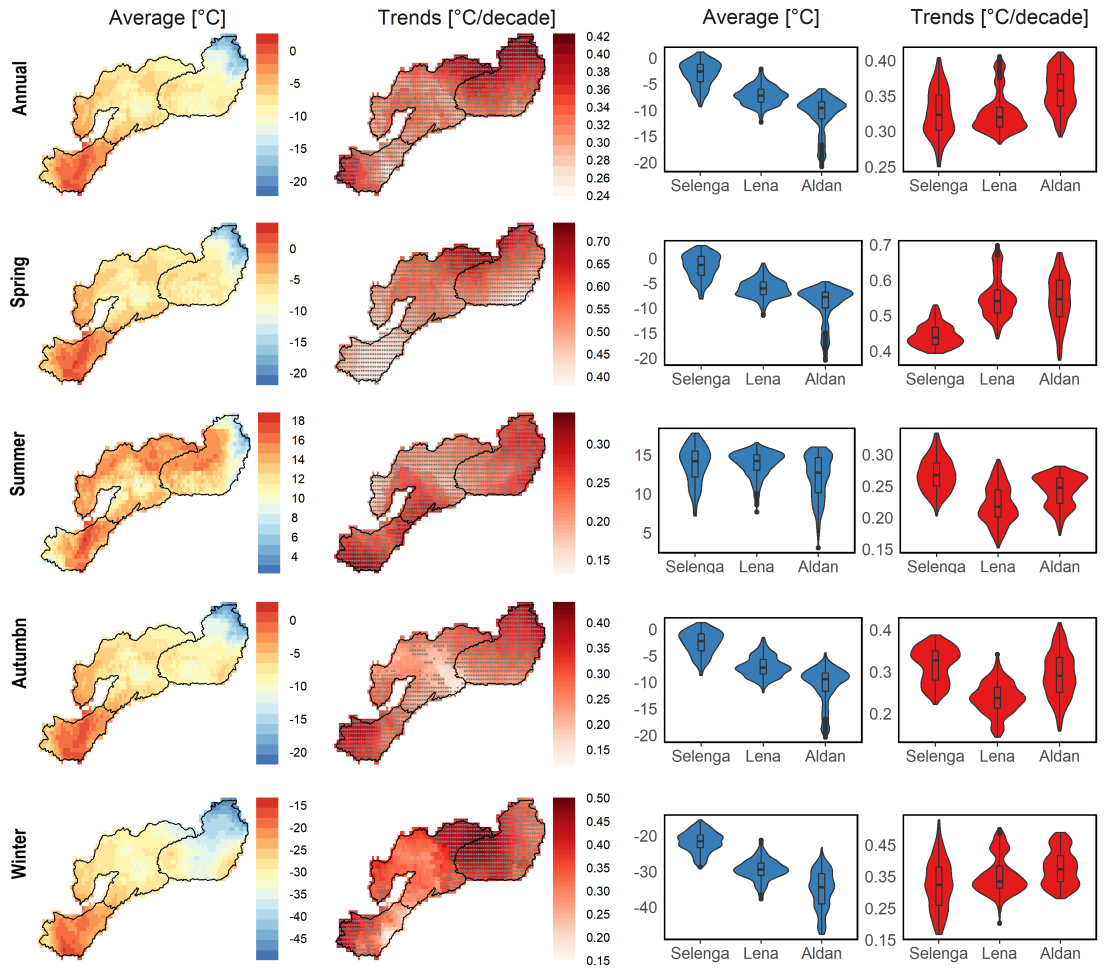

Figure 3.1: The spatial distribution of the long-term (1954-2013) average and trends of mean annual air temperature (MAAT) and mean seasonal air temperature (MSAT) based on the CRU dataset. In the second columns, the dots in grey denote the trends with statistical significance ($p \leq 0.05$). First and third columns are the spatial pattern and the probability density functions (PDFs) for the MAAT and MSAT, with the horizontal axis being the density of probability; second and fourth columns are the PDFs of 60-year trends for the MAAT and MSAT.

temperature difference existing between north and south. The extent of the PDFs of the MAAT and MAST in Aldan is much broader than those in Lena and Selenga, indicating a much more significant spatial heterogeneity in temperature in the north of southern Siberia. Nevertheless, for most of the region, nearly all the mean temperatures, except MSAT in summer, are below 0 °C.

The trends of the temperature reveal statistically significant warming throughout the entire southern Siberia. The most pronounced warming is observed in the northern latitudes region of Aldan and the mountainous region of the western Selenga, which means that the temperature increases more rapidly in the colder region than in the warmer region. More Specifically, the MAAT trends in the north region of the Aldan and Lena range from 0.32 to 0.42 °C/decade, while MAAT trends over the middle valley region of the Selenga and Lena basins extend from 0.25 to 0.30 °C/decade. In addition, the most significant spatial difference in MAAT trend is observed in Selenga, ranging from

0.25 °C/decade in the eastern region to 0.40 °C/decade over the western mountainous region.

At seasonal scale, the most significant warming trends are found in spring over the entire study area, where all the three basins have recorded a warming rate larger than 0.40 °C/decade. Specifically, the higher warming rates during spring are found in several parts of the Lena and Aldan basin, ranging from 0.6 to 0.75 °C/decade. The PDFs of the MSAT trends in spring exhibit the most extensive range of spatial differences among all the seasons, with an almost 0.2 °C/decade difference between the Aldan (Lena) and Selenga basin. For the MSAT during summer and autumn, the gridded trends show less consensus among these three basins. During winter, strong warming rates are also recorded throughout the entire Aldan basin. However, the warming trends of winter MSAT in the Selenga basin show significant spatial heterogeneity, with more than 0.4 °C/decade differences between the highest and lowest rates of warming.

Additionally, more than half of the area in Selenga and Lena experience non-significant warming rates during winter. This absence of the statistic significance in the rising of the winter temperature could be attributable to the recent cooling condition in Northern Eurasia since the 1990s (J. L. Cohen et al., 2012), which has been attributed to the potential linkage between the Arctic region and middle latitudes that is known as "warming arctic, cooling Eurasia" (WACE) (J. L. Cohen et al., 2012; Mori et al., 2019, 2014)

3.1.2 Precipitation

Different from the latitude-dependent distributions in the air temperature, the distributions of the mean value and trends in precipitation differ substantially across the entire region (Fig. 3.2). The annual precipitation of all the three catchments is characterized by a considerable spatial heterogeneity, with more than 300 mm of difference between the highest and lowest gridded precipitation (as shown from the corresponding PDFs). The extremely high precipitation is found in the southeastern coastal area of Aldan and the northern boundary of Selenga due to the modulation of the local climate over Lake Baikal. Nevertheless, most of the annual precipitation is distributed close to the center of the PDFs over all three catchments. Seasonally, the summer precipitation is distributed in the same range for the entire region. However, the PDFs of the precipitation in spring, autumn, and winter posse less similarity, with lower values being noticed in Selenga as compared to those in Lena and Aldan.

During the period of record from 1954 to 2013, the long-term trends of annual and seasonal precipitation present non-uniform changes over all the three southern Siberian basins. In the middle area of the Lena basin and the western part of the Aldan basin, the most considerable increased annual precipitation is noticed. In contrast, the most decreased trend in annual precipitation is registered in the south of Aldan. From the PDFs perspective, the trends in annual precipitation are almost evenly distributed around 0 mm/decade in Aldan and Selenga. However, most of the trends in Selenga are not statistically significant.

At the seasonal scale, the PDFs show that spring is the only season that experiences a widespread precipitation increase across all three basins. Nevertheless, there is a

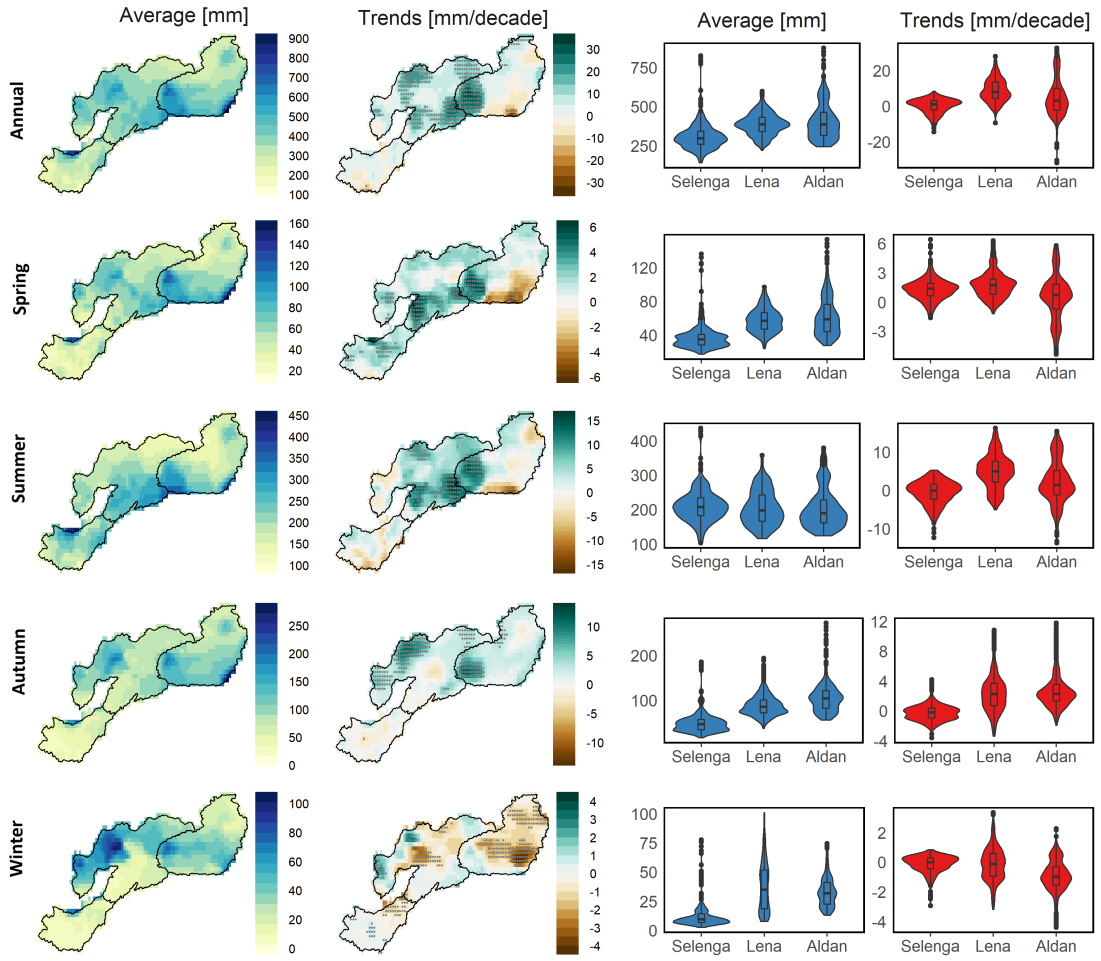

Figure 3.2: Same as Fig. 3.1, but for precipitation. The precipitation data is taken from GPCC dataset.

substantial spatial contrast in Aldan, with both statistically significant upward and downward trends being observed in the southern part of this basin. Thus, the spatial variations in spring precipitation in Aldan are much more significant than those in the other two basins. The PDFs of the trends in summer precipitation have similar shapes with respect to the distributions of the spring trends but with different peaks and more extensive ranges. As to the autumn precipitation, although there is only a slight change being observed in the Selenga basin, statistically significant upward trends are recorded in the large parts of the Lena and Aldan basin. This has contributed to a basin-wide rise in the autumn precipitation over two northern basins. The winter precipitation is relatively lower than in other seasons. However, it is the only season that is characterized by basin-wide decreased precipitation over all three basins.

3.1.3 Potential evapotranspiration

Since the potential evapotranspiration (PET) largely depends on the local radiation, wind speed, cloudiness, and the moisture available in the atmosphere (Trenberth et al., 2014), thus, the values and trends of the PET exhibit substantially distinct patterns in

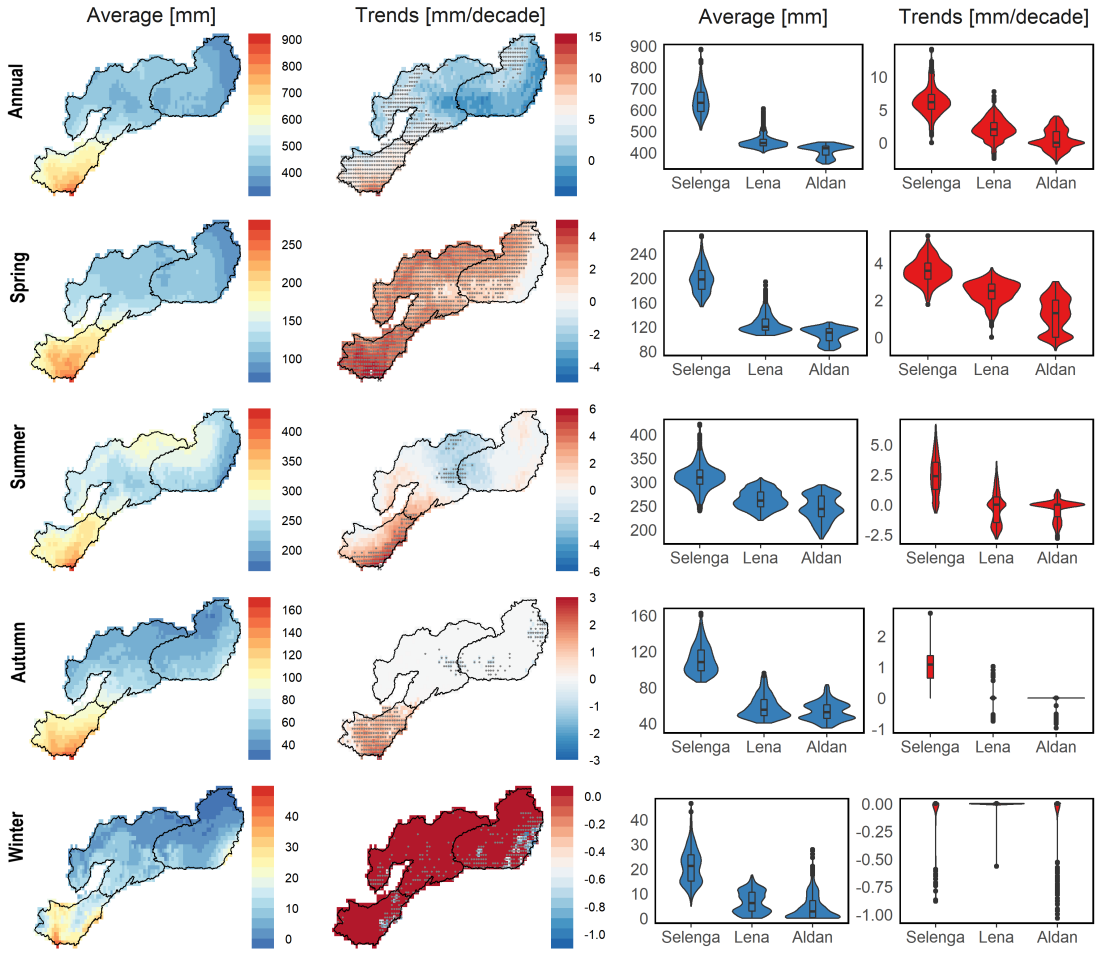

Figure 3.3: Same as Fig. 3.1, but for PET. The PET data is taken from CRU dataset.

comparison to that in the air temperature and precipitation. The PET in the south is much larger than that in the north: in the semi-arid Selenga, the highest annual PET is as large as 900 mm; whereas in the Boreal Lena and Aldan basins, the annual PET ranges between 250-500 mm. As a result, the PDFs of annual and seasonal PET in Selenga show a larger range than the other two basins, indicating a strongly latitudinal governing pattern in PET.

A distinct spatial contrast between the north part (Lena and Aldan) and the south part (Selenga) is also exhibited in the PET trends at both annual and seasonal scales. High trends are generally observed in the region characterized by high PET as well. Especially, the southeastern part of Selenga has the highest trend of 5-7 mm/decade in the summertime. However, the summer PET in Aldan and Lena shows no significant trends in most parts of the region. Furthermore, spring is the only season where all the three basins have an increasing trend in PET, despite the non-significant declines in the eastern area of Aldan. Due to the low availability of energy during winter, the PET is extremely small and has no significant trend.

3.2 Climatic signal of the changed frozen soil and permafrost

3.2.1 Changes of 0 °C isotherm of MAAT

The 0 °C isotherm of MAAT is a line on the map where mean annual air temperature (MAAT) equals to 0 °C. It serves as an efficient signal for representing the thermal condition in the seasonal frost and permafrost environment (Evans & Ge, 2017). Fig. 3.4 shows the changes of the 0 °C isotherm of MAAT between two 30-year periods before and after the year 1984 (i.e., 1954-1983 in dark and 1984-2013 in blue). A clear northward shift in the 0 °C isotherm of MAAT between these two periods is observed in the southwestern and southeastern area, implicating a potential northward migration of permafrost domain in the southern Siberian region.

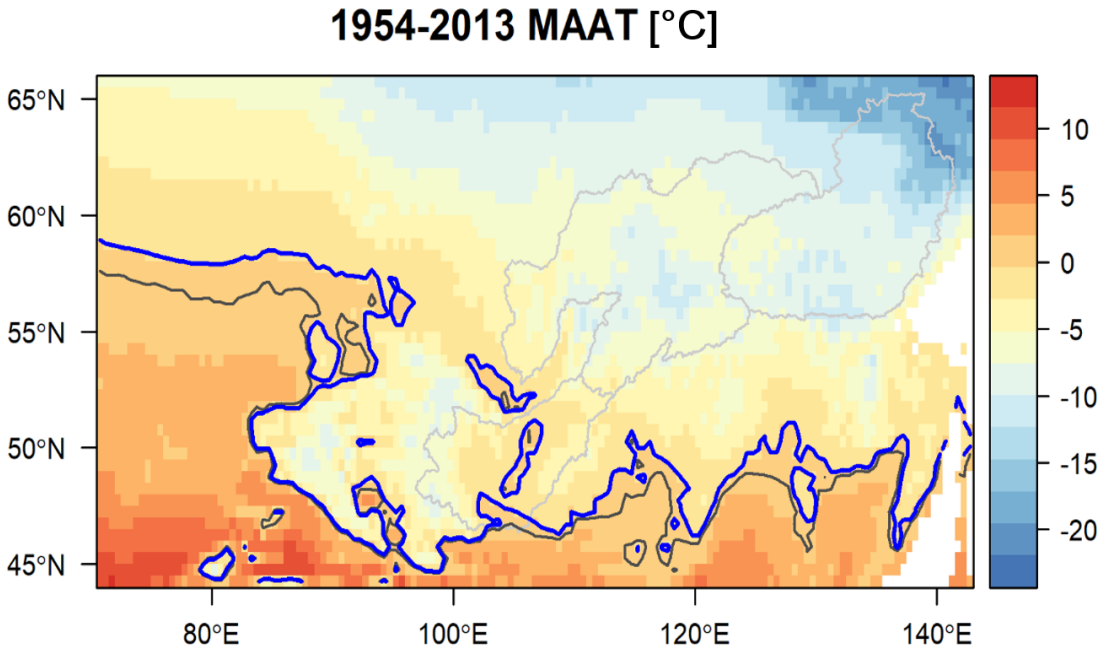

Figure 3.4: Spatial distribution of the mean annual air temperature (MAAT) during 1954-2013 based on the gridded CRU dataset. The two contours (in black and blue) are the isolines for the gridded cells with MAAT equaling to 0 °C over 1954-1983 (black) and 1984-2013 (blue).

Among these three catchments, the significant shift in the thermal regime is primarily noticed in the Selenga basin located in the southern boundary of the permafrost domain. In particular, it is observed not only in the southern region but also in the middle valley region. These significant shifts in 0 °C isotherm of MAAT suggest an increased sensitivity of local thermal conditions to the ongoing global warming. Given that permafrost distribution is susceptible to changing local thermal conditions, these evolution patterns also suggest an enhanced lateral degradation with increased permafrost-free area in the Selenga basin.

3.2.2 Spatial-temporal pattern and variability of FI, TI, and ALT

Based on the Stefan methods in Sec. 2.3.2, here we use the gridded CRU temperature datasets to calculate the freezing index (FI), thawing index (TI), and active layer thickness (ALT) for each of the gridded cells during the period of 1954-2013. Specifically, FI represents the accumulation of temperature in cold-season (below 0 °C), TI is aggregated from warm-season temperature (higher than 0 °C). Usually, ALT can be measured by field observation, however, only over small scales and with a short time span. Previous studies (T. Zhang et al., 2005) find that there is a linear dependence between ALT and TI. Therefore, here we determine the long-term, large-scale ALT from the TI during 1954-2013, with the spatially dependent coefficient being derived from Peng et al. (2018).

All these three indices can reflect the thermal ground conditions related to permafrost (Frauenfeld et al., 2007; Peng et al., 2018). We calculate both the long-term average (i.e., climatology) and trends of FI, TI, and ALT for each gridded cells (Fig. 3.5), which could delineate the spatial distribution of the general state and the historical variations in permafrost condition. In particular, we compared different climatology and trends in three different periods, namely 1954-2013, 1954-1983, and 1984-2013, to investigate potential changed thermal state (Figs. 3.6 and 3.7).

3.2.2.1 Climatological features of FI, TI, and ALT

Fig. 3.5 shows the long-term mean value (i.e., the climatology) of FI, TI, and ALT during 1954-2013. The spatial distribution of FI exhibits a large range of variations, with a maximum of 8000 °C-days in the north, and a minimum around 2000 °C-days in the south (Fig. 3.5). This spatial disparity, as much as 6000 °C-days, indicates the large latitudinal dependence of FI. Besides, there is also a large range of differences among these three catchments. In Aldan, the FI is characterized by the most substantial spatial contrast between the south and north. On the contrary, the FI in Selenga resembles uniformly low value over the entire basin.

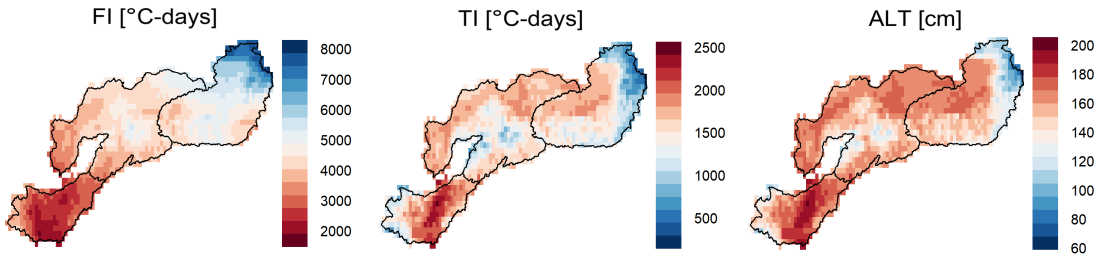

Figure 3.5: The spatial distribution of the long-term climatology of freezing index (FI), thawing index (TI), and active layer thickness (ALT) during the 60-year period from 1954 to 2013. The three indices are calculated by the Stefan method based on the gridded monthly air temperature data from the CRU dataset. In general, both FI and TI have a large range of spatial differences: for the warm, tropical region where has no monthly mean air temperature below 0 °C, FI may equal to 0 °C-days, but TI shows high values. On the contrary, for the high latitude and altitude region where have a longer period of the cold season, FI might be or even larger than 10000 °C-days while TI can be close to 0 °C-days (Frauenfeld et al., 2007).

In the case of TI, its climatology decreases from 2500 °C-days in the valley region of the Selenga River basin to less than 500 °C-days in the northern region of Aldan (Fig. 3.5). In comparison to FI, the TI also exhibits stronger spatial contrast within each basin. In Selenga, for instance, the TI ranges from 700 °C-days in the western mountainous region to almost 2500 °C-days in the middle valley region. This 1800 °C-days difference implies that the large altitude disparity has induced substantial heterogeneity of the thermal condition in the Selenga region.

Similar to the pattern in TI, the climatology of ALT varies from 200 cm in the middle region in Selenga to 60 cm in the northern area of the Aldan basin. From the basin-wide perspective, the long-term (1954-2013) averaged ALT is around 165 cm in Selenga, 158 cm in Lena, and 145 cm in Aldan. In Selenga, ALT declines from 200 cm in the valley region to 120 cm in the southwest mountainous region. In Aldan, the ALT climatology also shows more considerable spatial differences, ranging from 180 cm in the middle reaches to less than 100 cm in the northeast region. As to the Lena basin, ALT is around 160 cm to 180 cm, which is more evenly distributed over the entire basin except for the middle region with thinner ALT.

3.2.2.2 Spatial distribution of trends in FI, TI, and ALT

Fig. 3.6 illustrates the spatial distribution of trends and their PDFs for these three indices during 1954-2013, 1954-1983, and 1984-2013, respectively. During 1954-2013, FI shows significant, decreased trends over the entire southern Siberian region (Fig. 3.6a), with the most significant reduction being recorded in the northern Aldan region, where is also characterized by the highest long-term averaged FI. On the contrary, lower FI in the middle region of the Selenga basin exhibits the smallest decline compared to the other region. These spatial changes in FI indicate that the colder region (basin) has experienced the most substantially rising of temperature in cold seasons.

However, the spatial distribution of the 30-year-periodical trends (Figs. 3.6d-j) shows different pictures as compared to the 60-year period (Fig. 3.6a). During 1954-1983, although there are strong negative trends exhibited over the entire region, only small areas in Selenga and Lena have been characterized with statistically significant reductions (Figs. 3.6d,j). Whereas during the latter 30-years period from 1984 to 2013, most of the region experienced increased FI, despite an absence of statistical significance, and only the northern Aldan region has noticed significantly declined trends in FI (Figs. 3.6g,j). This phenomenon is coincident with the recent cooling winters discussed in Sec. 3.1.

Since the year-to-year ALT series is calculated from TI based on the linear relationship with the coefficient varies from basin to basin. Nevertheless, the long-term trends of ALT show similar patterns with the trends in TI (Figs. 3.6b,c). Thus, here we describe the trends of these two indices in the same context. First, there are extensively increased trends in the TI (ALT) over the entire region during 1954-2013, with the most significant upward trend being noticed in the middle reaches of the Selenga basin, where is also characterized by the largest TI (ALT). This spatial pattern reveals that the warmer region (basin) has experienced the most pronounced rising temperature in the warm season. However, this spatial pattern is not observed in the first 30-year periods during 1954-1983 (Figs. 3.6e,k). Only the middle valley region of Selenga exhibits the significantly increased TI (ALT), and most of Aldan and Lena are characterized by negligible

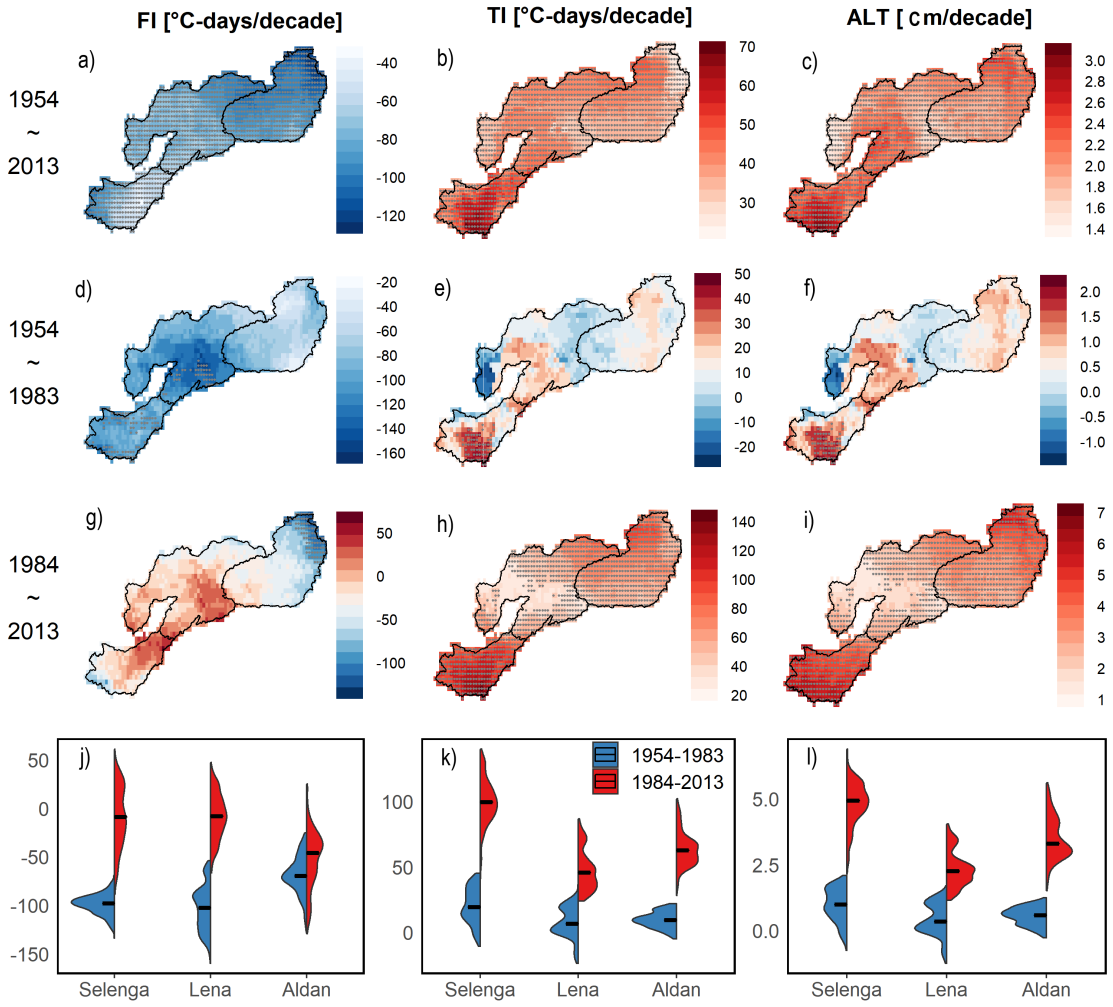

Figure 3.6: The spatial distribution of the long-term trends and the basin-wide distribution of the freezing index (FI, left panel), thawing index (TI, middle panel), and active layer thickness (ALT, right panel). The first row is the trends throughout the 1954-2013 period, the second and third rows are the 30-year period trends during 1954-1983 and 1984-2013, respectively, and their basin-wide distributions are illustrated in the bottom violins plot with the left and right side represents the two 30-years periodical trends before and after 1984. The dots in grey in the graphs a-i denote the trends with statistical significance ($p \leq 0.05$).

trends in TI (ALT). However, the TI (ALT) in the second 30-year period has experienced significant, increased trends (Figs. 3.6h,k). The most significant increase in TI (ALT) is recorded in the Selenga basin, with the observed trends being more than double of the trends during the first 30-year period. In addition, widespread positive trends are also observed in Aldan during 1984-2013, leading to a clear shift in the trend PDFs compared to that in the earlier 30-year period. These substantial differences between the two trends strongly suggest a dramatic shift in the thermal condition in southern Siberia from the middle 1980s onwards.

Inspired by different trends between the earlier 30 years (1954-1983) and the latter 30 years (1984-2013), in Figs. 3.7a-c, we show the difference of the values of each index in the earlier and later 30-year periods. This could allow us to investigate the potential

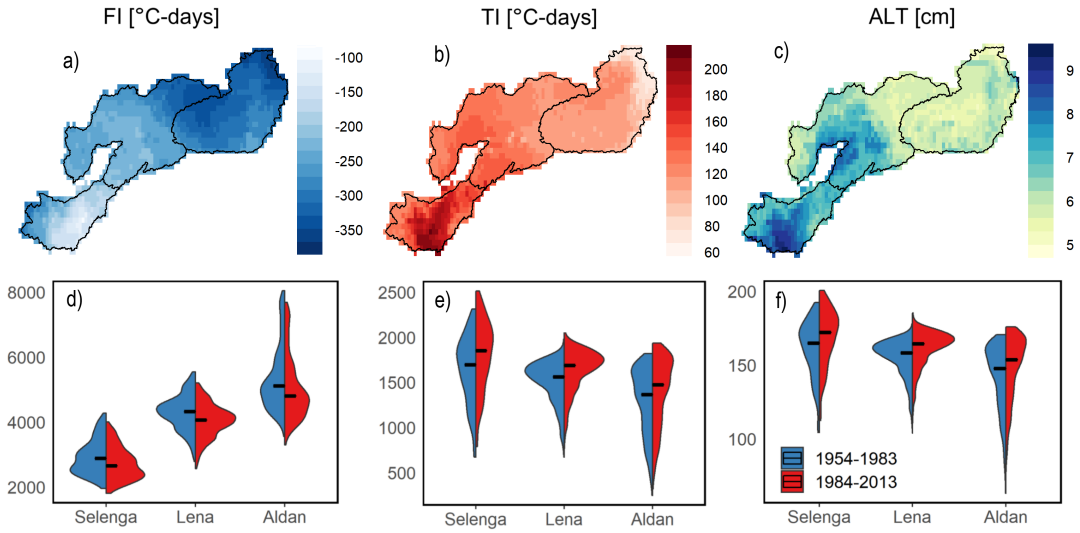

Figure 3.7: The periodical deviation of FI, TI, and ALT between two 30-year periods (i.e., the 1954-1983 and the 1984-2013), and the below row is the basin-wide distribution of the climatology during these two periods. The left (blue) and right (red) violins represent 1954-1983 and 1984-2013 periods, respectively.

shift of the 30-year state of FI, TI, and ALT (Figs. 3.7d-f). The FI shows an apparent deviation between these two periods (Figs. 3.7a,d). All these three catchments have seen lower FI during 1984-2013 as compared to the first 30-year period, with the most significant shift being recorded in the cold Aldan basin (around 350 °C-days differences), indicating a general warm winter during the recent 30-year period in this region. There are also substantial shifts in the states of TI for the entire study area (Figs. 3.7b,e). The most pronounced deviation is noticed in the valley region of the Selenga basin, implying a potential transformed thermal state in this region which is located in the southern boundary of the permafrost domain. Similar to the state differences in TI, the ALT also exhibits widespread changes between two 30 years periods (Figs. 3.7c,f), with the most substantial shifts (almost 10cm) existing in the middle valley region of the Selenga basin. Given that the TI and ALT are essential indicators of permafrost condition, these extensively increased trends in TI (ALT) might implicate an overall vertical degradation in southern Siberia.

3.3 Summary

On average, the mean annual average temperature (MAAT) in southern Siberia has increased by 2.7 °C during the period 1954-2013. The spatial distribution of annual precipitation shows that most parts of the Lena basin and few parts of Aldan exhibit an increasing trend. However, in basin-wide precipitation, we will show in Sec. 4.1 that only Lena has exhibited an increasing trend, and Aldan and Sselenga have no significant trend. The annual PET shows a widespread increase over the entire Selenga basin and a small part of the Lena basin. However, it shows a slight decrease in most of Aldan.

The FI, TI, and ALT have shown widespread variations from 1954 to 2013, however,

with different directions of change. Specifically, FI exhibits a decreased trend during 1954-2013, with most of the significant change registered in Aldan. In contrast, TI and ALT show increasing trends, with the most significant trend being registered in Selenga during the later 30-year period (1984-2013). During the later 30-year period, these significant trends have led to a substantial shift in the thermal state, implicating a potentially enhanced permafrost degradation in southern Siberia.

Chapter 4

Long-term hydro-climatic changes and relevant processes

According to Chap. 3, prevalent warming has been observed in three southern Siberian catchments (Selenga, Lena, and Aldan) during the period from 1954 to 2013. As a result, permafrost has also experienced explicit warming conditions, which is supported by the temperature-based index (TI/FI/ALT) shown in Fig. 3.6. Thus, in this chapter, we show how permafrost degradation may affect the hydrological processes under such warming conditions. To achieve this goal, we first examine the historical changes and associated processes in hydroclimatic variables over the three southern Siberian catchments. With the moving average method, we identify the manifestation of natural atmospheric oscillations on the hydrological dynamics. Then we introduce cross-correlation between runoff and precipitation to verify the potential role of permafrost degradation on runoff generation processes. After that, we apply these seasonal dynamics to describe and interpret the inter-annual variability in precipitation and runoff.

4.1 Trends and periodical oscillations

4.1.1 Hydro-climatic change at annual scale

The long-term inter-annual variability of hydro-climatic variables, namely air temperature, potential evapotranspiration (PET), precipitation, and river runoff, was investigated in Fig. 4.1 for the three basins (i.e., Selenga, Aldan, and Lena). Significant warming has been registered from 1954 to 2013, with the mean annual air temperature (MAAT) has increased by 1.9 °C/60 yrs ($p<0.001$), 2.3 °C/60 yrs ($p<0.001$) and 2.0 °C/60 yrs ($p<0.001$) in the Selenga, Aldan, and Lena, respectively. Such robust warming has led to a significantly increased PET in the Selenga and Lena basin (0.66 mm/yr, $p<0.001$ and 0.21 mm/yr, $p\leq0.05$), however, the PET in the Aldan basin shows a negligible trend (0.04 mm/yr, $p>0.05$). These divergent trends in PET reflect the different land-atmosphere interactions over the semi-arid, transition, and boreal ecosystems.

The precipitation in Lena resembles a significant increase during the period of record (1954-2013), while it shows no significant persistent long-term trends over Selenga and Aldan. Nevertheless, short-term oscillations are noted by the moving average analysis (dashed lines in Fig. 4.1) over all the three basins, resembling a seesaw pattern between the Selenga and Aldan (Lena): when the precipitation decreases in the Selenga basin, it rises in the Aldan and Lena basin and vice versa. These alternative oscillations between

dry and wet regimes in the precipitation correspond well with the atmospheric circulation between Northeast Asia and Siberia (Iwao & Takahashi, 2006), which can be related to the propagation of Rossby waves and associated development of atmospheric wave train structure over the Eurasian continent (Fujinami et al., 2016; Hiyama et al., 2016; Iwao & Takahashi, 2006).

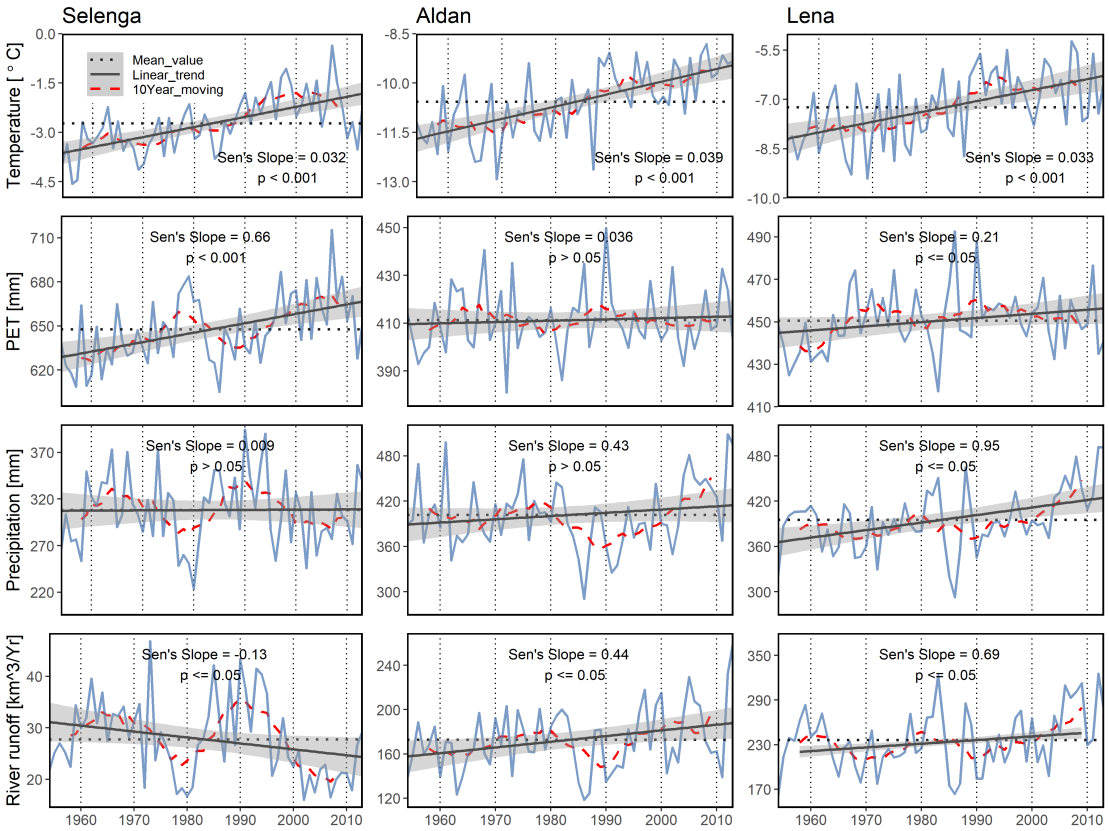

Figure 4.1: Time series for annual mean temperature (°C), annual PET (mm), annual precipitation (mm) and annual runoff (km^3/yr) from 1954 to 2013 (blue lines). Black solid lines show the linear trend, grey shading bands indicate the 95% confidence level interval for uncertainty, black dot lines represent long-term average and red dash lines show the 10 years moving average. The basin-wide monthly series of temperature and PET are extracted from CRU dataset, and precipitation is from GPCC dataset. The river runoff data is from GRDC dataset.

The aforementioned oscillation patterns in the annual precipitation result in a similar alternation of high (wet) and low (dry) flow periods with the abundance of the runoff in the Selenga and Aldan (Lena) basins, respectively (Fig. 4.1). Such a runoff-precipitation consistency is identified from the significant positive correlations between the annual precipitation and runoff Table. A.3 over both the Selenga (+0.76, p<0.001), Aldan (+0.68, p<0.001), and Lena basin (+0.80, p<0.001). As to the long-term variability, the annual runoff in Lena follows the significant increasing trend in the annual precipitation, resembling a similarly increased trend (0.69 km^3/yr, p≤0.05) during 1935-2000 (Ye et al., 2009). With regards to Selenga and Aldan, the annual runoff over both basins yields much more pronounced trends during 1954-2013 in comparison to the insignificant long-term trends in the precipitation over this period. The divergent trends in the runoff, i.e., declining in the Selenga (-0.13 km^3/yr, p≤0.05) but increasing in the Aldan (0.44 km^3/yr, p≤0.05), also agrees with previous findings obtained based on different

runoff datasets (Tananaev et al., 2016; Törnqvist et al., 2014), and strongly indicate the different role of the warming-related process on the hydrologic dynamics under different permafrost conditions.

4.1.2 Hydro-climatic change at seasonal scale

Fig. 4.2 shows the interannual variability in the air temperature (T), potential evapotranspiration (PET), precipitation (P), and river runoff (R) for each season over Selenga, Aldan, and Lena basins. Similar to the robust increase of MAAT over the three basins, rapid and significant warming trends are clearly evident over each season. Notably, a sharp rise in the summer air temperature is noted since the middle of the 1980s for each basin. Following this pronounced warming trend, there are significant increases in the seasonal PET from spring to autumn in the Selenga basin. Nonetheless, the seasonal PET shows the lower magnitude and minor changes in the Aldan and Lena basins, indicating relatively limited energy available in these two boreal catchments. For the precipitation, the insignificant trends in the annual time series shown in Fig. 4.1 are reflected by the non-apparent seasonal trends illustrated in Fig. 4.2. In addition, the pronounced seesaw-like precipitation oscillations between Selenga and Aldan (and

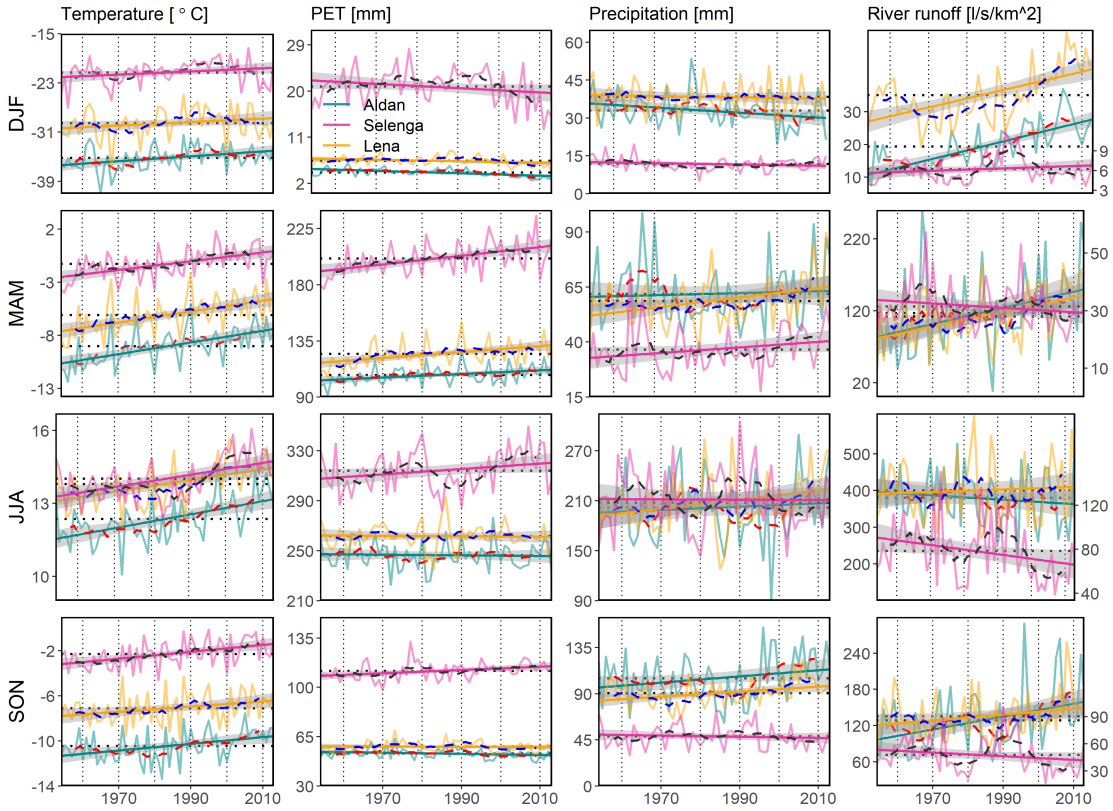

Figure 4.2: Time series of seasonal mean air temperature (°C), seasonal total precipitation (mm) and seasonal total runoff (l/s.km^2/yr) in the Aldan (turquoise colored lines), Selenga (red colored lines) and Lena (orange colored lines) basins between 1954 and 2013. The graph shows the linear trends (as black solid lines), the 95% confidence level intervals for predictions (in grey shading), the long-term averages (black dotted lines), and the 10 year moving averages (red dashed lines).

Lena) mainly appear in summer, which is primarily driven by the large-scale atmospheric oscillations, as we mentioned previously.

For seasonal runoff, the oscillation patterns of summer runoff in the Selenga, Aldan, and Lena basin shows the same short-term pace as the summer precipitation (Fig. 4.2). Consequently, clearly contrary oscillations have emerged in the summer runoff between these three basins: with wet-dry-wet-dry patterns in the Selenga but dry-wet-dry-wet states in the Aldan (and Lena). Interestingly, similar oscillation patterns have also been noticed in the runoff from autumn to spring, even though the precipitation among these seasons shows no apparent oscillation patterns. Such cross-season oscillations reflect how the characteristics of the summer precipitation are propagated to the runoff in the concurrent and subsequent seasons through the lagged runoff-precipitation response.

4.2 Runoff-precipitation response under permafrost degradations

In order to understand the potential change in the runoff-precipitation response under warming conditions, we used cross-correlation analysis to investigate the lagged relationship between seasonal precipitation and runoff (Fig. 4.3). In Figs. 4.3a-c, we present the 60-year period correlations, then illustrate the changes in the correlations between the earlier(Figs. 4.3d-f) and later 30 years (Figs. 4.3h-j). The comparison of the two 30-year periods allows us to detect changes in the runoff-precipitation response that were likely induced by enhanced permafrost degradation. In general, summer (JJA) precipitation shows strong, significant correlations with the runoff of the concurrent and subsequent seasons in both basins. This phenomenon reflects the strong lagged relationship between runoff and precipitation that is induced by the thawing of the active layer during the warm season (Frampton et al., 2011; Sjöberg et al., 2013; Ye et al., 2003).

When comparing the three basins, the magnitudes of the cross-correlation between the summer (JJA) precipitation and the runoff in a given season in the Selenga basin are always larger than the corresponding values in the Lena and Aldan basin. This suggests that summer precipitation plays a dominant role in the generation of runoff in the semi-arid Selenga basin. Furthermore, the seasonal runoff-precipitation correlations show a more prolonged time lag in Selenga as compared to Lena and Aldan. We attribute this to the different types of permafrost coverage (sporadic vs. discontinuous/continuous) present in the three basins. It may therefore be the case that regions with less permafrost extent and more developed subsurface connections have stronger and longer runoff-precipitation responses (Walvoord & Kurylyk, 2016).

A comparison of the earlier and later 30-year periods indicates that both basins have experienced warming-enhanced permafrost degradation since 1984. For instance, during the earlier 30-year period, the strong lagged correlation (with ρ>0.5) between the JJA precipitation and subsequent runoff continues into the winter in Selenga and into autumn in Aldan (Figs. 4.3d-f). However, during the latter 30 years, it has been extended by one season into spring and winter for Selenga and Aldan (Lena), respectively (Figs. 4.3h-j). Rising temperatures over the past 30 years have affected the underground hydrogeological structure by activating the development of previously impermeable flowpaths (Kurylyk et al., 2014). These newly formed flowpaths allow for greater infiltration

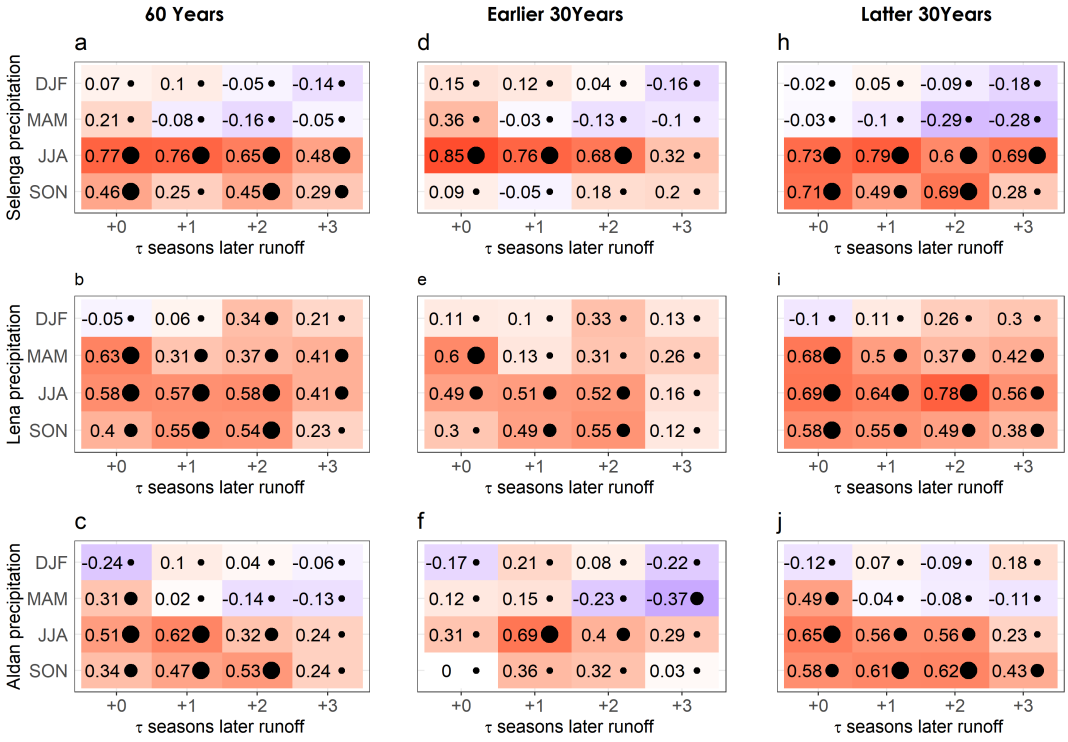

Figure 4.3: Cross-correlation matrices (Spearman's correlation coefficient) between precipitation and runoff during three periods: 1954-2013, 1954-1983, and 1984-2013. Relationships for the Selenga basin are shown in the top row; the middle and bottom rows show the conditions in the Lena and Aldan River basins. The lagged response between runoff and precipitation is expressed by the "τ seasons later" axes. The colors and numbers represent the magnitude of the correlation, whereas the size of the dots denotes the p-value significance of the correlation. Blue colors indicate negative correlations, red colors indicate positive correlations. Large dots show highly significant correlations (p <0.001), medium dots indicate significant correlations ($p \leq 0.05$), and small dots correspond with non-significant correlations (p >0.05).

and percolation into the subsurface soil layer and groundwater system during summer and autumn. The increased storage of water in the soil sustains surface runoff for a longer period of time, thereby extending the precipitation-to-runoff lag. This enhanced hydrological input is reflected in the shift in the runoff regime during 1984-2013 as compared to the 30-year period prior to 1984. In particular, the later period shows less intra-annual variability due to the increase in winter runoff and the decrease in summer runoff (e.g., runoff regime in Selenga and Aldan in Fig. A.4).

Another phenomenon is the advent of solid and significant correlations between autumn (SON) precipitation and the seasonal runoff in the second 30-year period (Fig. 4.3h-j). One may assume that it is the result of enhanced runoff response to autumn precipitation. However, we argue that these enhanced cross-correlations might also be a consequence of the strong similarities between the precipitation in summer and autumn from 1984 to 2013. Furthermore, the small, unexpected correlations between summer precipitation and summer runoff in the Aldan basin during the earlier 30 years (Fig. 4.3f) are mainly the result of divergent change patterns between spring and summer precipitation (Fig. 4.2). These phenomena indicate that, when performing cross-correlation analysis, the change patterns of the time series must be taken into account to exclude

random results.

4.3 Inter-annual variability in precipitation and runoff

At a decadal scale, precipitation and river discharge fluctuate between the dry (below-normal) and wet (above-normal) state that is mainly driven by the large-scale atmospheric circulations over southern Siberia (Iwao & Takahashi, 2006). These decadal-scale hydrological behaviors, together with extreme anomalies such as heavy rainfall (and corresponding floods) and droughts, might induce abrupt change (or step change) to the hydro-climatic time series. The occurrence of these abrupt variabilities could suppress or strengthen the long-term behavior of the hydroclimatic variables, which may also bring difficulties to the detection and attribution of long-term trends in these variables. Here, we focus on the time series of anomalies in precipitation and runoff at both annual and seasonal scales to evaluate the occurrence, magnitude, and duration of the abrupt changes in water availability in the three southern Siberian catchments (Figs. 4.4-4.6). The anomalies are divided into four categories based on three thresholds that we introduced in Sec. 2.3.2. Especially, the anomalies above 80% percentile of the average are called extremely high condition (blue), whereas the anomalies below the 20% percentile of the average are called extremely low condition (red).

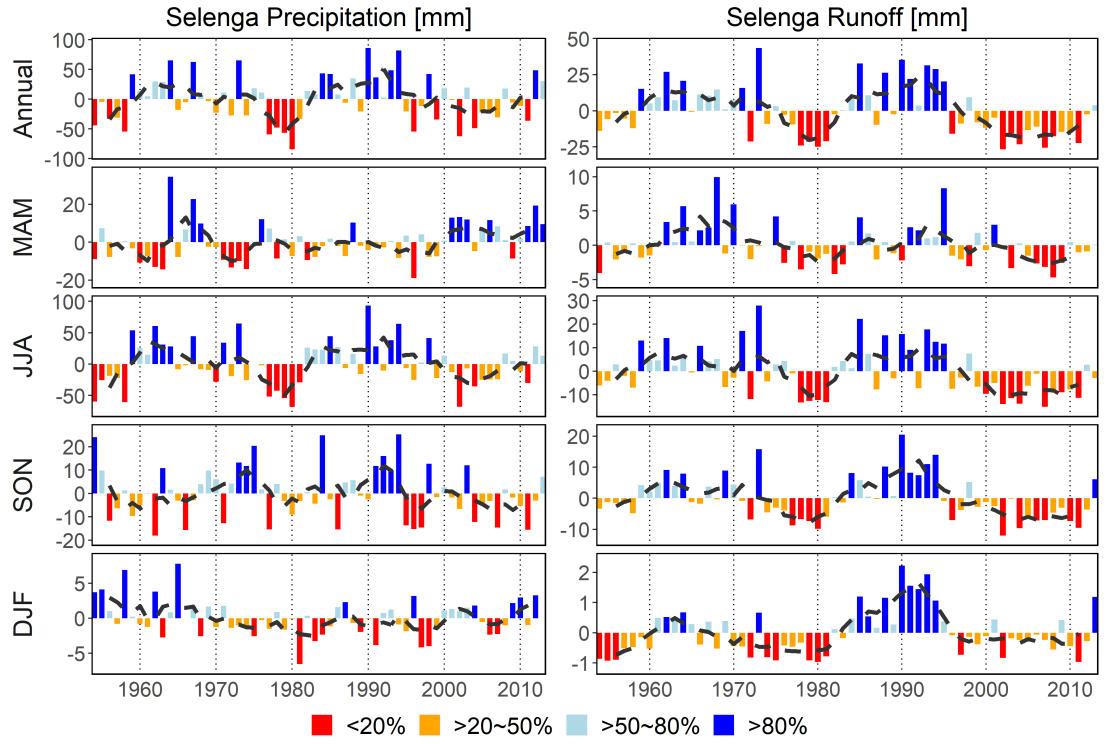

Figure 4.4: The standardized deviation for the hydrological variable at annual and seasonal scale in the Selenga River basin during 1954-2013. The blue (and orange) color indicates value above the long-term average, and red color denotes amount below long-term average. The four categories are based on the the percentiles ranking analysis introduced in Sec. 2.3.2.

In Selenga, extremely high annual precipitation (exceeding 80% percentile) occurs primarily during two wet periods over 1959-1967 and 1984-1994 (Fig. 4.4). As precipitation generates direct input to the hydrological system, these extremely high precipitation anomalies are also manifested in river runoff. However, differences in terms of the occurrence and intensity also exist between runoff and precipitation at annual and seasonal scales. Firstly, anomalies in annual runoff exhibit stronger intensity than that in annual precipitation. Examples are the years of 1962 and 1971: though annual runoff experiences extreme high conditions (above 80% percentile) during these two years, annual precipitation only exhibits moderate above-normal wet condition (ranges from 50%-80% percentile). This might result from different seasonal patterns in precipitation. Specifically, precipitation in summer and autumn shows opposite change patterns during these two years that might cancel each other when they aggregate together to the annual value. In contrast, runoff in autumn and winter may mirror the precipitation pattern in the prior season(s) due to lagged runoff-precipitation response modulated by the subsurface system. The increased lagged summer precipitation could compensate for the deficit in autumn precipitation. As thus, the accumulated annual runoff may also follow the dominant pattern in summer precipitation. In addition to these differences in magnitude, there are also different behaviors with regard to the occurrence of extreme anomalies. For instance, the year 1995 has seen severe wet conditions (exceeding 80% percentile) in runoff over both annual and seasonal scales (spring and summer) despite that precipitation has experienced below-normal conditions throughout the year. Reasons for this could be that runoff in 1995 has lagged the higher-than-normal precipitation in the preceding year (1994) despite the slightly decreased precipitation in 1995. This reflects a long-lasting runoff-precipitation response cycle in this permafrost-affected region.

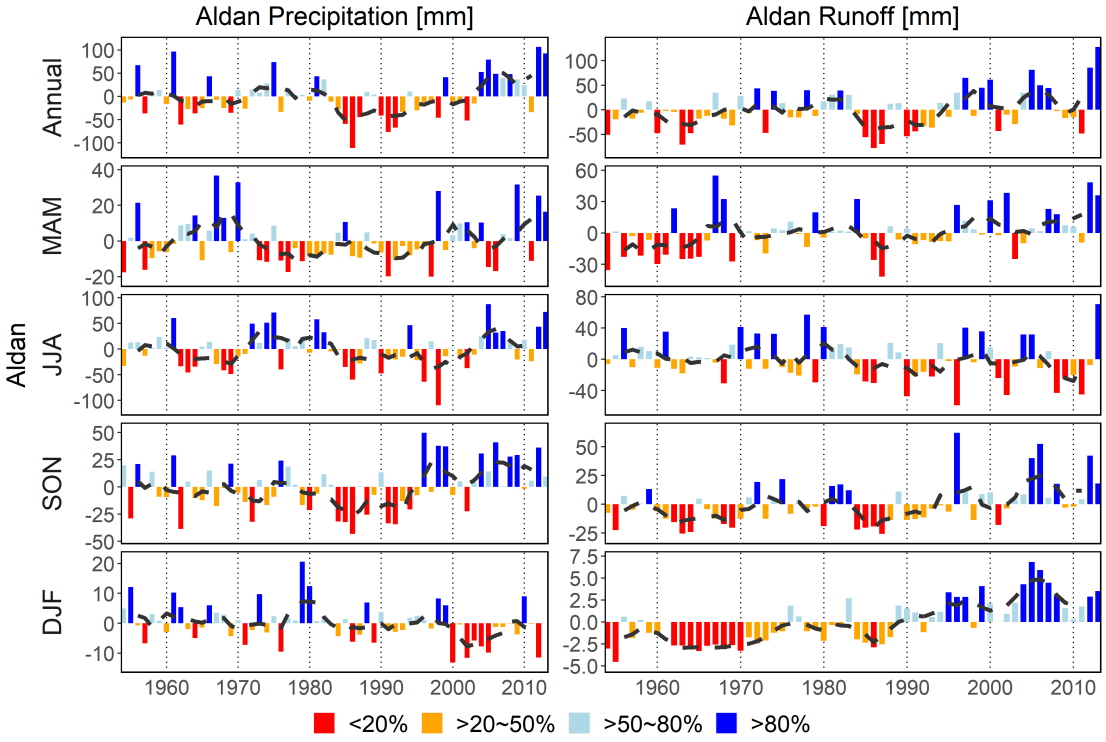

Figure 4.5: Same to Fig. 4.4, but for the Aldan River basin.

Below-normal precipitation and runoff in the Selenga basin are prevalent over three periods during the time scale of record: 1954-1958, 1970-1981, and 1996-2011. However, the correspondence patterns are different during these three periods. Runoff anomalies fluctuate consistently with the precipitation deficits during the first two dry periods, whereas it stays much longer in below-normal conditions during the last dry period as compared to anomalies in precipitation. Especially, although precipitation in 2000, 2003, and 2008 has positive annual and seasonal anomalies, runoff still shows below-normal conditions during these three years over both scales. This out-of-pace pattern between precipitation and runoff indicates that the hydrological system in Selenga experiences a step-change in the context of runoff-precipitation response during the second dry period.

In the Aldan basin, though the precipitation and runoff experience alternatively wet and dry states during 1954-2013, extreme anomalies and step-change are also resembling during the period of record (Fig. 4.5). Since 1984, precipitation experiences a shift in variance that is accompanied by significantly lower and higher anomalies than the period before 1984. The most remarkable shift is registered in autumn. Specially, there are more than half of the years (7/11) have experienced low precipitation during the first dry period from 1984 to 1994. After that, a step change is noticed since 1996, with almost 75% of the precipitation being higher than the long-term average, and over half of which exceed the 80th percentile of precipitation. This strong shift in the past envelope of autumn precipitation also resembles over other seasonal and annual scales but with lower amplitudes.

In response to the shifted variances in precipitation from 1984 to 2013, runoff also experiences extreme anomalies during this period, but with different amplitudes and

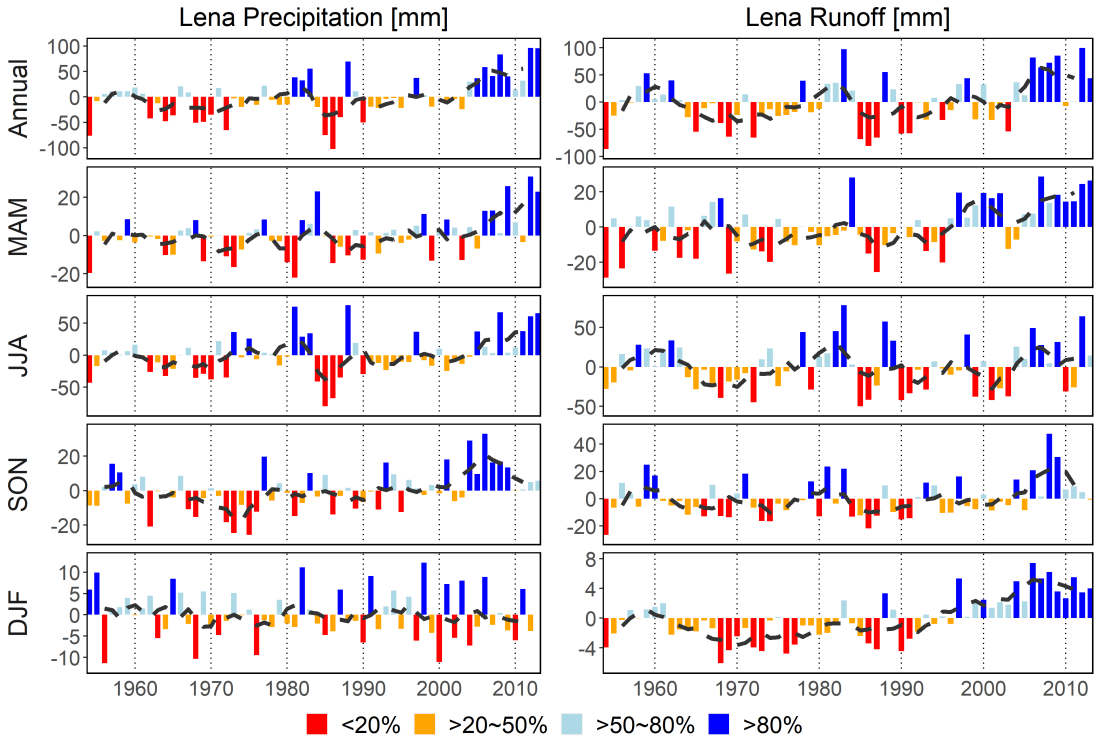

Figure 4.6: Same to Fig. 4.4, but for the Lena River basin.

seasonal patterns. For instance, there are two clear wetting periods resemble in summer precipitation, i.e., 1972-1983 and 2004-2013. However, summer runoff during the second period exhibits distinct patterns of variability as compared to summer precipitation. Specifically, although summer precipitation during 2001-2003 and 2008-2011 only resembles slight declines, the summer runoff shows a substantial reduction during these years. This leads to larger differences between summer runoff and precipitation during the last decade. This increased difference between runoff and precipitation might be attributable to the intensified summer evapotranspiration and enhanced subsurface infiltration due to the warming-induced deeper thawing of permafrost. Furthermore, the substantial reduction in summer runoff in the context of increased summer precipitation is accompanied by considerable positive anomalies in winter runoff. This coincident pattern between decreased summer runoff and increased winter runoff reflects the modulation of subsurface processes on runoff generation, hinting a potential role of warming permafrost on hydrologic processes in the permafrost-affected region.

As to the Lena basin, following the periodical fluctuations between wet and dry (Fig. 4.6), the recent decade has experienced a considerably higher than normal water condition. More than half of the significantly higher than normal conditions (over 80% percentile) between 1954 and 2013 occurs during this decade. On a seasonal scale, most seasons have also experienced widespread above-normal precipitation anomalies during the last decade. Winter is only season exhibits strongly year-to-year fluctuation between the extremely wet and dry condition in precipitation. Runoff shows more considerable fluctuation as compared to the precipitation over both annual and seasonal scales. Like the Aldan basin, though summer precipitation shows widespread wet conditions, summer runoff has experienced dry anomalies during the last decade. Meanwhile, winter runoff has seen continuous higher than normal conditions despite the changeable winter precipitation. The similar seasonal behavior in runoff and precipitation between Aldan and Lena in the last decade suggests the potentially changed runoff-precipitation response due to the warming-induced permafrost thawing during this period.

4.4 Discussion

Quantitative understanding of the historical change and its drivers at multiple scales is essential for predicting future changes in regional water availability. Based on the moving window average visualization, our study has identified two dry and two wet regimes during the 60-year period in both the southern region (Selenga) and the northern region (Aldan and Lena). While the wet and dry regimes appear alternatively in both south (Selenga) and north (Aldan and Lena), the wet-dry-wet-dry oscillation pattern in the south (Selenga) is clearly in contrast to the dry-wet-dry-wet pattern experienced in the north (Aldan and Lena), resembling the spatial seesaw mechanism of the temporal atmospheric circulations between the Northeast Asia and the Siberia (Iwao & Takahashi, 2006). This means that, despite the substantial drying and wetting states observed during 1999-2013 in the Selenga and Aldan (Lena) basins, respectively, in the 15 years after 2013, the seesaw circulations may shift the Selenga (or Aldan/Lena) basin from the drying (or wetting) regime to an alternatively wetting (or drying) regime. However, in addition to these short-term oscillations, the river runoff also bears long-term decreasing (drying) and increasing (wetting) trends in the Selenga (Aldan/Lena) basin. As a consequence, the long-term drying (wetting) trend in Selenga (Aldan/Lena) may suppress

the coming up short-term wetting (drying) conditions in Selenga (Aldan/Lena) for the period after 2013.

The direct evidence of permafrost evolution and its effect on regional hydrological processes can be obtained from field observations (V. E. Romanovsky et al., 2010; Walvoord & Kurylyk, 2016). However, they are usually based on small spatial scales and short temporal coverage (Brutsaert & Hiyama, 2012). From a long-term perspective, many groups have applied the historical base flow (river runoff sustained by groundwater system) records to investigate the permafrost evolution based on the basin-scale permafrost-hydrology dynamics (Brutsaert & Hiyama, 2012; S. Lyon et al., 2009). However, the base flow is based on daily streamflow and suffers from large uncertainties in southern Siberia (Shiklomanov et al., 2006). Thus, other approaches based on the long-term runoff records are demanding. The cross-correlation used in this study, i.e., the seasonal runoff-precipitation correlation, provides evidence of the basin-scale permafrost evolution in response to a changing climate.

Generalizing the findings obtained from small-scale *in situ* observation to large basin scales can improve our physical understanding of the integrated hydrologic systems (McDonnell et al., 2007). Our investigations of basin-scale drying and wetting dynamics are consistent with previous field observations over both basins. In the Selenga basin, evidence of permafrost degradation has been provided by field observations (Ishikawa et al., 2005; Kopp et al., 2014): though the permafrost below the north-faced forest slopes is characterized by a vertical degradation with wet active layer, the permafrost below the flat pasture plain suffers from complete thawing that may lead to lateral degradation with dry soil layer. Our results indicate that this field-scale phenomenon of lateral degradation with a decreased permafrost extent may widely happen over the entire Selenga basin under rapid summer warming. Indeed, this is true because the 0 °C isotherm of MAAT in the Selenga basin has moved northward during the latter 30 years from 1984 to 2013 in comparison to the first 30-years period Fig. 3.4. As a result, it stimulates the northward migration of the southern boundaries of permafrost in this region (Davaa & Jambaljav, 2014). Furthermore, the strong vertical permafrost degradation and associated wetting mechanism assumed from our basin-scale analysis in Aldan and Lena can be proved by previous field observations (Iijima et al., 2014) at a station approximately 190 km to the northwest of the basin. These consistent drying or wetting condition between those *in situ* observations and our basin-scale investigations suggest that significant climate warming has already led to widespread permafrost degradation throughout the southern Siberian region.

Previous studies on detecting hydro-climatic changes in the Siberian region suggest potential uncertainties exist in the dataset. For example, the accuracy of precipitation data is affected by poor distribution of gauges in Siberia with a remote and harsh environment (Bring et al., 2016; Groisman & Gutman, 2012; McClelland et al., 2004). Similarly, there is also uncertainty in the river discharge measurements during winter months when the gauging technique (stage-discharge relationship) is affected by the presence of river ice (Shiklomanov et al., 2006). However, these uncertainties will not affect the coherent cross-correlations (i.e., strongly lagged correlations between summer precipitation and winter runoff). Thus, it will not modify our conclusions on the enhanced seasonal runoff-precipitation relationship induced by permafrost degradation under a warming climate. Furthermore, in the Selenga basin, the fast population growth (Malsy et al., 2017) and ongoing economic development (e.g. rapid growth of mining activities,

urbanization, and agriculture) may also increase the water consumption that eventually reduces the water storage and supply (Priess et al., 2011; Wang et al., 2019). This also makes it difficult to distinguish the summer runoff reduction induced by enhanced infiltration under permafrost degradation from that caused by the human activities in this basin. Nevertheless, human consumption normally has an immediate consequence on the magnitude of water availability. However, permafrost degradation usually exerts lagged effect on the seasonal runoff distribution. Thus, this cross-season effect can be detected from the cross-correlation analysis used in this study, with the increased winter runoff being evidence as well (Fig. 4).

The existence of extreme anomalies (a higher or lower value than normal conditions) may bring difficulties in detecting and attributing the change patterns in hydro-climatic variables at long-term and decadal scales. For instance, Selenga has experienced severe drying conditions during 1970-1981 and 1996-2012 (Fig. 4.4); however, there are also extremely higher than normal values existing during these two dry periods (i.e., 1973 and 1998). The reason for these two extremes might be due to the strong El niño events in these two years that can substantially affect the local precipitation and river runoff (Lin & Qian, 2019). The existence of these abnormalities might disturb the decadal dry state and associated long-term patterns in precipitation and runoff. In addition, misunderstanding may also exist in accumulating seasonal value to annual value. Examples are the year of 1996 and 1998 in the Aldan river basin (Fig. 4.5). These two years have seen the recorded high precipitation during autumn, while the annual total precipitation even experiences negative anomalies during these two years. This could be attributable to the cancellation between summer and autumn precipitation, which oscillates in opposite directions during these two years. This suggests that one should always consider the potential uncertainties due to the seasonal cancellation when detecting the change pattern in annual value.

4.5 Summary

Our study has examined the historical (1954-2013) change patterns of water availability, and the corresponding driven mechanism at multiple-temporal scales over three southern Siberian basins with diverse landscape characteristics: the semi-arid Selenga, characterized with the mixed permafrost from sporadic to isolated permafrost; the boreal Aldan, underlain by continuous permafrost; and the Lena represents a transition area between the other two basins that is characterized with discontinuous permafrost. These three river basins respond differently to the changing climate: during the 60-years period from 1954 to 2013, the river runoff bears a significantly decreased trend (-7.8 km^3/60yrs, $p \leq 0.05$) in the Selenga, but a robustly increased trend (26.4 km^3/60yrs, $p \leq 0.05$) in the Aldan basin (41.4 km^3/60yrs, $p \leq 0.05$ in Lena basin). These considerable changes cannot be directly explained by changes in precipitation over each basin. Many other factors, such as actual evapotranspiration and human intervention, can also contribute to these divergent changes. However, the different permafrost degradation scenarios over the two basins may be the primary driver. The enhanced lagged runoff-precipitation, showed by our seasonal runoff-precipitation cross-correlation analyses, indicates the intense permafrost degradation over all three basins. However, the sporadic and isolated permafrost in the Selenga basin mainly experiences lateral degradation that stimulates direct vertical loss of the surface water. Different from the case in the Selenga, the

continuous permafrost in the Aldan and discontinuous permafrost in the Lena still have a low-permeable frozen layer during the warm season. Thus, in these two basins, warming primarily induces vertical permafrost degradation, i.e., a deepening active layer that sustains more water to the surface hydrological processes (i.e. runoff and ET).

Chapter 5

Drying and wetting under enhanced warming

Based on the findings in Chap. 4, the hydrological processes in southern Siberia are significantly governed by the natural variability of atmospheric circulation. As a result, the runoff in the Selenga catchment has experienced a wet-dry-wet-dry oscillation during 1954-2013, whereas the runoff in the Aldan and Lena catchments has noticed a dry-wet-dry-wet pattern (Fig. 5.1). In this chapter, we focus on the intra-annual hydro-climatic regime of the later 30 years (1984-2013), to understand how the runoff-generating processes may differ between the wet and dry periods. This period is of great importance because the warm season temperature experienced an abrupt rise (Fig. 4.2), implicating an intensified warming condition and probably enhanced permafrost degradation.

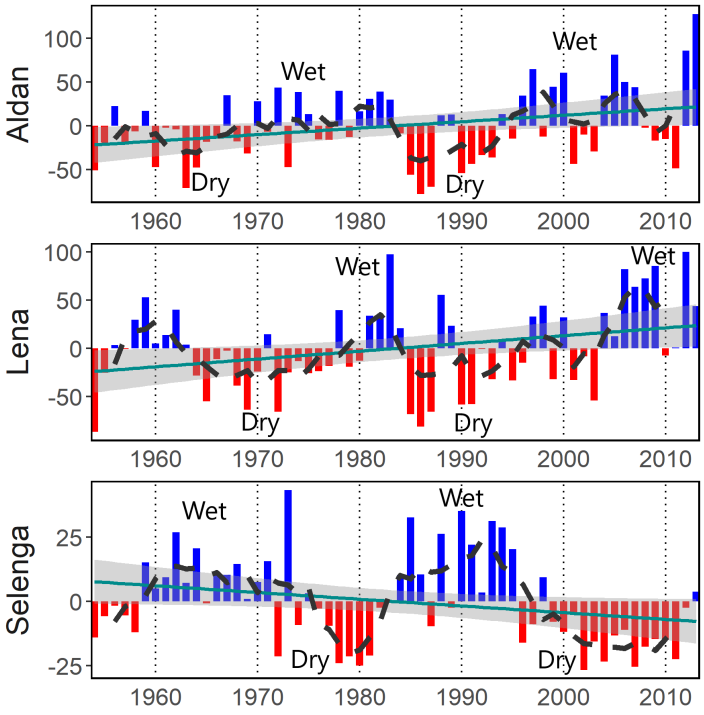

Figure 5.1: Runoff anomaly (mm) during 1954-2013 shows the periodical oscillations between dry and wet states over the three catchments. Runoff data is taken from GRDC dataset.

Since the terrestrial water storage (TWS) data is also available in this period, it is used to reflect the spatial characteristics and variations of the water availability in this

region and to unravel the spatial relevance of subsurface water conditions on the runoff generating process. Furthermore, we investigate the regime shifts of water distribution on the basis of the conceptual steady-state Budyko framework. This enables us to detect the potential consequence of the changed land-atmosphere interactions on regional water availability. Finally, the historical evolution in the aridity index at a regional scale is examined. It provides insights into the spatial disparity and historical evolution of terrestrial water availability in response to climate change and permafrost degradation in southern Siberia.

5.1 Shifted hydro-climatic regime

In order to provide quantitative implications for the potential changes in hydro-climatic connections, the intra-annual regimes of the precipitation (P), river runoff (R), and evapotranspiration (ET), within the periods of 1984-1998 and 1999-2013 were investigated (Fig. 5.2).

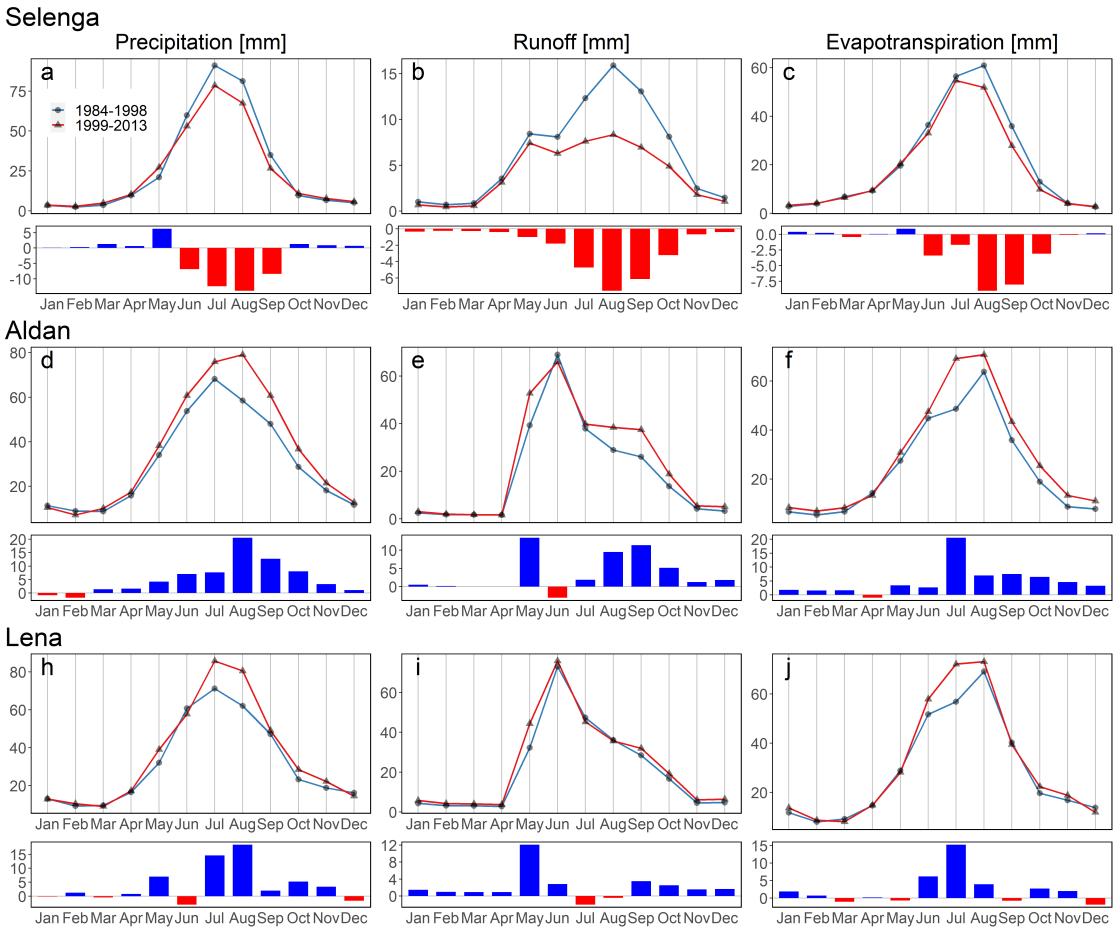

Figure 5.2: Periodical regime and deviation of precipitation, river runoff and evapotranspiration during two 15-year periods: 1984-1998, 1999-2013. The precipitation is based on GPCC dataset, river runoff data is taken from GRDC dataset, and the evapotranspiration is from TRAIN simulation.

In the Selenga catchment, compared to the slightly changed regime in the precipitation (Fig. 5.2a) and ET (Fig. 5.2c), the river runoff resembles two distinct regimes before and after 1999 (Fig. 5.2b). The runoff of the first 15-year period is characterized by a summer-rain-dominated regime with a significant difference between the spring and summer runoff peaks, whereas this peak-difference becomes very negligible during the second 15-year period, leading to a flat intra-annual distributed runoff regime. As to the absolute change, the monthly precipitation during June to September show a remarkable drop in 1999-2013 compared to that in the first 15-year period (Fig. 5.2a), which is primarily a result of the large scale atmospheric circulation (Iwao & Takahashi, 2006) noted in Chap. 4. Following this substantial reduction in the warm-season precipitation after 1999, both the river runoff and ET resemble pronounced drop during the second 15-year period (Figs. 5.2b,c). Such a drop in all the three hydro-climatic variables indicates the governing role of the summer precipitation on the surface hydrological processes in the water-limited semi-arid Selenga catchment.

However, the Selenga runoff and ET, in August and September, drop much more (Figs. 5.2b,c) than the precipitation in the concurrent months (Fig. 5.2a). This suggests that the reduced surface water availability is also likely to be affected by the warming-induced permafrost degradation. In general, the active layer can sustain a wet surface condition due to the presence of permafrost (Iijima et al., 2014). As the temperature increase, the Selenga catchment, characterized by discontinuous, sporadic, and isolated permafrost, is tended to experience a lateral degradation such as formation of the open (or lateral) taliks and whole-scale permafrost loss (Fig. 3.4) (Davaa & Jambaljav, 2014; Ishikawa et al., 2005). Under these warming-induced subsurface changes, the soil layer is expected to become drier due to the enhanced infiltration and percolation. This has led to less water available for the surface hydrologic processes (i.e., ET and runoff) in the later summer and earlier autumn, resulting in a potentially drier hydrologic system.

In the Aldan catchment, however, widespread positive shifts are observed during 1999-2013 for all the three variables (Figs. 5.2d-f), indicating a pronounced wetting hydro-climatic state over this period. This wet state is also a consequence of the large-scale atmospheric oscillation, but represents a seesaw pattern (Iwao & Takahashi, 2006) with respect to the dry state in the Selenga catchment. The considerable rise in the summer precipitation during the latter 15 years is accompanied by a shift of the precipitation peak from July to August. Following this shifted precipitation regime, the runoff has also experienced a clear rise in August and September, resulting in a significant regime shift from a snow-fed to a snow-rainfall-fed runoff regime with a plateau through July to September. This apparent plateau in river runoff, in distinct difference with respect to the sharp precipitation changes, reveals the enhanced lagged runoff response to precipitation induced by permafrost degradation that we already discussed in Sec. 4.2.

Furthermore, the Aldan runoff in May shows a much stronger upward shift than that in the precipitation, but the runoff peak in June suffers from a substantial loss despite the increased precipitation during this month. Since runoff in June is mainly fed by snowmelt, it indicates warming-enhanced earlier snowmelt in the latter 15 years: most of the accumulated snow has melted to contribute to the runoff in May. In addition, the ET in June and July exhibit a much more significant increase (Fig. 5.2f) in comparison to the precipitation and runoff (Figs. 5.2d,e). This can be primarily attributed to the thickening and moistening active layer induced by vertical permafrost degradation under rapid warming (Ford & Frauenfeld, 2016; Iijima et al., 2014): the deepening of the

active layer is able to maintain more liquid water since the remaining permafrost can still prevent water from draining away. Consequently, this thicker active layer with saturated moisture can result in an enhanced ET fraction during the warm season in a warmer climate, reducing the surface runoff fraction in the corresponding months (e.g., June and July).

Similar to the Aldan catchment, there is a positive shift in the hydroclimatic regime in the Lena catchment, especially in May when the spring melting process is prevailing (Figs. 5.2h-j). The increased precipitation in the Lena catchment is mainly observed in the summer month: July and August, which results in an increased ET during these two months but with different intensities of change. In addition to these increases, the Lena catchment has also experienced significantly decreased runoff in the warm season months due to the enhanced evapotranspiration. Nevertheless, the significant rise in precipitation in August is accompanied by decreased runoff and slightly increased ET, which indicates an enhanced infiltration process in the melting season in the Lena catchment with discontinuous permafrost.

5.2 Spatial-temporal patterns and variabilities in water availability

5.2.1 Precipitation and TWS

Fig. 5.3 displays the regional occurrence of the spatial patterns and temporal variations in precipitation (P) and terrestrial water storage (TWS) based on the gridded GPCC data and GRACE-REC data, respectively. Normally, the general pattern of hydro-climatic variables can be reflected by the multi-annual average. However, the GRACE-REC data only provides anomalies of TWS other than the absolute value. It means that these yearly anomalies may cancel each other when they were aggregated into long-term average, and the final accumulation might be relatively close to 0 as we have shown in Fig. A.5 in the appendix. This indicates that the multi-annual average might not be an informative description for the general condition in TWS anomalies. As thus, here we apply the empirical orthogonal functions (EOF analysis, see the detail of this method in Sec. 2.3.2) to each grid cell of P and TWS anomalies. The upper panel in Fig. 5.3 shows the first mode (EOF1), accounting for 32% and 51% of the total variance, which delineates the dominated spatial patterns in P and TWS, respectively. Despite the difference in the percentage of the representation, both of the spatial structures of P and TWS resemble similar wet (positive) and dry (negative) contrast between the northern and southern catchments. This similarity indicates the governing role of precipitation on the drying and wetting distribution in TWS during the 30-year period from 1984 to 2013.

The lower panel in Fig. 5.3 resembles the spatial distribution of the linear trends in P and TWS anomalies during 1984-2013. The trends in P vary regionally, ranging from -6 mm/yr to 10 mm/yr. The grid cells with decreased trends are mainly noticed in the southern Selenga catchment, while the substantial increase is observed primarily in the Lena and Aldan catchments. Similar spatial patterns of trends exist in the TWS anomalies. This suggests that the variations in P have been imprinted on the evolution

of the terrestrial water storage at a specific region.

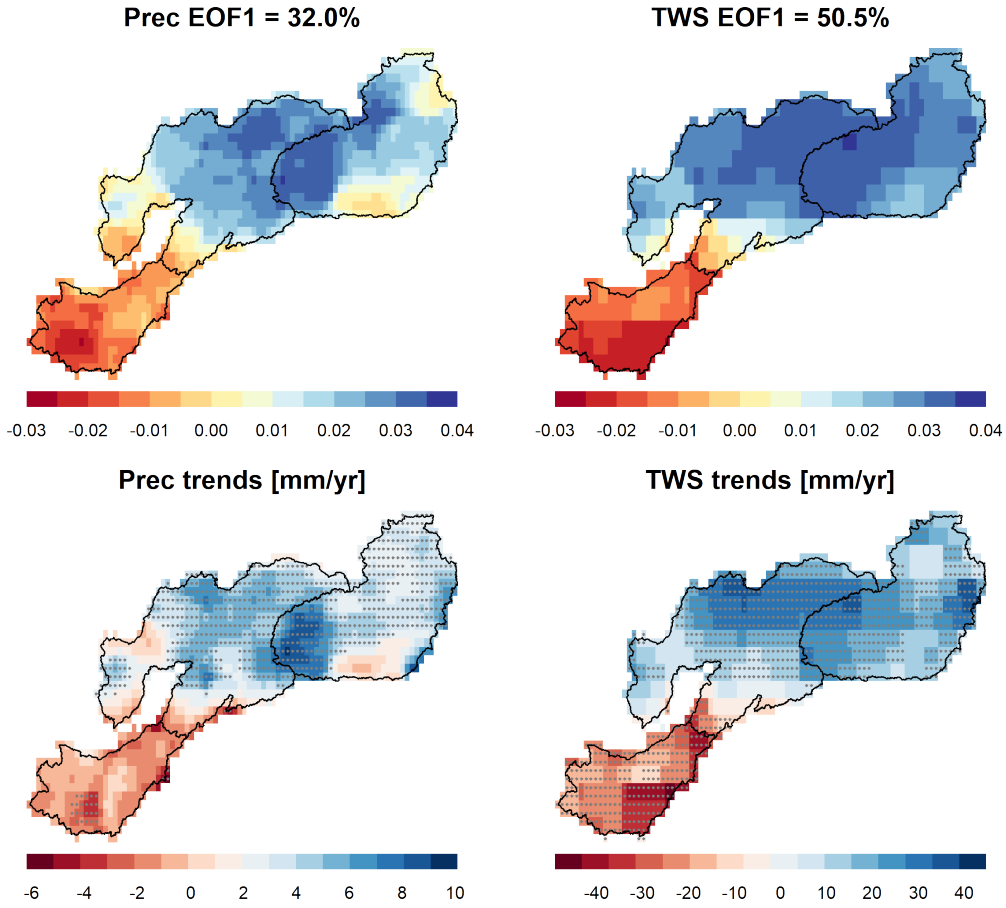

Figure 5.3: Spatial-temporal characteristics in precipitation (P) and terrestrial water storage (TWS) during 1984-2013. The upper panel presents the spatial patterns of the first modes (EOF1) of P and TWS, and the percentage denotes the explanation for the variance of EOF1. The below panel displays the trends of P and TWS for each grid cell in the study area; the dots in grey denote the trends with statistical significance ($p \leq 0.05$). Precipitation is from GPCC dataset and the TWS data is extracted from GRACE-REC dataset (Humphrey & Gudmundsson, 2019).

Both the EOF patterns and the temporal trends provide insight into the spatial characteristics and temporal dynamics of water availability in southern Siberia. Most part of the Lena and Aldan catchments, characterized by relatively wet conditions, has experienced an overall increase in both precipitation and TWS, resulting in a wetter state in water availability. On the contrary, the semi-arid Selenga in the south undergoes a widespread reduction in P and TWS, leading to a much drier condition in water availability. These contrast behaviors in water availability suggest a pattern that "wet gets wetter while dry gets drier". This phenomenon is also identified in other regions around the globe such as China (Ding et al., 2008), Europe (Stahl et al., 2010), and Australia (A. Chen et al., 2021), despite that there still lacks an overall picture throughout the global continent (Greve et al., 2014).

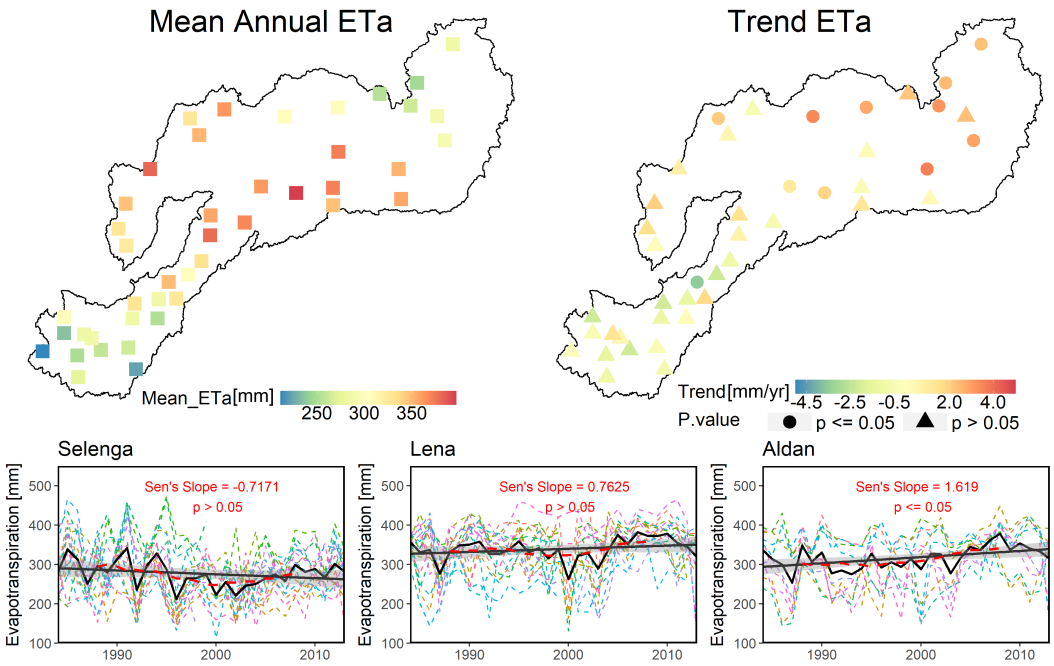

Figure 5.4: Spatial distribution and time series of mean annual and trends for the TRAIN simulated ET in the Selenga, Lena, and Aldan catchments from 1984 to 2013.

5.2.2 Evapotranspiration based on TRAIN model

As evapotranspiration (ET) is an essential component in both the water cycle and energy cycle of the hydro-climate system, its variations can reflect the states of the terrestrial water availability. Here we further present the spatial distribution and temporal variations in evapotranspiration (ET) based on TRAIN simulation (Fig. 5.4). The graph on the upper left shows the average ET condition. The stations with higher ET are mostly noticed in the Lena catchment, whereas the stations with lower ET mostly exist in the Selenga and Aldan catchments. Though the air temperature and PET in Selenga are relatively higher than the other two catchments, ET shows a relatively lower value. The lack of high ET in Selenga could be attributable to the lower precipitation in this region (Fig. 5.3, up left). In contrast, the relatively low ET in Aldan is mainly a result of the limited energy availability (i.e., the cold temperature and low PET) for evaporating water in terrestrial (Fig. 4.1). This highlights the different driven mechanisms of regional ET dynamics with regard to the competition between moisture control and energy control in southern Siberia.

As to the trends in ET during 1984-2013, despite the pronounced warming and increased PET in Selenga (Fig. 4.1), most of the stations have experienced decreased ET during the period, which results in a decreased ET (-0.72 mm/yr, $p>0.05$) for the entire catchment. This reduction in the annual ET might result from the decreased precipitation (-1.42 mm/yr, $p\leq0.05$) during this period, indicating limited water availability for the surface latent heat flux in this dry semi-arid region. In Aldan, half of the stations exhibit significantly increased ET from 1984 through 2013, leading to a catchment-scale increased ET (1.62 mm/yr, $p\leq0.05$). There is also an increased ET trend in the Lena

catchment (0.76 mm/yr, p≤0.05), with most of the stations resembling an upward tendency. However, this increased ET trend is relatively smaller than that in the Aldan catchment, despite that the precipitation shows a similar increased tendency over both catchments (i.e., 3.9 mm/yr, p<0.001 in Lena and 4.1 mm/yr, p<0.001 in Aldan, respectively). Considering that the PET over both catchments only shows a slight change from 1984 to 2013 (Fig. 4.1, second row), the different behaviors of the ET trends over these two catchments is primarily controlled by the change patterns in the air temperature (i.e., 0.51 °C/30 yrs, p>0.05 in Lena and 0.84 °C/30 yrs, p>0.05 in Aldan, respectively), indicating the strong sensitivity of the ET dynamics to the thermal condition in the boreal climate system.

5.3 Control on runoff generation: precipitation and TWS

The presence of permafrost is expected to prevent the precipitated water from downward infiltration. If the entire land surface is underlain by frozen soil throughout the year, the catchment should directly respond to the precipitation, with a strong relationship between runoff and precipitation. However, there are only several parts of the study region that show strong correlations between runoff and precipitation (Fig. 5.5). Especially, there are weaker correlations between precipitation and runoff in the Selenga catchment than that in the Aldan and Lena catchments. On the contrary, the correlations between TWS and runoff decrease from south to north as permafrost distribution increases.

These contrary strengths of the relationship between runoff-precipitation and runoff-TWS reveal the different dominant control of runoff generation among these three catchments. The less permafrost coverage in the Selenga and Lena catchments can allow more precipitation to infiltrate to the subsurface. As thus, the runoff-TWS correlation in these two catchments is much stronger than that in the Aldan catchment. Furthermore, the runoff-TWS correlation in the Selenga and Lena catchment is also more significant than

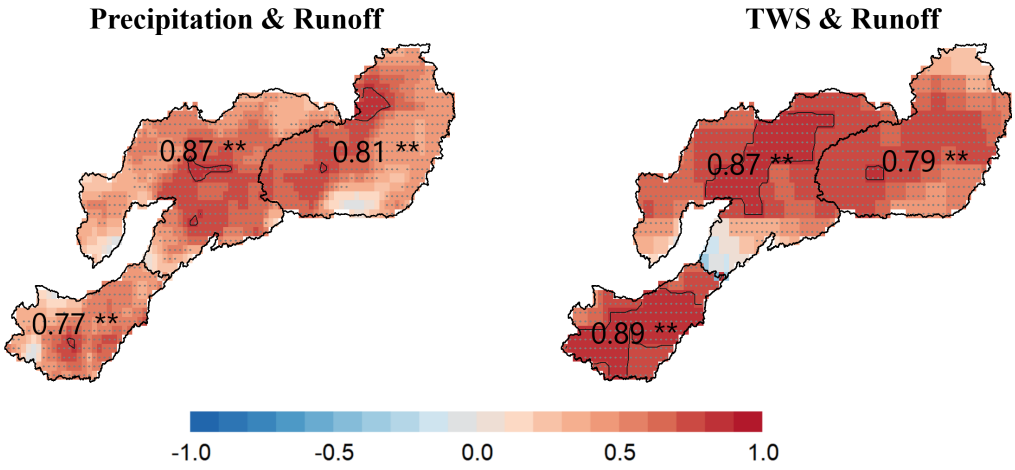

Figure 5.5: Correlations between annual precipitation and runoff, TWS and runoff, respectively, during the period of 1984-2013. Contour in black solid line delineate the correlation larger than 0.8. The black dot represents the significance of the correlations, with p value being smaller than 0.05.

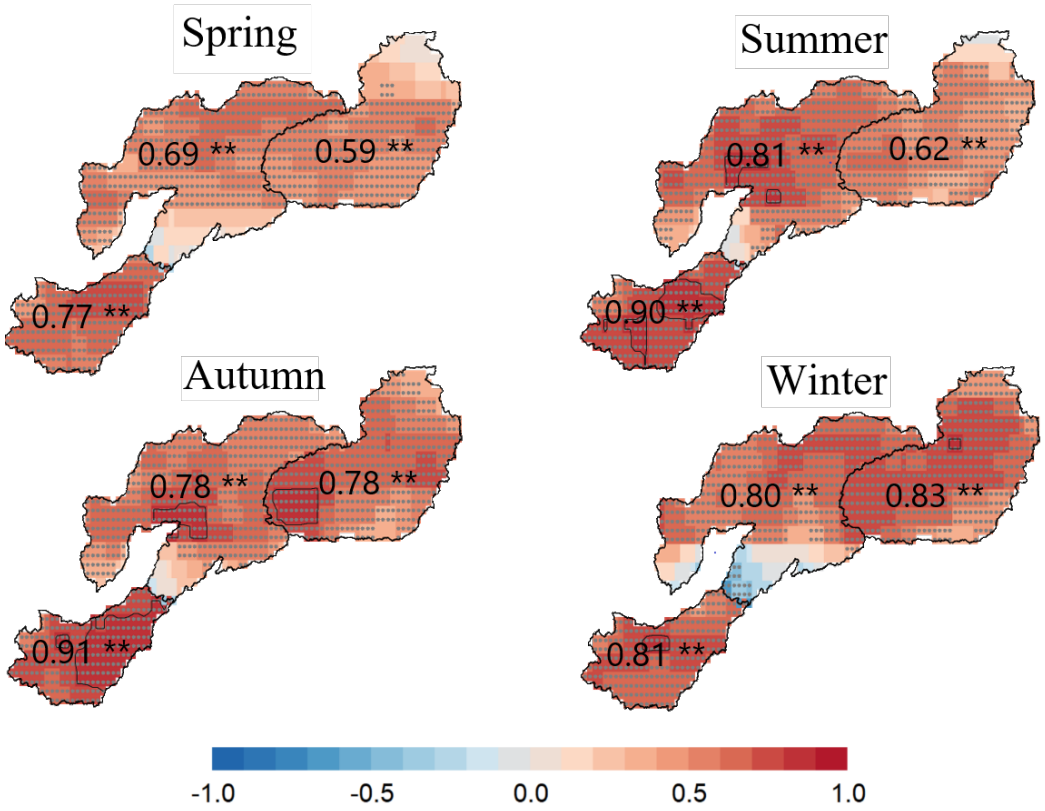

Figure 5.6: Correlations between annual TWS and runoff for each seasons during the period of 1984-2013. The message on this figure is same to Fig. 5.5.

the runoff-precipitation correlation, suggesting the increased importance of the subsurface system on the runoff generation in these two catchments. Specifically, permafrost degradation (i.e., the decreased permafrost extent) can increase the connections between surface and subsurface. This enhancement is evidenced by the enhanced runoff-TWS correlations during the thawing season (from summer to autumn, Fig. 5.6). These high runoff-TWS correlations in the Selenga catchment indicate that there are stronger connections between surface and subsurface water systems in this region with sporadic permafrost. Whereas for the other two catchments with higher permafrost coverage, the surface and subsurface system show less strong connections, thus have weaker runoff-TWS correlations. Differently, all the three catchments have similar runoff-TWS correlations during winter, implying a relatively stable relationship between surface runoff and subsurface groundwater systems in the cold season.

5.4 Consequence of climate change and permafrost degradation

5.4.1 Drying and wetting dynamics

The drying and wetting dynamics in these three catchments can be detected by the Budyko framework from a land-atmosphere coupling perspective (Fig. 5.7). Depending on the magnitudes of DI, we divide the dry condition into three categories: wet or energy-limited (DI $\leq$ 1.5), transition (1.5 $<$ DI $\leq$ 2), and dry or water-limited (2 $<$ DI $\leq$ 5) (UNEP & Thomas, 1992). The Selenga catchment is a typical example of a catchment at the threshold between the transitional and water-limited regimes. In the second 15 years period (1999-2013), a higher dryness index, i.e., higher atmospheric water demand (PET) in comparison to the available water supply (precipitation), is noticed in this catchment. Given the pronounced decrease in precipitation during this

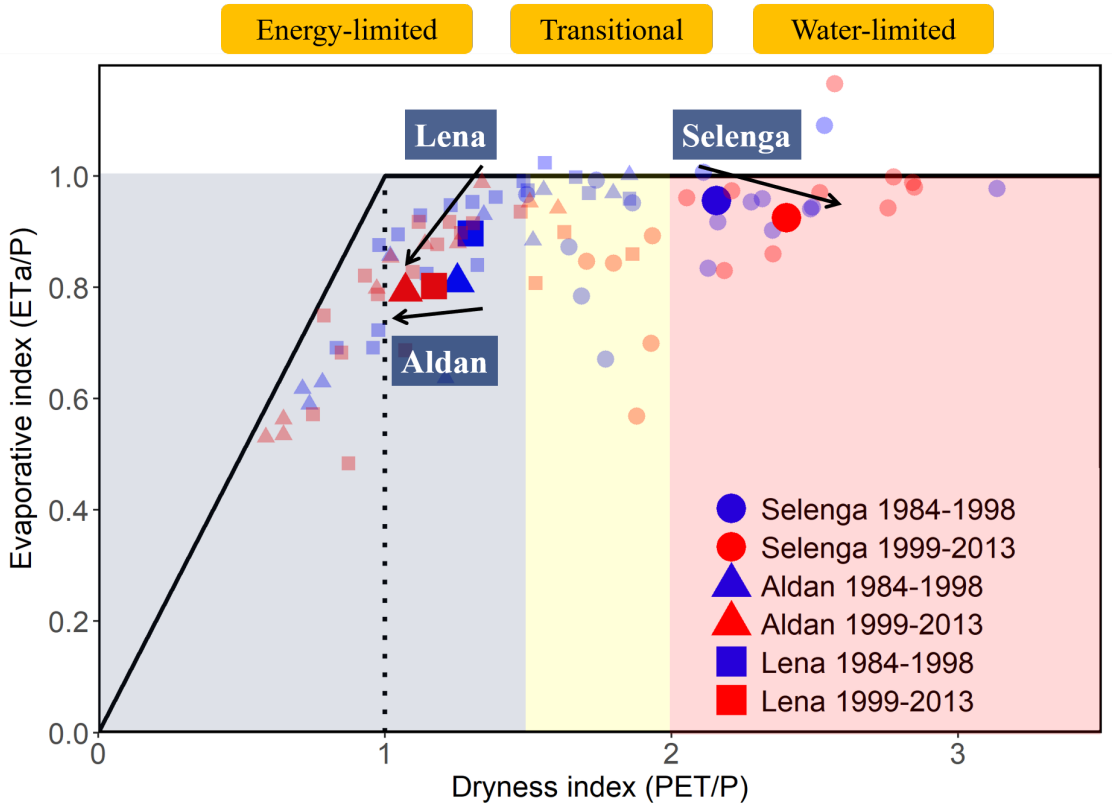

Figure 5.7: Budyko framework for Selenga, Lena, and Aldan: Annual average evaporative index (EI) plotted against dryness index (DI) for the Selenga catchment (circle), the Lena catchment (square), and the Aldan catchment (triangle) for two 15 years periods: 1984-1998 and 1999-2013. The 15-year-average value of the 17, 19, and 10 stations (shown in Figure 3) in the Selenga, Lena, and Aldan catchment are denoted by small circles, squares, and triangles, and the average of the 17-, 19-, and 10-station are depicted with bigger circles, square, and triangles, respectively. The horizontal dark line is the water-limit, where 100% of P becomes ET, and the diagonal dark line is the energy-limit, where 100% of available evaporative energy (i.e., PET) is converted to latent heat. To the left of the dashed line are energy-limited conditions, and to the right are water-limited conditions.

period (Fig. 5.2a), the substantially increased dryness index indicates that the water-limited (dry) Selenga catchment gets even drier under the warming and drying climatic condition. This drying condition is consistent with the severe droughts in the middle-latitude regions of Central, and East Asia described by Huang et al. (2016). Additionally, the evaporative index, i.e., evapotranspiration partition to the precipitation, also exhibits prevalent reduction during 1999-2013, despite the robust warming and enhanced PET during this same period (Fig. 4.1). Together with a persistent decline in the river runoff, this reduced evaporative index implies a significant surface water deficit via the enhanced infiltration induced by warming-associated lateral permafrost degradation (Fig. 3.4) in this water-limited catchment.

In the relatively humid zone where both Aldan and Lena belong to, however, most of the stations are located in the "energy-limited" (wet) region, with a few stations being in the transitional zone. The averaged dryness index shows a reduction during 1999-2013 compared to the first 15-year period over both catchments. The decreased dryness index indicates a wetter condition in the latter 15 years in response to the increased water supply (precipitation) (Fig. 5.2d,h). The wetting condition in the Aldan and Lena catchment agrees well with the prevalent wetting state in the southeastern Siberian region during this period (Boike et al., 2016; Fedorov et al., 2014; Iijima et al., 2014; Muskett & Romanovsky, 2009; Shiklomanov & Lammers, 2014; Velicogna et al., 2012). Meanwhile, a clear drop in the evaporative index is also noticed, especially in the Lena catchment. This implicates that the limited energy availability (PET) in the boreal ecosystem is not able to sustain enough energy consumed by the saturated or near-saturated surface. As a result, the surplus water could yield higher runoff in these two energy-limited catchments, since the infiltration is still blocked by the underlain continuous or discontinuous permafrost. Therefore, the wetting state in the energy-limited Aldan and Lena catchment is driven by the increased precipitation and intensified vertical permafrost degradation in the latter 15 years.

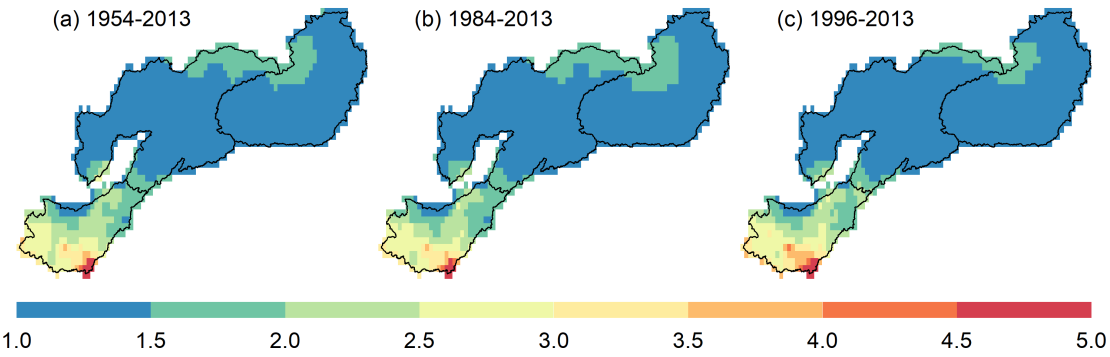

Figure 5.8: Spatial distribution of dry index (DI) over the three catchments in the southern Siberia based on the long-term averaged observation, (a) is for the entire 60 years period from 1954 to 2013 and (b) is for the latter 30 years during 1984-2013, and (c) is for the 1996-2013 period.

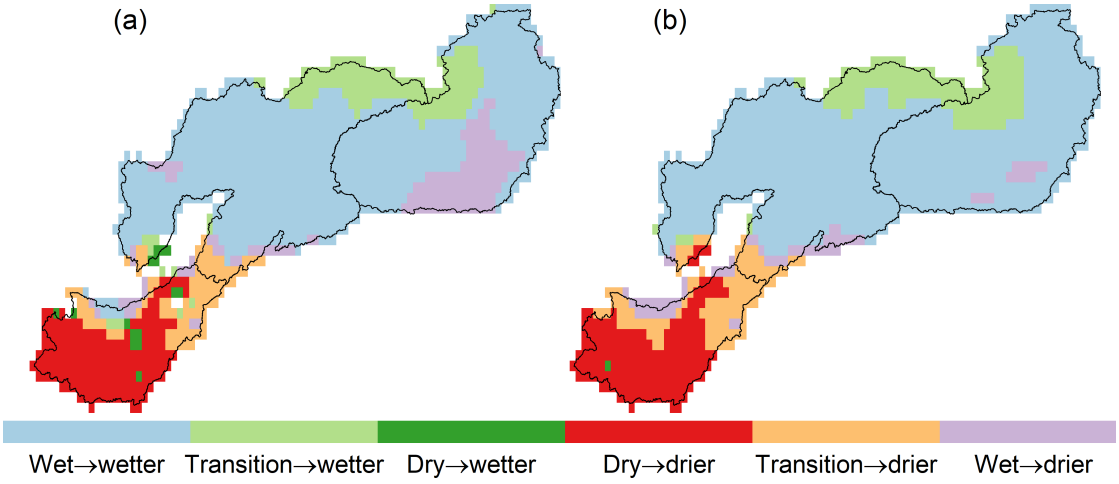

Figure 5.9: Evolution of drying and wetting conditions. Shown are the differences in DI during 1996-2013 in comparison to that during (a) 1954-2013 and (b) 1984-2013, respectively.

5.4.2 Evolution in regional aridity

Terrestrial aridity, described by dry index (DI), is the mean of the ratio between potential evapotranspiration and precipitation. It is primarily shaped by the complex interactions between the atmosphere and land surface, and can capture the spatial patterns in regional water availability. When DI rises, it represents a drier condition; if it declines, the conditions are becoming wetter. Figs. 5.8a,b,c show the spatial patterns of averaged DI during three periods of 1954-2013, 1984-2013, and 1996-2013, respectively. They reflect the general drying and wetting conditions over each period. The patterns in the Selenga catchment are characterized by drying conditions over all the three periods, and even show expanding drying areas over the recent period from 1996 to 2013, i.e., more regions have higher dry index. On the contrary, wetting conditions generally prevail in the Lena and Aldan catchment, with a growing area being in a humid condition (i.e., DI $\leq$ 1.5). These increased spatial contrasts in the aridity indicate that, due to the complex interactions and feedback in the hydrology-atmosphere-landscape system, regional hydrological response to changing environment is usually not uniform.

In order to identify the transformation of regional aridity and water availability during three periods shown in Fig. 5.8, the differences in DI during 1996-2013 in comparison to that during 1954-2013 and 1984-2013 are calculated. Based on the sign of the difference in the aridity, we define six types of transformations as shown in Fig. 5.9. Taken the transformation between Fig. 5.8b and Fig. 5.8c as an example: when the DI in 1996-2013 is smaller than that in 1984-2013, we call the transformation is from wet, transition, and dry to wetter for the DI in 1984-2013 being of wet, transition, and dry, respectively; otherwise we call the transformation is from wet, transition, and dry to drier, respectively. While Fig. 5.9a represents the transformation of aridity during the long-term (60-year) period, Fig. 5.9b denotes the transformation of aridity during the recent 30-year period. For both cases, the changes towards drier conditions are detected in most parts of the semi-arid Selenga catchment (red) and a small part of the wet Lena and Aldan catchments (violet). Regions with a dry condition that becomes wetter are sparse and primarily distributed in the middle valley region in the Selenga catchment

(green). In contrast, the wetting region is mainly found in the wet Aldan and Lena catchments (blue). Transition aridity mainly exists in two regions: one is the region between Selenga and Lena, the other is a cold and dry area in the north of Lena and Aldan. Fig. 5.9 shows that the first transition region is getting drier (yellow), while the second transition region is becoming wetter (light green). Since the difference between Fig. 5.9a and Fig. 5.9b is negligibly small, it means that the aforementioned transformation is only weakly dependent on the choice of the reference period, and the three southern Siberian catchments have experienced an extremely significant shift in the surface water availability over the recent period (1996-2013). These observed changes reflect a "dry gets drier, wet becomes wetter" phenomenon as we noted in Sec. 5.2, but it serves as evidence from a climatic perspective.

Furthermore, given the drying and wetting dynamics in the hydrology-permafrost-climate system as we discussed in Sec. 5.4.1, the "dry gets drier, wet becomes wetter" evolution from both terrestrial water availability and regional aridity perspectives implicates the potential influence of permafrost degradation on the hydro-climatic system. For the region with "dry gets drier", which is mainly observed in the Selenga catchment, the dominated lateral permafrost degradation has induced a drying land-atmosphere system, which could further accelerate the overlying lower-level atmosphere temperature by suppressing the evapotranspiration. Meanwhile, the drier and warmer atmosphere favors a clear sky that may reduce local precipitation, leading to a continued drying state in the land surface. This lateral-degradation-related dry and hot feedback loop could further induce a shift of "dry gets drier" in both land surface and atmosphere. On the contrary, the region with "wet becomes wetter" is primarily noted in Lena and Aldan, where have experienced enhanced vertical permafrost degradation. The corresponding wetting condition in land surface can sustain sufficient moisture to the atmosphere by evapotranspiration, thus leading to a relatively less fraction of sensible heat from land surface to atmosphere. As a result, this wet and cool feedback loop would promote a changing pattern with "wet becomes wetter" in regional water availability and atmospheric condition.

5.5 Discussion

From 1984 through 2013, the Aldan and Lena catchments, where already manifest a wet condition (i.e., with high precipitation, runoff, and TWS), are becoming wetter, whereas the semi-arid Selenga catchment gets drier from both the atmospheric and hydrological perspective. As we discussed in Sec. 4.1, these three catchments are found to be located in the two ends of the "seesaw-like" atmospheric circulations between Northeast Asia and Siberia (Iwao & Takahashi, 2006). The corresponding contrast precipitation oscillations during this 30-year period have led to an oscillation from dry to wet state in the Aldan and Lena catchment, but a shift from wet to dry pattern in the Selenga catchment. This means that the predominant wetter condition in Aldan and Lena and the drier condition in Selenga are mainly controlled by the oscillation patterns of precipitation. Nevertheless, the effect of warming-induced permafrost degradation on water availability (see detail in Chap. 4) is still pronounced. The lateral permafrost degradation stimulates the water loss in the Selenga catchment and led to a water-deficit runoff regime during a low precipitation state during 1999-2013. Whereas in the Aldan and Lena catchments, the vertical degradation sustains water-rich surface moisture and yields higher runoff

during the rainy season, resulting in a snow-rainfall-fed runoff regime.

Though the hydrological processes during a complete oscillation cycle (30-yr in southern Siberia) are expected to be dominated by precipitation (Z. Chen & Grasby, 2009; Hannaford et al., 2013; Pekárová et al., 2003), the corresponding connections between precipitation and runoff are disparate among these three catchments. This disparity is evidenced by differences in the regime pattern between runoff and precipitation (Fig. 5.2). As we mentioned in Sec. 4.2, a seasonal runoff-precipitation response is more dependent on the modulation of the subsurface system, which is primarily controlled by the thawing and freezing dynamics of permafrost in these three catchments. That is to say, the intra-annual behaviors in runoff-precipitation response could signify the critical role of the subsurface on the intra-annual distribution of river runoff.

These seasonal dynamics have also led to a disparity in the annual relationship between hydro-climatic variables, which is reflected by the different runoff-TWS and runoff-precipitation correlations in (Fig. 5.5). A higher runoff-TWS correlation in the Selenga catchment implicates that the subsurface system is becoming more critical in runoff generating processes in this sporadic permafrost region, where already suffers an enhanced lateral permafrost degradation (Fig. 3.4). This insight into the increasing role of groundwater on runoff generation has also been suggested by studies in other permafrost region (St. Jacques & Sauchyn, 2009; Walvoord & Striegl, 2007) as well as by modeling investigation (Lamontagne-Hallé et al., 2018). In the case of two northern (Lena and Aldan) catchments, the relationship between runoff and precipitation shows less differences as compared to that between runoff and TWS, indicating that the hydrological processes (both runoff and TWS) in these two catchments covered by higher permafrost extent are mainly controlled by precipitation. Nevertheless, the relatively larger R-TWS correlation in Lena than that in Aldan suggests that the subsurface system in the Lena with discontinuous permafrost is more developed (connected) than the Aldan with continuous permafrost. As warming continues, permafrost conditions are expected to experience a one-direction evolution from continuous to discontinuous and further to sporadic, and eventually totally disappear (Walvoord & Kurylyk, 2016). Consequently, the associated hydrological system in these three permafrost-affected catchments underlain by different permafrost distributions is likely to exhibit a potentially irreversible transformation (Devoie et al., 2019; Lenton, 2012; Nitzbon et al., 2020).

Hydrological processes are tightly coupled in the land-hydrology-atmosphere system (Seneviratne et al., 2010). The interactions and feedbacks between climate factors, hydrological variables, and land surface properties are expected to alter both the water and energy cycle for a given region (Fig. 1.2). In the Selenga catchment, the combination of the declined precipitation and permafrost-degradation-enhanced soil moisture loss has led to the decreased ET, indicating a reduced latent heat flux and evaporative vapor from the land surface to the atmosphere. In turn, this will result in an increased sensible heat flux partition that can potentially increase the temperature in the troposphere (Jung et al., 2010). Consequently, the drier and warmer atmospheric condition in this semi-arid region is likely to trigger a more frequent occurrence of heatwave events that further exacerbate land surface drying (Erdenebat & Sato, 2016), leading to a drier land-hydrology-atmosphere system (Ford & Frauenfeld, 2016; P. Zhang et al., 2020). On the contrary, the wetting surface condition in Aldan and Lena is intensified by warming and the associated thickening of the active layer. The atmospheric moisture will be increased mainly through the higher latent heat flux, leading to a humid low-level

troposphere with more cloud covering in this region (Vecellio et al., 2019). As a result, the moistening and cloudy atmosphere will induce a higher probability of precipitation that could contribute more moisture supply to the water balance (Iijima et al., 2014), causing a wetter land-hydrology-atmosphere system over this boreal region. These two patterns of drier and wetter systems would eventually lead to a transformation in the terrestrial water availability as shown in Fig. 5.9 and potential migration of climate zone in the future as suggested by Seneviratne et al. (2006).

Moreover, the severe drying condition in the semi-arid Selenga catchment, and enhanced wetting conditions in the boreal Aldan and Lena catchments, might also bring adverse and inevitable ecological consequences. In the water-limited Selenga catchment, the ecosystem is fragile and sensitive to the climate changes (Karthe et al., 2017). As air temperature rise continuously, the warming-associated processes, such as enhanced lateral permafrost degradation and increased potential evapotranspiration (PET), together with limited precipitation, might result in a more substantial water deficit on landsurface (Cook et al., 2014). This changing climate-induced water stress may not only threaten forest and grassland growth (Bao et al., 2014; Wang et al., 2019) but also lead to increased frequency of wildfires in the Selenga region and beyond (A. E. Hessl et al., 2018). Following those severe wildfire events, accelerated permafrost degradation has been observed (Bartsch et al., 2009; Kopp et al., 2017; Munkhjargal et al., 2020). Furthermore, in the wet Aldan and Lena catchments, the thawing of the upper ice-rich permafrost might cause thermokarst subsidence and formation of depression (Iijima et al., 2014; Séjourné et al., 2015). Forest fire events induced by natural or human disturbance could change the energy balance between land surface and atmosphere, which may also accelerate the continuous permafrost degradation over this boreal region (Boike et al., 2016). Meanwhile, the saturated (or near-saturated) surface and soil condition will reduce the canopy stomatal conductance of the forest (Iijima et al., 2014), thus, affect the growth of boreal forest and change the vegetation classes in the Boreal ecosystem.

5.6 Summary

We highlight the strong spatial wet-dry contrast in the distribution and variation of terrestrial water availability during the period 1984-2013 in the three southern Siberian catchments. The two northern catchments (Lena and Aldan), where already manifest a wet condition (i.e., with high precipitation, runoff, and TWS), are becoming wetter; whereas the semi-arid Selenga catchment located in the south gets drier from both atmospheric and hydrological perspectives. This disparity between north and south is also reflected in the shifted intra-annual regime. By combining these strong contrasts with spatial correlations between runoff and precipitation (TWS), we expose the different runoff generating processes over these three catchments underlain by different permafrost conditions. Precipitation plays a dominant role for Lena and Aldan, with higher permafrost coverage. Whereas for the southern Selenga catchment covered by less permafrost extent, the river runoff is more dependent on the subsurface discharge induced by lateral permafrost degradation. Furthermore, our investigations suggest that the lateral permafrost degradation in Selenga stimulates water loss from the increased permafrost-free area and leads to a water-deficit condition in this region. Whereas in the Aldan and Lena catchments, the vertical degradation sustained a water-rich surface moisture condition and yielded higher runoff during the rainy season, resulting in a wet

state. These two permafrost-degradation-induced surface water states further affect the overlying atmospheric condition, which may result in a potential transformation in the hydro-climatic system.

Chapter 6

Irreversible water deficits in semi-arid Selenga

Drought is one of the most devastating natural hazards that disrupt human life and socio-economies, challenge ecological systems, and complicate water resources management. In Chap. 5, we have noticed an intensified drying condition in the semi-arid Selenga River basin during 1996-2012. In the study based on tree ring record (P. Zhang et al., 2020), this dry spell has also been recognized as one of the most severe and prolonged droughts over the last two hundred years across Inner Central Asia. In this chapter, we investigate this record-setting drought from a hydrological perspective, with a specific focus on the compound effect of atmospheric circulation and permafrost degradation observed in previous chapters. Additionally, given the unprecedented dry condition during this period, we further discuss whether the identified hydrological transformation in this semi-arid region is irreversible.

We first examine how the drought propagates from precipitation (P) reduction to deficits in runoff (R) and terrestrial water storage (TWS), and how such propagation is related to the enhanced thermal condition from land surface to atmosphere. This is demonstrated by comparing the inter-annual and intra-annual anomalies of hydro-climatic variables, namely P, R, TWS, air temperature (T), and potential evapotranspiration (PET). We then discuss the potential effects of the enhanced permafrost degradation on the propagation of hydrological drought via the regression between thawing index and runoff deficits. After that, we assess the reduced runoff efficiency during this long-lasting dry period, namely, partitioning of precipitation into runoff (Chasmer & Hopkinson, 2017; Martin et al., 2020). Finally, such runoff deficits are also examined in the tributaries of the Selenga River.

6.1 Characteristics of dry spell during 1996-2012

Driven by the large-scale atmospheric circulations as we discussed in Sec. 4.1, the precipitation and runoff in Selenga regularly manifest periodical oscillations between dry and wet conditions during 1954-2013. Consequently, there are two noticeable dry periods in 1974-1982 (dry1) and 1996-2012 (dry2), and two apparent wet periods in 1960-1973 (wet1) and 1983-1995 (wet2). In order to distinguish the severe drought from the normal dry condition, we further employ the percentile ranking analysis (Sec. 2.3.2) to divide each hydro-climatic variable into four categories of conditions: very dry (<20%), dry (20-50%), wet (50-80%), and very wet (>80%). Similarly, the temperature is divided

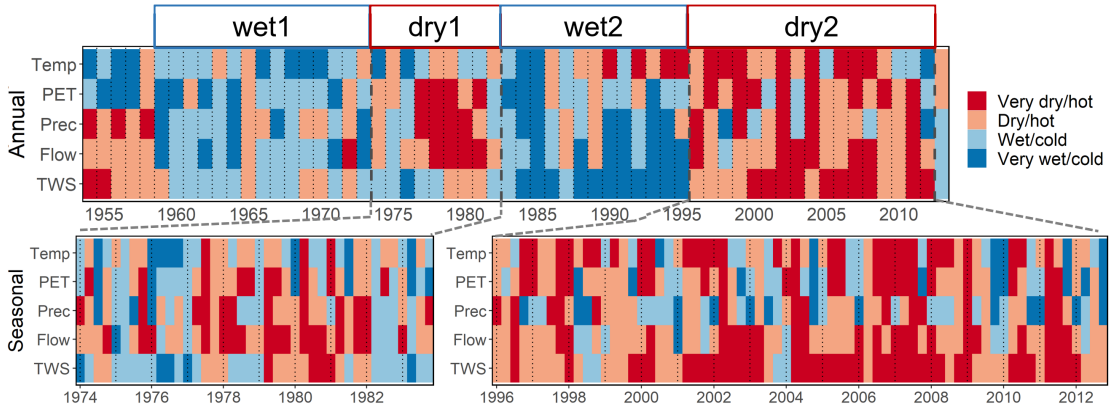

Figure 6.1: Dry and wet spells based on the percentile ranking analysis, during the period of 1954-2013. The upper and lower panels display the four hydrological and heat conditions based on annual and seasonal hydro-climatic variables, respectively. Temperature and PET are from the CRU dataset, precipitation is from the GPCC dataset, river flow is from the GRDC dataset, and the TWS is from the GRACE-REC dataset (Humphrey & Gudmundsson, 2019).

into very cold, cold, hot, and very hot. The results are shown in Fig. 6.1. The upper panel of Fig. 6.1 presents the plot based on annual variables, where the dry and wet conditions are obvious. Since we mainly focus on the two dry periods (dry1 and dry2), the enlarged properties of dry1 and dry2 based on seasonal variables are displayed in the lower panel of Fig. 6.1.

6.1.1 Severer hydrological droughts with longer duration

From the upper panel in Fig. 6.1, the water deficits start from precipitation during both dry1 and dry2, then gradually propagate over months to years through the hydrological system that eventually leads to water deficits in the river runoff and subsurface storage (TWS). However, different patterns also exist between these two dry periods: despite the precipitation deficits in dry2 showing less strong intensity than that in dry1, the dry condition in river runoff and TWS during dry2 are much longer in duration and more vigorous in intensity. Specifically, there are several wet conditions for annual precipitation in 2000, 2003, 2008, and 2012 during dry2. However, the river discharge always stays dry from 1999 to 2012. Such severe and prolonged runoff deficits trajectories are also detected in TWS anomalies, with much severer reduction. The dry condition in TWS only exhibits a slight recovery until 2013 after two successive years of wet precipitation in 2012 and 2013. It suggests that the reduced water availability during this intensified and prolonged dry period can only be mitigated by a consecutive increase in precipitation.

The persistent hydrological deficits have also been manifested by seasonal variables, shown in the lower panel in Fig. 6.1. This is particularly pronounced during summer and autumn when the precipitation experience a more significant reduction. Among these two seasons, the runoff and TWS show much severer and more persistent shortages than the precipitation. As to the spring and winter, the runoff and TWS resemble continued deficits despite the widespread rise in precipitation during this period from 1996 to 2012. This is because the runoff (TWS) during these two seasons are mainly controlled by

precipitation in the warm season due to the lagged runoff generation (Sec. 4.2) through the groundwater system.

6.1.2 Drying with intensified warming

The prolonged hydrological drought during 1996-2012 is also accompanied by significantly hot air temperature and large PET. This coincide phenomenon is especially strong in summer, during when the precipitation and temperature are highly coupled with the atmospheric system. These concurrent land-atmosphere extremes indicate potentially enhanced interactions of the landsurface-hydrology-atmosphere coupling under this long-lasting dry period (P. Zhang et al., 2020). The elevated air temperature will increase the atmospheric water demand. However, drying land surface can not provide sufficient water for this higher demand from the atmosphere. Consequently, this has led to enhanced atmospheric vapor pressure deficits that could further accelerate water loss from the land surface, resulting in a prolonged and intensified drying condition in the hydrological system. This intensified landsurface-hydrology-atmosphere coupling is also supported by the conjunction of positive anomalies among air temperature and 500-hPa geopotential height (Z500) (Fig. A.6 in Appendix).

The co-occurred positive anomalies in air temperature (PET) and hydrological deficits indicate that the enhanced atmospheric demands driven by rapid warming may exert an accumulative influence on the water flux generation in surface and subsurface systems. This may further affect the subsequent recovery of catchment function in the semi-arid Selenga basin as the resulted hydrological deficits require a longer period (more than one year) of above-average precipitation conditions to be restored.

6.2 Potential causes of enhanced drying condition

6.2.1 Enhanced summer atmospheric dynamics in Mongolia

Fig. 6.2 resembles the spatial distribution of the linear trend in summer mean 500-hPa (Z500) during 1954-2013. The summer mean Z500 has experienced a widespread increase in the mid-latitude, with the most considerable rise occurring over the Mongolia Plateau. This upward trend in Z500 across the Mongolian region has also been observed by studies based on other geopotential height datasets such as JRA25/JCDAS (Fujinami et al., 2016) and JRA-55 dataset (Hiyama et al., 2016). It indicates an enhanced atmospheric dynamics over Mongolia, which might produce warming summer air in this region.

In addition to the long-term trend, here we further examine the anomalies of both 500-hPa and 850-hPa geopotential height over both two dry periods as compared to the long-term condition during 1954-2013 (Fig. 6.3). We found that the recent dry spell from 1996 to 2012 has also experienced an amplification of the positive anomalies for both the 500-hPa (Z500) and 850-hPa (Z850) over the Selenga basin relative to the other southern Siberian region. The high pressure blocking patterns in both the middle- and lower-level atmosphere (Z500, Z850) over Mongolian Plateau can prevent air moisture flow and precipitation to the Selenga River basin. Furthermore, the positive anomalies in Z500 and Z850 could dynamically induce clear skies, warm atmosphere, and prolonged

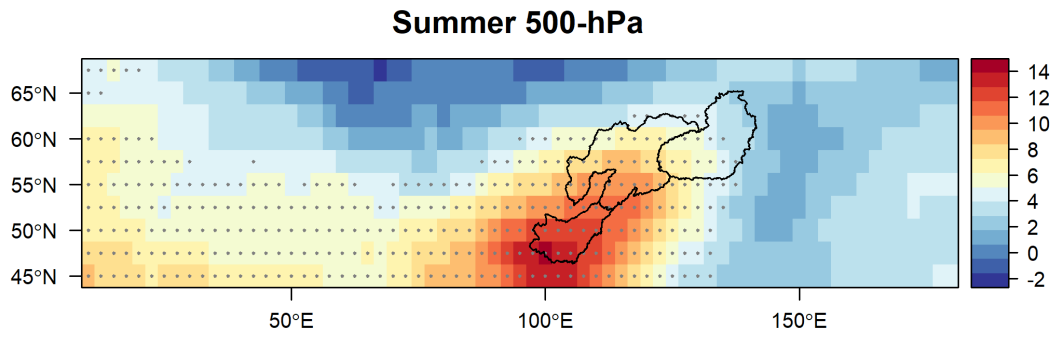

Figure 6.2: Linear trend of 500-hPa (gpm) geopotential height (Z500) during 1954-2013. Solid dots denote gridded geopotential height with trends that are statistically significant at the 95% confidence level. The geopotential height reanalysis data is from the National Centers for Environmental Prediction-National Center for Atmospheric Research (NCEP-NCAR).

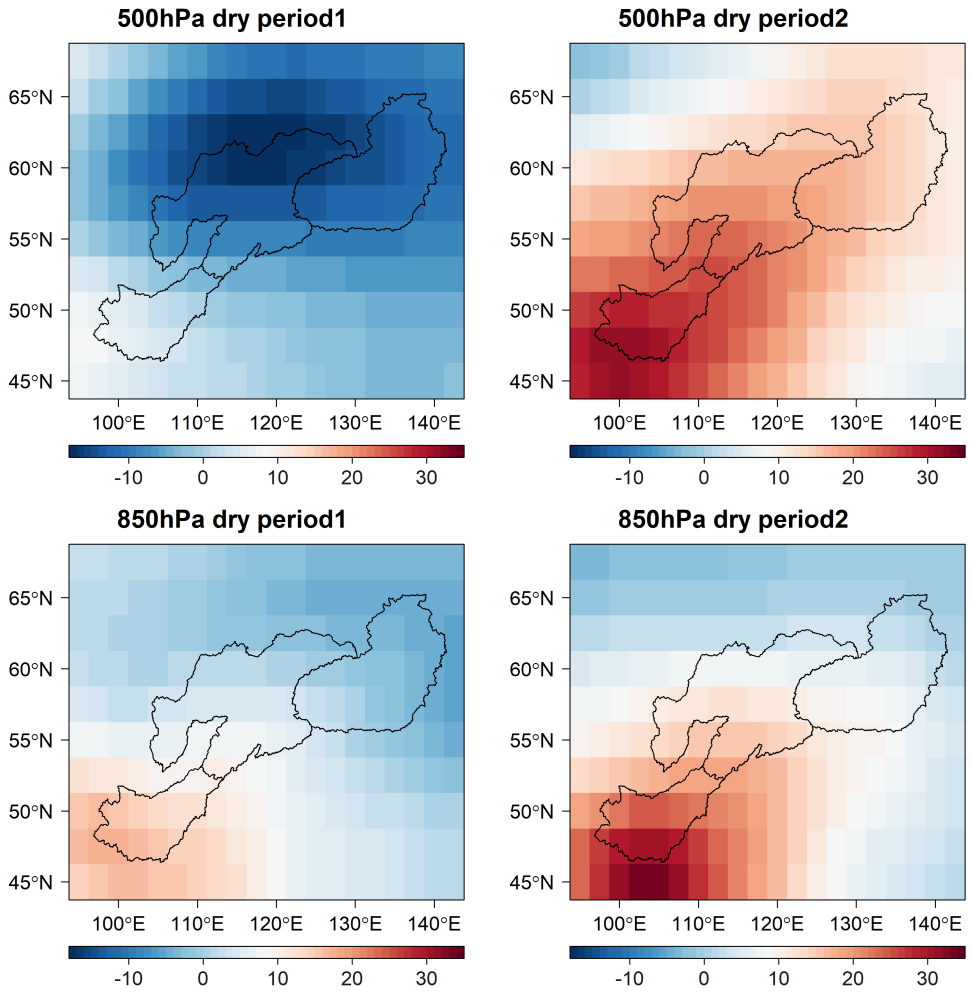

Figure 6.3: Anomalies of 500 hPa and 850 hPa (gpm) for two dry periods: 1974-1983 and 1996-2012 relative to the base period from 1954 to 2013.

hot state on the land (Meehl & Tebaldi, 2004). This could eventually produce severe heatwaves on the land surface (Meehl & Tebaldi, 2004; Sato et al., 2019). In contrast, no such enhanced blockings exist in the geopotential height during the dry period from 1974 to 1983, though it is also characterized by deficit moisture conditions. The different land-atmosphere behaviors during these two dry periods strongly suggest that the highly coupled land-hydrology-atmosphere system under rapid warming climate might produce more intensified drying conditions with enhanced intensity and longer duration.

6.2.2 Co-occurred dry and hot conditions in atmosphere

The severer hydrological deficits, namely, the very dry conditions in runoff and TWS anomalies, can also be exacerbated by the co-occurrence of high temperature and low precipitation (M. E. Mann & Gleick, 2015). This is especially apparent in dry2 from 1999 to 2012. During this dry period, there is a high chance of such co-occurrence (Fig. 6.4), especially during summer. For example, during 1954-2013, 22 out of the 60 summers (37%) have exhibited positive temperature anomalies as well as precipitation deficits (Fig. 6.4, left), with half of them come from the second dry period during 1996-2012. Particularly, the summer of 2002 had an extremely severe atmospheric condition with high temperature and the recorded lowest precipitation, and consequently a recorded driest hydrological condition in both the runoff and TWS. This implicates a potentially increased importance of warming on the occurrence of multi-year droughts.

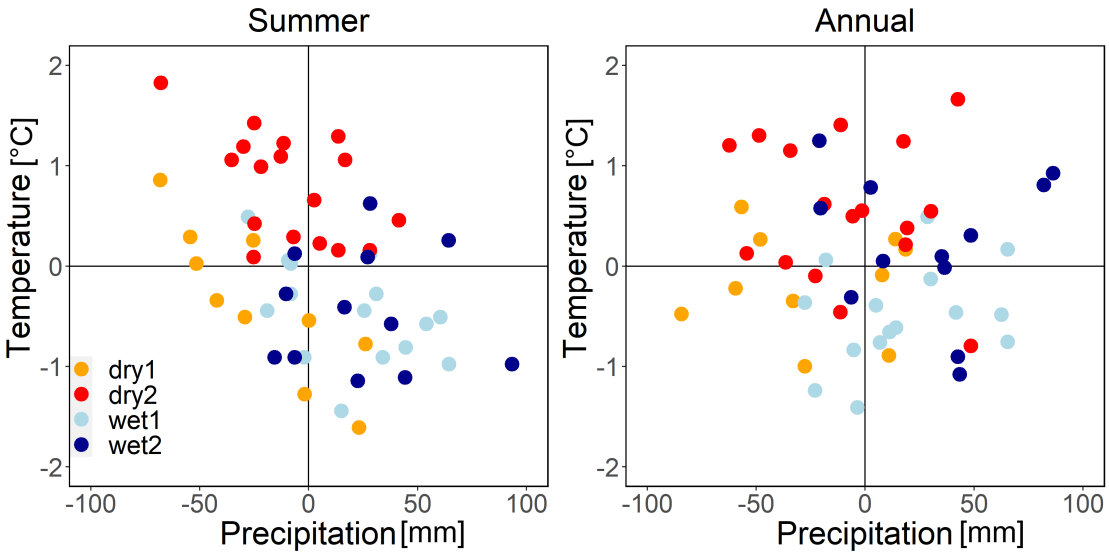

Figure 6.4: Regression of anomalies for precipitation and temperature during each dry and wet period.

6.2.3 Potential role of permafrost degradation on runoff deficits

In Sec. 3.2 we introduced thawing index (TI) as an indicator of permafrost thermal condition, with high TI referring to intensified thawing. Fig. 6.5 presents the long-term (1954-2013) variability of TI anomalies in the Selenga catchment. Overall, TI

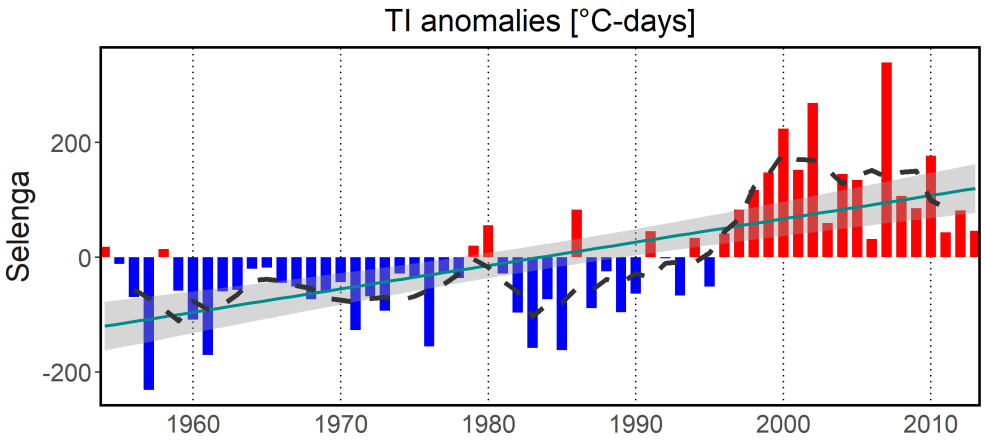

Figure 6.5: Inter-annual variability of TI anomalies during 1954-2013 over the Selenga catchment. TI is calculated by the Stefan method based on the gridded monthly air temperature data from the CRU dataset.

resembles an upward trend during 1954-2013, indicating a continued warming condition in permafrost. Interestingly, an evident step change has been exhibited since 1996, with all the yearly TI anomalies exhibiting positive value. This long-lasting positive pattern in TI is consistent with the drying condition during 1996-2012, which hints a potential connection between the permafrost degradation and runoff deficits.

In order to verify this assumption, in Fig. 6.6, the regression between TI and runoff deficits over each dry and wet period are presented. Generally, TI is negatively related to runoff during the entire period of record from 1954 to 2013, indicating that thawing permafrost may enhance the runoff deficits. This is because warming permafrost conditions could increase the connections between surface and subsurface systems, which can further trigger the downward movement of soil moisture. As a consequence, the en-

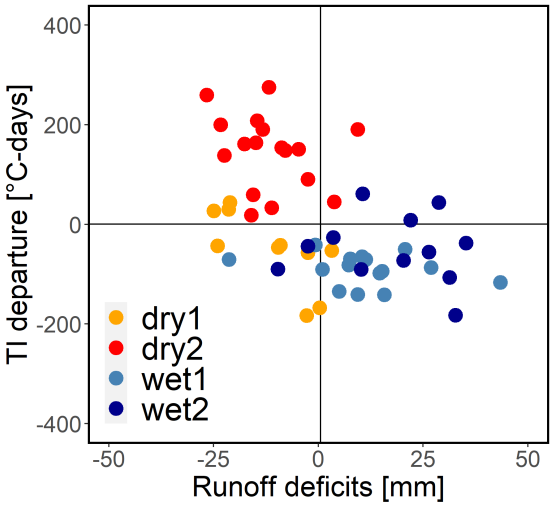

Figure 6.6: Regression of anomalies for thawing index (TI) and runoff deficits during each dry and wet period.

hanced infiltration due to permafrost degradation might induce decreased runoff. This behavior is most pronounced during the long-lasting dry spell from 1996 to 2012, when the runoff deficits co-occurred with greater positive TI.

Furthermore, the warming-induced lateral permafrost degradation in this region may also reinforce the runoff deficits. As we noticed in Fig. 3.4, there is a clear northward movement in the 0°C isotherm of MAAT during 1984-2013 as compared to the earlier 30-year period, implying that permafrost has experienced a significant lateral degradation pattern in this region. That is to say, as warming continues, there would be more permafrost-free areas in this region, which can induce higher infiltration and percolation. Due to these enhanced subsurface processes, there might be less surface water. The notable co-occurrence of runoff deficits and TI anomalies, together with the northward migration of permafrost domain in the Selenga basin, suggest that the permafrost degradation due to warming climate may substantially exacerbate the drying condition in this vulnerable region.

6.3 Consequence of the intensified drying condition

6.3.1 Transformation in runoff generation

Based on previous sections, hydrological variables (i.e., runoff and TWS) show much more severe deficits than precipitation in dry2. In order to identify the potential changes in the runoff generation processes during this long-lasting dry period, here we further consider the corresponding relationships between runoff and precipitation, runoff and TWS (Fig. 6.7).

A considerable difference has been observed in hydro-climatic relationships between dry and wet periods. During the dry periods, i.e., 1974-1983 and 1996-2013, the generated runoff from precipitation is much lower in comparison to that in the wet periods

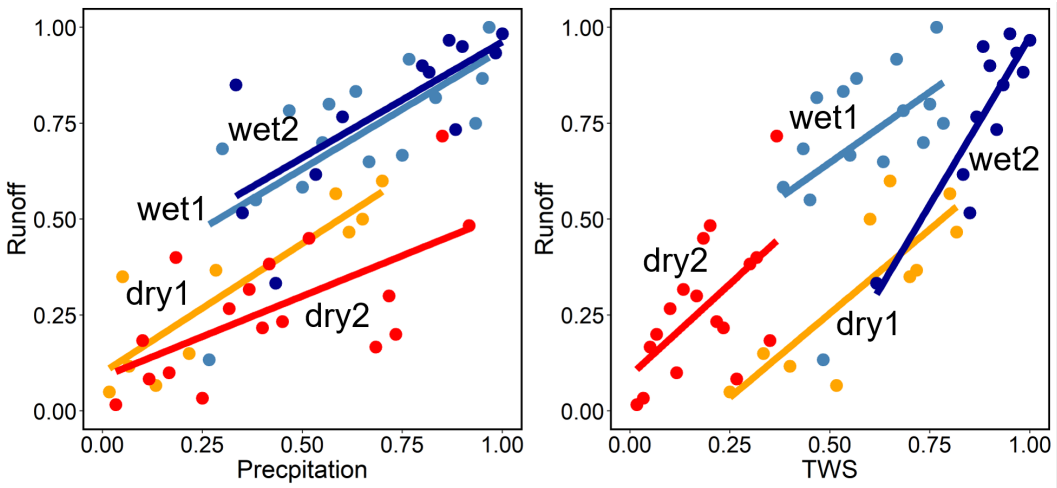

Figure 6.7: Changed runoff-precipitation and TWS-precipitation relationships during dry and wet periods in the Selenga basin.

during 1959-1973 and 1984-1995 (Fig. 6.7, left panel). This indicates that the hydrological system requires more input water from precipitation during dry periods to sustain surface water availability. This low precipitation conversion behavior is even more significant during dry2 from 1996 to 2012. With a relatively flat regression line between runoff and precipitation, it indicates a considerable reduction in runoff efficiency, namely, partitioning of precipitation into the runoff.

When comparing the runoff-TWS regression between the two dry spells, the same TWS can generate higher runoff during the recent long-lasting dry period (dry2) than in the first dry period during 1974-1983 (Fig. 6.7, right panel). That is to say, during 1996-2012, runoff responds more sensitively to TWS than the first dry period. This increased relationship implicates a stronger connection between surface runoff and groundwater systems along with permafrost degradation during this period.

6.3.2 Decreased runoff efficiency in subbasins of Selenga River

Driven by the reduction in precipitation, widespread runoff deficits conditions are also registered in the upstream subbasins of the Selenga River (Fig. 6.8). Since the river discharge data for subbasins of the Selenga River is only available during 1982-2010, our comparison between dry and wet states will only focus on two periods before and after 1996, i.e., 1982-1995 and 1996-2010.

Although the river runoff over all the subbasins responds well to the precipitation during the period before 1996, it exhibits less consistency with the variations in precipitation during the dry period from 1996 to 2010. This out of pace between river runoff and precipitation is consistent with the changed runoff-precipitation response in the large Selenga basin (Fig. 6.7, left panel). It is particularly notable in subbasins such as Orkhon (gauged at Sukhbaatar) and Eg (gauged at Khantai).

Different runoff-precipitation variations are also noticed among each subbasin with different landscape properties. For instance, river runoff in the mountainous subbasin like Delgermeren (gauged at Muren) shows stable moisture conditions before and after 1996, despite the relatively decreased precipitation around the 2000s. Differently, subbasins located in flat valleys like Orkhon (gauged at Orkhon) experiences a much more significant decrease in runoff as compared to the variations in precipitation. This indicates that the propagation of hydrological droughts in subbasins is strongly dependent on their specific location and landscape characteristics.

Though the river discharge data for the subbasins is limited to the period of 1982-2010, the long-term meteorological data can be obtained from gridded GPCC and CRU data sets. Here we further use the meteorological data to derive the dry index (PET/P) during 1950-2012, which can reflect the historical evolution in the drying condition in each subbasin (Fig. 6.9, left panel). Since the meteorological droughts are highly dependent on the large-scale atmospheric circulation (Trenberth et al., 2014), the historical evolution of the drying conditions shows a similar pace among each of the subbasins. During 1974-1983, a strong drying condition occurs across all the subbasins. This strong drying period is followed by a relatively wet state during 1984-1995. Since then, all the subbasins undergo a long-lasting drying condition during 1996-2012. These variations between dry and wet states over the subbasins are consistent with the patterns we observed in the

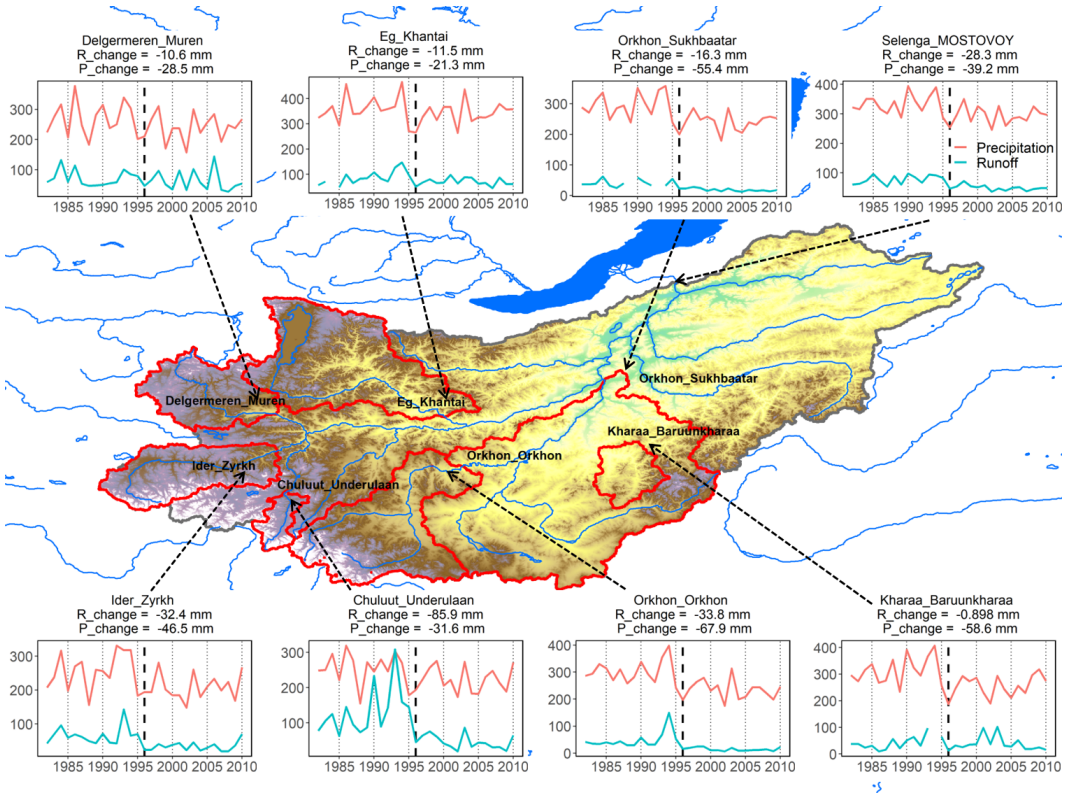

Figure 6.8: Location of the selected seven subbasins of the Selenga River, and time series in annual runoff (mm) and precipitation (mm) during 1982-2010 for each subbasins and the outlet in Mostovoy. The change in annual runoff and precipitation represents the differences in the mean average between two periods before and after 1996.

large Selenga basin (Fig. 6.1), which highlights the importance of meteorological controls in this semi-arid region.

In addition to the direct comparison in the variations of runoff and precipitation, the changed runoff-precipitation response can also be revealed by the runoff-precipitation ratio (R/P). Our investigations reveal that although the meteorological drying condition shows a similar pattern among all the subbasins, the runoff-precipitation response resembles significant differences across subbasins (Fig. 6.9, right panel). In general, the subbasins in the southern region, such as Chuluut, Orkhon, and Ider, are characterized by a strong reduction in the runoff-precipitation ratio during 1982-2010. These decreased R-P ratios indicate stronger sensitivity of runoff to precipitation and potentially lower efficiency in precipitation conversion to runoff in these subbasins. In contrast, the runoff in the northern mountainous region like Delgermeren and Eg shows a smaller decrease between the two periods before and after 1996. Particularly, the R-P ratio in the Kharaa River basin (gauged at Baruunkharaa) shows an unusual increase during 1998-2005. This increased R/P suggests that the runoff in this subbasin is also contributed by other sources such as warming-accelerated thawing permafrost.

Changed runoff-precipitation response also manifests in the shift of the regime in precipitation and runoff between the two periods before and after 1996 (Fig. 6.10). Though the regime in precipitation shows a similar pattern over all the subbasins, the runoff

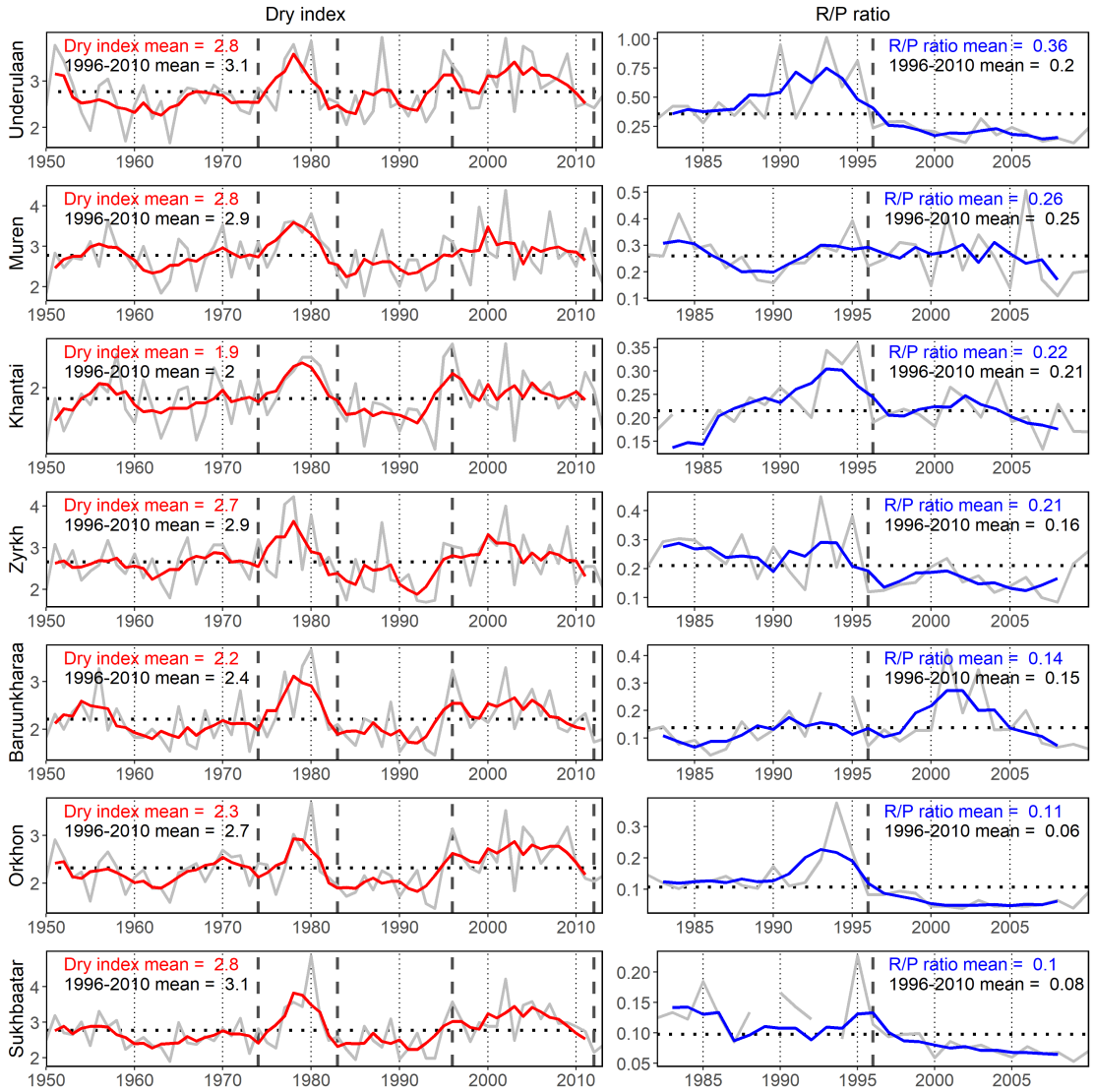

Figure 6.9: Time-series of the dry index (1950-2012) and runoff-precipitation ratio (1982-2010) for the selected seven subbasins in Selenga River basin. In the left panel, the grey line represents the yearly dry index, with soild red line being their 10-year moving average. In the right panel, the grey line denotes the yearly R-P ratio, with the solid blue line being their 10-year moving average.

regime exhibits substantial divergence across these subbasins. The most significant shift in runoff regime is observed in the southern subbasins include the Chuluut, Orkhon, and Ider, where also experience the most substantial reduction in the annual runoff (Fig. 6.8). In contrast, river runoff of the Delgermeren, Eg, and Kharaa subbasins shows a consistent pattern with precipitation.

Finally, our investigation reveals that warming-related alternations in runoff regimes such as enhanced spring melting and reduction in summer runoff are also observed in these three subbasins. For instance, increased spring runoff peaks are observed in the rivers such as Delgermeren, Ider, and Kharaa. This indicates an increased contribution from spring thawing under a warming climate. At the same time, the runoff peak in summer shows a widespread decline over all the subbasins, with the most notable

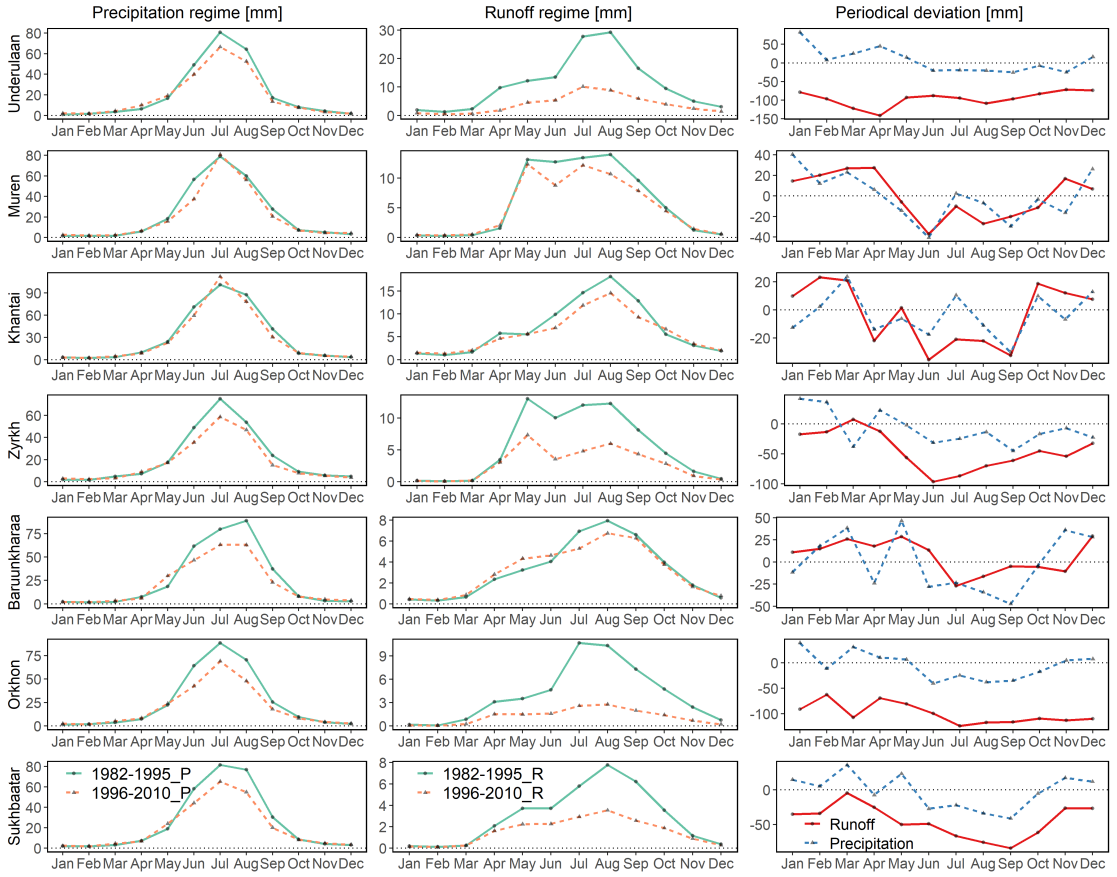

Figure 6.10: Regime of precipitation (left panel) and runoff (middle panel) during two periods, i.e., 1982-1995 and 1996-2010, and the corresponding deviation between these two periods (right panel) for both precipitation and runoff in the seven subbasins in Selenga.

reduction being in Orkhon, Chuluut, and Ider rivers in the southern region.

6.4 Discussion

The terrestrial water availability (precipitation, river runoff, and TWS) in the Selenga River basin exhibits the most prolonged dry period during 1996-2012 as compared to the preceding dry period over 1974-1982. This dry period in the hydro-climatic system mainly results from periodical atmospheric oscillation mentioned in Sec. 4.1. During this long-lasting period, the precipitation and associated hydrological processes exhibit severe water deficits. However, the water deficits condition in runoff and TWS are much severer and long-lasting than those in precipitation. Furthermore, this period also experienced unprecedented warming. Given this co-occurrence between severe water deficits and high air temperature, it indicates that precipitation deficits are more likely to yield consecutive drying conditions in the terrestrial hydrological system when they occur in a warmer climate. This co-occurrence pattern, namely dry hydrological system and hot atmosphere, is also observed in Europe and America (Diffenbaugh et al., 2015; Martin et al., 2020; Meehl & Tebaldi, 2004), reflecting a potential increased co-occurring of droughts and heatwaves under a warming climate.

Furthermore, our results reveal an overall reduction in runoff efficiencies across both Selenga River and its tributaries, with a clear regime shift since the middle 1990s. Given the rapid warming during recent decades, it suggests that the excess heat from the warming atmosphere is diminishing the runoff efficiencies from precipitation (Martin et al., 2020), indicating a potential shortage in water supply in this semi-arid region. It also hints that rapidly increasing temperatures are becoming a critical contributor to the drought risk in the semi-arid Selenga basin. Meanwhile, enhanced anticyclonic circulation anomalies are also observed during this long-lasting dry period. These intensified anticyclones overlap well with the water deficits, indicating a strong co-occurrence of heatwaves and droughts (Schubert et al., 2014). This increased probability of compounding heatwave and drought suggests potential enhanced feedback from the land surface to the atmosphere in the semi-arid Selenga basin (P. Zhang et al., 2020).

The terrestrial water availability is, of course, primarily controlled by water from precipitation, but it also relies a lot on how the water is distributed into infiltration, evapotranspiration, and river runoff (Brutsaert et al., 2005). This means that hydrological droughts are also highly dependent on the fluxes and storage of water available in the surface and subsurface hydrological systems (van Loon, 2013). As thus, the warming-induced permafrost degradation (Sec. 3.2) might also intensify the hydrological droughts in the Selenga basin. This potential drying consequence of permafrost degradation on surface and subsurface water systems is also evident by studies based on field observation (Ishikawa et al., 2005; O'Donnell et al., 2012) and remote sensing survey (Chasmer & Hopkinson, 2017), which indicates the crucial role of permafrost dynamics on regional water availability. Though it is of great importance, existing studies on detecting the drying condition in northern Mongolia Plateau have not considered the historical evolution in permafrost in this region (A. Hessl et al., 2013; A. E. Hessl et al., 2018; P. Zhang et al., 2020). Our investigation fills this research gap, and finds a robust negative relationship between thawing index (TI) and runoff deficits (Fig. 6.6), which provides evidence to the potential linkage between permafrost degradation and hydrological droughts. On the other hand, given the substantial reduction in river runoff, this negative connection between TI and runoff deficits also suggests a potential irreversible, enhanced permafrost degradation under an ongoing warming climate in this transboundary region.

Drought might have more severe consequences for humans and the ecosystem in the semi-arid region like Selenga, as water availability in such a region is already low under normal climate condition (Dai, 2011). Selenga is a vital transboundary river between Mongolia and Russia, and it is also the largest tributary of Lake Baikal. Increased water demand from ecological systems and human consumption is expected to approaching the limited water supply in the semi-arid Selenga basin (Karthe et al., 2017; Priess et al., 2011). Warming-induced processes such as increased atmospheric moisture demand and enhanced permafrost degradation may further strengthen the water deficits in this region. Such extreme water deficits can disrupt human life and socio-economies, endanger ecological systems, and challenge the water resources management between upstream Mongolia and downstream Russia (van Loon, 2013). This study, covering a comprehensive investigation on the change in water availability in response to changing climate and thawing permafrost, can provide fundamental information for the water resource managers and policymakers to build a water-sharing agreement that could balance the competing water demands and defuse potential conflicts.

6.5 Summary

In this chapter, we have investigated the long-lasting drying period in the Selenga River basin during 1996-2012 from a hydrological perspective. We found that the severity of hydrological deficits is likely to be intensified when precipitation deficits co-occur with higher temperature conditions. These co-occurring hot-dry meteorological conditions, accompanied by an intensified anticyclonic atmospheric condition, overlap well with a significant shift to decreased runoff efficiency throughout the region. Furthermore, a strong negative relationship between thawing index and runoff deficits provides evidence of the potential linkage between permafrost degradation and hydrological droughts. It suggests that warming-induced lateral permafrost degradation may strengthen the runoff deficits and further intensify the drying surface condition. These correspondences between the atmosphere, hydrological system, and land surface processes suggest an enhanced land-atmosphere coupling, which may induce an irreversible hydro-climatic shift under a warming climate. Our results also highlight an increasing influence of rising temperature on drought propagation in the Mongolian Plateau.

Chapter 7

Hydrologic extremes in Boreal Lena and Aldan

The studies in previous chapters are mainly based on accumulated annual or seasonal hydrological variables. The analysis of these variables has provided general insights into the long-term annual and seasonal patterns. However, it smoothes out the extreme events, such as floods, that could have devastating impacts on both natural systems and human society (Diffenbaugh et al., 2013). Such impacts are likely to become more severe under a changing climate (Blöschl et al., 2017; Trenberth et al., 2015). Given the remarkable warming and corresponding permafrost degradation during summertime in southern Siberia, it is therefore essential to explore and predict the characteristics, processes, and dominated controls of the hydrologic extremes.

Especially in Sec. 5.1, we have noticed a remarkable regime shift in the Aldan River runoff during 1984-2013, with an apparently increased runoff in August and September after 2000. In this chapter, we employ daily runoff data, which is available for the period of 1950-2011, to further explore more detailed changes in runoff regime by investigating the corresponding hydrographs of the subbasins in the Lena and Aldan River basins. This data could also allow us to identify the maximum and minimum of daily river streamflow, i.e., the maxiflow and miniflow, respectively, and use them to represent the hydrologic extremes. Furthermore, we investigate the historical change in the magnitude and timing of the extreme events based on a moving-averaged daily runoff with a 10-day time window. In order to reveal the sensitivity of extreme events to a warming climate and associated alterations in permafrost conditions, we also conducted the correlations between the extreme flows and climate variables, and permafrost indices.

7.1 Background

In a warming climate, hydrologic extremes are expected to occur more often and more intense (Allan & Soden, 2008; Min et al., 2011; Trenberth et al., 2003). However, accurate descriptions of hydrologic extremes and attribution of their changes are still not well understood yet, mainly because the variations in hydrological regimes are connected with complex climatic and landscape interactions at multiple spatial and temporal scales (Slater et al., 2021). Nevertheless, we can still use the maxiflow and miniflow to understand how hydrologic extremes respond to changing climate and landscape. Since the maxiflow and miniflow determine the range of hydrograph within a year, the ratio of maxiflow and miniflow (RMMF) can be used to reflect a specific characteristic of the

seasonality in river runoff (Ye et al., 2009).

Due to the existence of permafrost, rivers in southern Siberia show higher differences between maxiflow and miniflow as compared to rivers in the temperate region (Woo, 2012). The frozen layer of permafrost has low hydraulic conductivity and limited storage capacity, especially during cold season when the ground is completely frozen. This property has led to a lower baseflow (lowflow) during winter, and thus a higher RMMF in the permafrost-affected region (Ye et al., 2009). In a warming climate, the coverage of permafrost is expected to decrease. This reduced distribution of permafrost can thus affect the runoff regime, such as RMMF. Therefore, the inter-annual variations in maxiflow, miniflow, and the RMMF can be used to reflect the changes in river flow shaped by changing climate and the associated evolution of permafrost condition (Gautier et al., 2018; Ye et al., 2003, 2009). This study mainly focuses on the Lena and Aldan River basins. There are 4 and 3 river flow gauges in Lena and Aldan, respectively (Fig. 7.1b). The daily river flow records are available from 1950 to 2011.

7.2 Intra-annual distribution and changes in river runoff

7.2.1 General condition in river runoff regime

The annual hydrograph reveals how the daily runoff distributes within the year for each tributary of the Lena and Aldan River basin (Fig. 7.1a). In general, there are two runoff peaks emerge in each tributary. The first runoff peak occurs around 150-190 day of the year (DOY), varying from the end of May to the beginning of July, and is governed by snowmelt. The secondary runoff peak, emerging around 200-270 DOY, is primarily caused by heavy rainfall in summer or autumn. The large value of first peak and remarkable difference between the two peaks imply that the runoff generation over these subbasins is primarily sustained by spring snowmelt.

Furthermore, Fig. 7.1a also reveals the different runoff regimes between Aldan and Lena. Both the first and second runoff peaks in Aldan subbasins are higher than those in Lena subbasins. Especially in the upstream of Aldan, the river runoff gauged at Ust Mil shows the most pronounced first peaks, which could be caused by dense snow cover in this region. In contrast, the runoff regimes in the Lena River subbasins show a relatively flat pattern with smaller differences between the spring peaks and the secondary peaks generated during summer and autumn. Despite these differences between Aldan and Lena, both runoff gauged at the outlets (Vtrchoyanski Perevoz in Aldan and Tabaga in Lena) show lower peaks compared to the runoff in the upstream. Moreover, the occurrence of spring melt, thus the first peak, in the upstream (i.e., Aldan Ust Mil and Lena Zmeinova) are earlier than that in the downstream. This is mainly because the upstream region is usually warmer than the northern downstream region due to the latitude-dependent temperature condition.

Lowflow (or flow during the cold season) normally occurs during winter, which only accounts for a small fraction of annual runoff compared to the runoff peak. Among all the subbasins, the lowest magnitude of lowflow is observed in the Aldan River basin gauged at outlet Vtrchoyanski Perevoz, where is characterized by the most extensive permafrost coverage. Since lowflow in the permafrost region is primarily sustained by

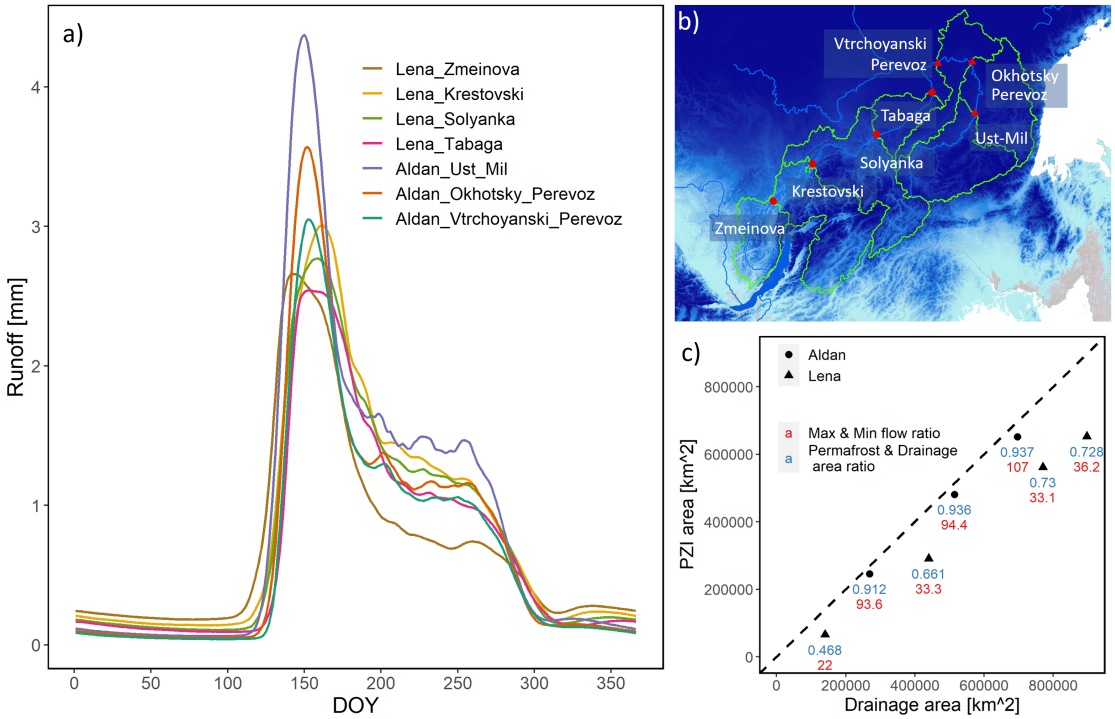

Figure 7.1: Basic runoff condition in the subbasins of the Lena and Aldan River basin; a) daily runoff regime based on the reference period during 1950-2011 for each tributary in the Lena and Aldan River basin; b) gauges of each tributary and subbasins in the Lena and Aldan River; and c) geographic distributions of the ratio between permafrost area and the drainage area as well as the averaged ratio of maximum and minimum flow (RMMF).

groundwater (Walvoord & Kurylyk, 2016), the relatively small lowflow is primarily due to the extensively existed permafrost that prevents water exchange between groundwater system and surface river streamflow during the cold season.

Fig. 7.1c shows the geographic distribution of the RMMF in the context of permafrost coverage over all the subbasins. The RMMF is generally larger in the basins with higher permafrost coverage. This is evident in two aspects. First, the subbasins in Aldan are underlain by a larger permafrost extent than that in the Lena subbasins (Fig. 7.1b), i.e., continuous permafrost in Aldan, whereas discontinuous in Lena. Accordingly, the lowflow of each subbasin in Aldan (continuous permafrost) is larger than that in the Lena basin (continuous permafrost). Second, the RMMF of the subbasins in downstream is larger than that of the headwaters. For example, there is more permafrost cover in the northern downstream region due to the latitude-dependent temperature condition across the Aldan River basin, with the permafrost extent increase from 91% in the upstream to 94% in the downstream basin. In response to such a difference in permafrost coverage, the RMMF also increases from 94 in the headwaters to 107 in the downstream. A similar pattern is also detected in the Lena River basin. Along with the increased permafrost extent (from 47% to 73%), the RMMF between the headwater and the downstream increases from 22 to 36. These corresponding patterns in the RMMF and permafrost coverage are indicative of permafrost for the runoff generating processes in the permafrost-affected southern Siberian region.

7.2.2 Shifts in runoff regime and RMMF

In this subsection, we use both mean annual hydrograph and RMMF to detect change patterns in the seasonality of river runoff. In the left panel of Fig. 7.2, the runoff timeseries is divided into six 10-year periods, namely, from the 1950s to 2000s. These 10-year mean annual hydrographs reflect that there is a clear leftward regime shift induced by the earlier spring melt. Specifically, in order to directly compare the shift between the first and last decades, the distribution range of the daily runoff on each DOY of the two corresponding 10-year periods is depicted by the two shading areas: blue for the 1950s and red for the 2000s. For a given DOY, the upper and lower bounds of the shading area represent the largest and smallest daily runoff on that date, respectively, during the corresponding decade.

In the three subbasins of Aldan, the distribution range of the decadal hydrograph also manifests a clear leftward shift in the first runoff peak during the 2000s as compared to those in the 1950s. There also exhibit increased magnitudes in these peaks. However, in the subbasins of Lena, though the distribution range reflects a leftward shift in the onset of the spring-snowmelt runoff generation, there is no apparent change in the timing of the first runoff peaks. These shifted patterns reveal the increased influence of rising temperature on snowmelt timing and the associated onset of runoff peaks across southern Siberia, especially the Aldan River basin.

In addition to this apparent shift in the first runoff peak, the secondary runoff peak has also experienced a substantial shift in the occurrence timing. Especially for the subbasins located in the downstream region in both Lena (Solyanka, and Tabaga) and Aldan (Okhotsky Perevoz and Vtrchoyanski Perevoz), which has noticed a pronounced delay in the secondary runoff peak, from 210 (DOY) during the 1950s to 270 (DOY) in 2000s, has a marked shift in the runoff peaks from summer to autumn. This pattern is even more obviously illustrated from the upper bounds of the distribution range. These pronounced shifts are mainly induced by a substantial increase in heavy rainfall in autumn after a step change since 1996, as we explained in Sec. 4.3.

Though the magnitude of the baseflow is only a small fraction in the annual runoff, its relative change governed by the subsurface condition can reflect the seasonal cycle of river runoff. We found that, all the subbasins have experienced higher lowflow during the 2000s than those in the 1950s. This indicates the potential role of permafrost degradation on runoff generation that we explained in Sec. 4.2. The detailed analysis of lowflow will be presented in the next subsection.

The right panel of Fig. 7.2 displays the historical evolution of RMMF over each subbasin. Despite the varying magnitudes of the trends, the RMMF of all the subbasins shows a downward pattern throughout 1950-2011. We will show in the following subsection that these significant reductions in RMMF are mainly due to the remarkable increases in the lowflow. As we noticed before, the subbasins with broader permafrost coverage have higher RMMF. Nevertheless, their lowflow is also highly sensitive to warming-induced permafrost degradation. Thus, these subbasins are found to have larger decline trends in RMMF. For example, the Aldan River basin is underlain by the most extensive permafrost coverage (about 94%), the RMMF (gauged at outlet Vtrchoyanski Perevoz) over the 60 years has decreased by almost 30%. In addition, the most considerable change in RMMF over Lena Region is noticed in the basin gauged at the

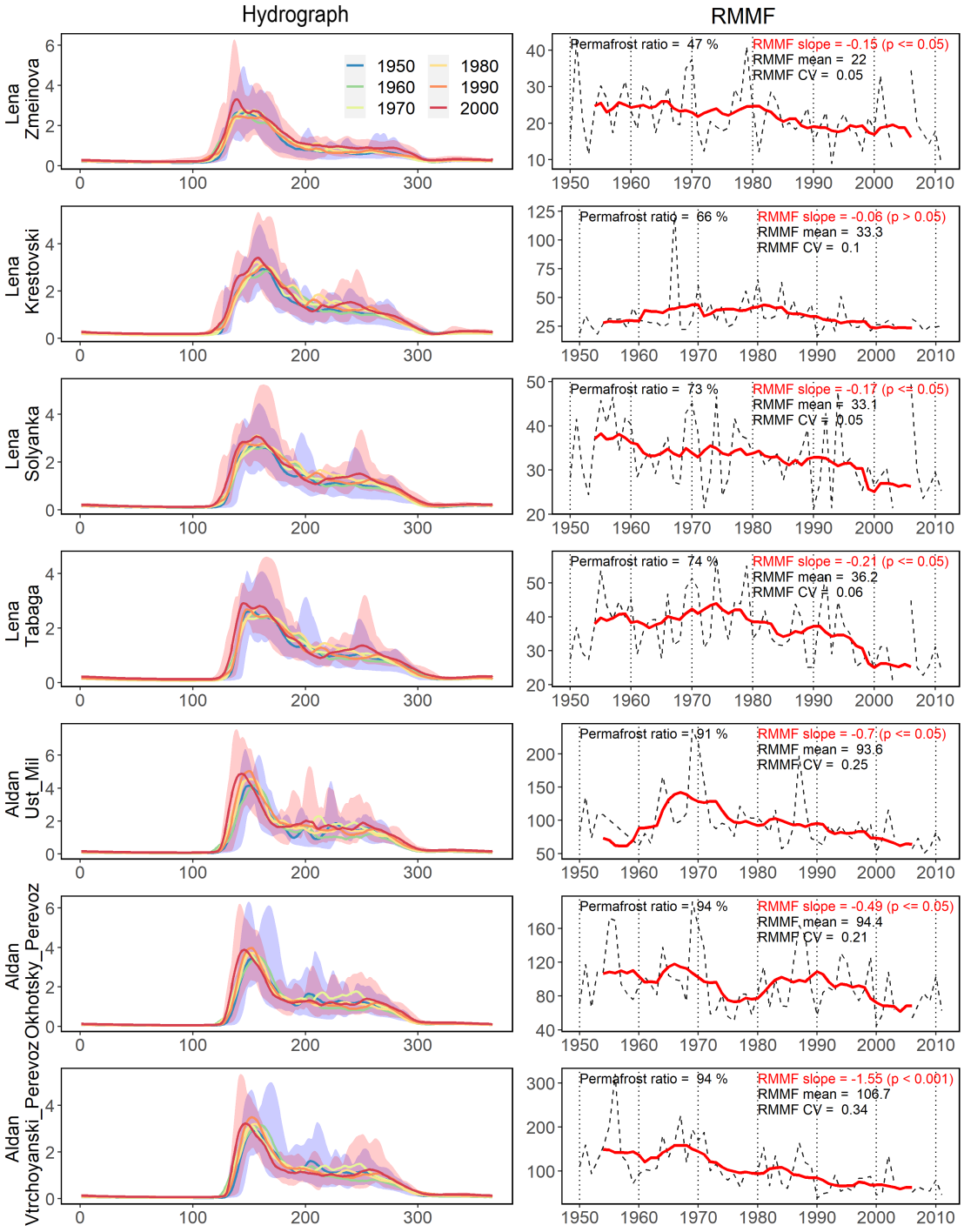

Figure 7.2: hydrograph based on 10-year averaged daily runoff (mm, left panel) and the time series of RMMF (right panel) during 1950-2011 for the seven subbasins in the Lena and Aldan River basins. In the left panel, the lines represent the averaged daily runoff during each decade; and the upper and lower bounds of the shading area (blue for the 1950s, red for the 2000s) are the maximum and minimum of daily flow, respectively, during two corresponding 10-year periods. In the right panel, the dashed grey line denotes the yearly RMMF, with the solid red line being their 10-year moving average.

outlet Tabaga. This basin is also covered by the most permafrost as compared to the other subbasins in Lena. These changes in RMMF highlight how the changing climate and associated evolution in permafrost have affected the runoff generation processes in southern Siberia.

7.3 Historical change in maxiflow and miniflow

Given the changes in the hydrograph and RMMF, one can expect corresponding changes in the associated hydrologic extremes. Thus, here we examined the long-term variations in the magnitude and timing of maxiflow and miniflow (Fig. 7.3), which are extracted from the 10-day moving average of daily river runoff.

7.3.1 Variabilities in magnitudes

Generally, miniflow exhibits a statistically significant increase ($p<0.05$) over all of the subbasins except one in Lena (gauged at Krestovski). The most substantial rise is registered in the Aldan River basin (gauged at outlet Vtrchoyanski Perevoz), which is accompanied by a clearly abrupt increase since the 1970s. A similar pattern is also noticed in the downstream region (gauged at outlet Tabaga) in Lena. Despite those considerable increases, there is also a significant reduction prior to this abrupt rise over both Aldan and Lena. The most substantial decrease is registered in the subbasin gauged at Krestovski, leading to a negligible trend in miniflow over this subbasin. This might be owing to the natural oscillation as we found in the seasonal runoff discussed in Sec. 4.1, however, the periodicity seems to be different and vary from subbasins to subbasins.

As compared to the substantial increase in the miniflow, maxiflow only exhibits a slight change over all the subbasins. Over the subbasins in Aldan, the variations in miniflow are much significant than those in maxiflow, thus, leading to a larger range of variations in RMMF (Fig. 7.2, right panel). On the contrary, the subbasins in the upstream of the Lena River have experienced a similar pattern between miniflow and maxiflow. Thus, the RMMF of these subbasins only exhibits a relatively slight change as compared to the other subbasins.

7.3.2 Shifts in timing

The right panel of Fig. 7.3 presents the year-to-year time series of the occurring timing of maxiflow and miniflow for each subbasin. Maxiflow occurs typically from May to June and varies between 146 to 161 days of the year (DOY), exhibiting a generally similar pattern over all the subbasins. However, for the subbasins in Aldan, the negative trends of the maxiflow DOY indicate that there is an earlier onset of runoff peaks. Given that the maxiflow of these subbasins are primarily sustained by snowmelt, the earlier occurrence of maxiflow is indicative of the earlier snowmelt due to a warming climate.

In the Lena River basin, however, there is no such significant change in the timing of maxiflow. Notably, in some individual years (such as the year 1973, 1981, 1988, 1998), the maxiflow in the Lena River subbasins occurs in the late summer or early autumn, during

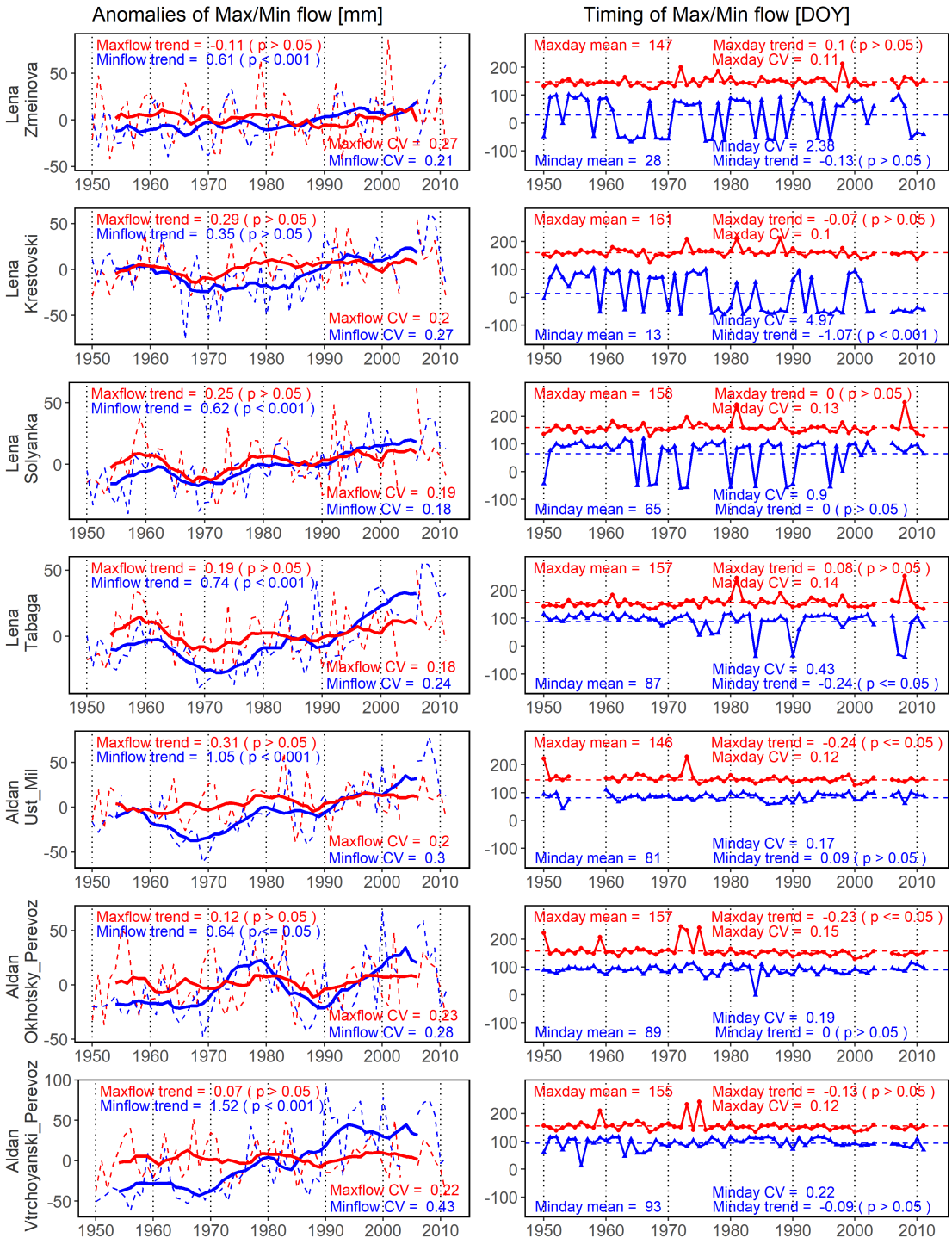

Figure 7.3: Time series of the magnitude in maximum and minimum flow, and the occurring timing of these flows for the seven subbasins in the Lena and Aldan River basins during the period of 1950-2011. The left panel shows the changes for the anomalies of the maxiflow and miniflow (mm). The right panel presents the timing changes, i.e., the occurrence day of the maxiflow and miniflow during the year (DOY, the day number starts from the first day of January). A negative value means that miniflow occurs in the preceding winter.

when the occurring timing of maxiflow is later than the average condition (i.e., during later spring to earlier summer). This delayed onset of runoff peak is mainly because the maxiflow of these years is primarily dominated by the summer rainfall other than the spring snowmelt. Interestingly, those individual years have experienced abnormally large rainfall, which is coincident with the occurrence of the strong El niño events. These consistencies implicate the potential remote connections between the Pacific ocean and the middle-latitudes owing to the large-scale atmospheric circulation (Lin & Qian, 2019).

In the case of miniflow, it might appear either in early winter or at the end of winter. This can be identified from the hydrograph shown in Fig. 7.2, which usually has two dips in the lowflow. One dip occurs at the end of winter (around 80-100 DOY). Throughout cold season, the water supply into the groundwater system is much smaller than the water depleted by runoff generation. This unbalance leads to a decreasing baseflow during the end of winter, before the contribution from snowmelt emerges. The other dip is in the early winter (around 310-320 DOY), when the upper zone of the soil layer and river channel is almost completely frozen, but the water sustained from the groundwater system is still not sufficient. Such appearance of miniflow in the early winter might result from several reasons. First, since the lowflow in late autumn and early winter is largely sustained by the moisture from the deep soil layer, thus, in a dry year with low precipitation, a corresponding reduction in the moisture in the deep soil layer may lower the dip during early winter. Second, the permafrost dynamics may also induce a lower dip in the early winter. Due to intensified percolation induced by permafrost degradation in a specific warm year, the water in the deep soil layer may further percolate downward to the even deeper groundwater system. This will eventually lead to a lack of water supply to the lowflow from the deep soil layer, and thus a lower dip during early winter. Third, in a warm winter, the snowmelt may start earlier and elevate the baseflow dip at the end of winter, which will leave the dip in the earlier winter as the lowest level in lowflow during winter.

Since the timing of the miniflow may jump between the two dips in the lowflow of the hydrograph, the occurrence of miniflow in each subbasin is much more variable as compared to the timing of maxiflow. This is especially true for the subbasins in the Lena River (Fig. 7.3, right panel). The most significant nonstationarity is observed in two upstream subbasins in Lena (gauged at Zmeinova and Krestovski). Differently, the timing of miniflow in the subbasins of Aldan is relatively stationary, and primarily occurs at the end of winter. A similar pattern also exists in the downstream Lena basin (gauged at Tabaga) before the middle 1970s. After that, however, the occurrence time of miniflow in Lena (Tabaga) had jumped several times to early winter. These jumps are coincident with the higher-than-normal miniflow in the corresponding years (Fig. 7.3, left panel), implying that such abrupt changes might be a result of the permafrost-degradation-triggered complex water movements in the subsurface system.

7.4 Role of changing climate on maxiflow and miniflow generation

In previous sections, we already identify widespread changes in the magnitude and timing of maxiflow and miniflow, as well as the corresponding RMMF. We proposed that such changes might be caused by permafrost degradation in a warming climate. Therefore, in

this section, we verify our assumptions by the cross-correlation analysis of the seasonal-lagged-response mechanism.

7.4.1 On magnitude of maxiflow and miniflow

Fig. 7.4 summarizes the Spearman rank correlations that relate the extreme events (maxiflow and miniflow) and RMMF to the climate factors (i.e., temperature and precipitation) in each subbasin. This includes their cross-correlation to the TI and precipitation in the previous warm season (P-warm) and to the FI and precipitation in the concurrent cold season (P-cold). The left panel of Fig. 7.4 shows that, for all the subbasins, the maxiflow only manifests a close linkage with precipitation in the cold season. This agrees with our previous finding that the maxiflow in Lena and Aldan is primarily controlled by the spring melting of the accumulated snowfall.

As to the miniflow that generally emerges in the cold season, its correlations with TI and P-warm in the preceding warm season are more pronounced (Fig. 7.4, middle panel). Especially, the precipitation in the preceding warm season (P-warm) exhibits the most significant correlation with miniflow. This represents the lagged runoff-precipitation relationship induced by permafrost dynamics as we discussed in Sec. 4.2. As we mentioned before, lowflow in the cold season is primarily sustained by groundwater, and the input of groundwater mainly comes from precipitation in the warm season that is substantially sensitive to the warming-induced permafrost degradation. Thus, these significant correlations between P-warm and miniflow provide additional evidence on this dynamic linkage.

In addition to these lagged runoff-precipitation relationships, miniflow might also be related to the thawing (TI) and freezing index (FI). There are significantly positive (neg-

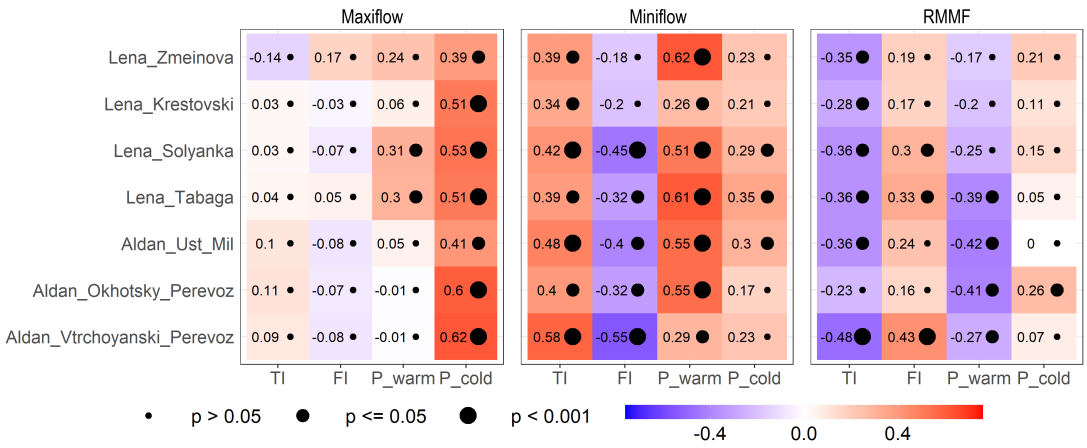

Figure 7.4: Correlations of maxiflow and miniflow, and RMMF against TI, FI, accumulated precipitation in preceding warm season and accumulated precipitation in cold season, respectively. The colors and numbers represent the magnitude of the correlation, whereas the size of the dots denotes the p-value significance of the correlation. Blue colors indicate negative correlations, red colors indicate positive correlations. Large dots show highly significant correlations (p <0.001), medium dots indicate significant correlations ($p \leq 0.05$), and small dots correspond with non-significant correlations (p >0.05).

ative) correlations between miniflow and TI (FI). This suggests that both the increase in TI and the decrease in FI (see detail in Sec. 3.2) exhibit comparable control on the variability in miniflow across all the subbasins. Specifically, the highest correlation is noticed in the Aldan River basin (gauged at Vtrchoyanski Perevoz), covered by continuous permafrost. This implicates that the lowflow generation in the cold region extensively covered by permafrost is highly susceptible to the increased temperature and associated permafrost conditions. Nevertheless, miniflow in the two subbasins in the upstream region of the Lena River shows a lack of correlations with FI. This might be owing to the abnormal change in the FI during the recent decade (from 2000 onward). Taken together, miniflow in most subbasins manifests a higher degree of correlation with the temperature and precipitation accumulated in the warm season (TI and P-warm) than that in the cold season (FI and P-cold). This hints the important modulation role of permafrost on runoff generation in southern Siberia.

The right panel of Fig. 7.4 displays the correlations between RMMF and climate factors. Since the variation in RMMF is highly dependent on changes in miniflow, it exhibits a similar linkage to all the climatic factors as compared to miniflow but in the opposite direction. Correspondingly, higher correlations between RMMF and temperature (precipitation) are generally noticed in warm seasons other than the cold season. This suggests the seasonality of river runoff in southern Siberia is particularly sensitive to climate conditions in the warm season, which could be related to the thawing and freezing dynamics of permafrost in this region. Indeed, the rising temperature in the warm season (i.e., increased TI) can promote enhanced infiltration and percolation that could eventually reduce the maxiflow. In contrast, the rising winter temperature (i.e., decreased FI) may stimulate subsurface water movements that could drive an increased lowflow in the cold season. Consequently, RMMF also responds sensitively to those changes in TI and FI. These remarkable correlations signify the substantial influence of permafrost on the seasonality of river runoff in southern Siberia.

7.4.2 On timing of maxiflow and miniflow

To further explain the variations in the timing of maxiflow and miniflow, in this part, we discuss their correlations to the permafrost condition (i.e., TI and FI) and to the temperature in the months when the maxiflow and miniflow emerge, namely, April to June for the maxiflow, January to March for the miniflow (Fig. 7.5).

In the case of maxiflow (Fig. 7.5, left panel), its timing exhibits the most notable negative correlation with the temperature in May (T-May). This significant relationship suggests that as T-May increases, the maxiflow occurs much earlier. As we mentioned previously, the runoff generation in May is primarily dominated by snowmelt, which responds sensitively to the change in temperature. Consequently, the occurrence of maxiflow driven by snowmelt responds directly to the T-May. These predominant negative correlations indicate that rising temperature in May is the primary cause for the earlier occurrence of maxiflow.

In addition to the control of temperature in May, the maxiflow in the Aldan subbasins also responds to the changes in TI and FI. It correlates negatively to TI but exhibits a positive correlation with FI. This suggests that the decreasing trend in the timing (earlier onset) of maxiflow is also governed by the thermal condition in permafrost. Indeed, the

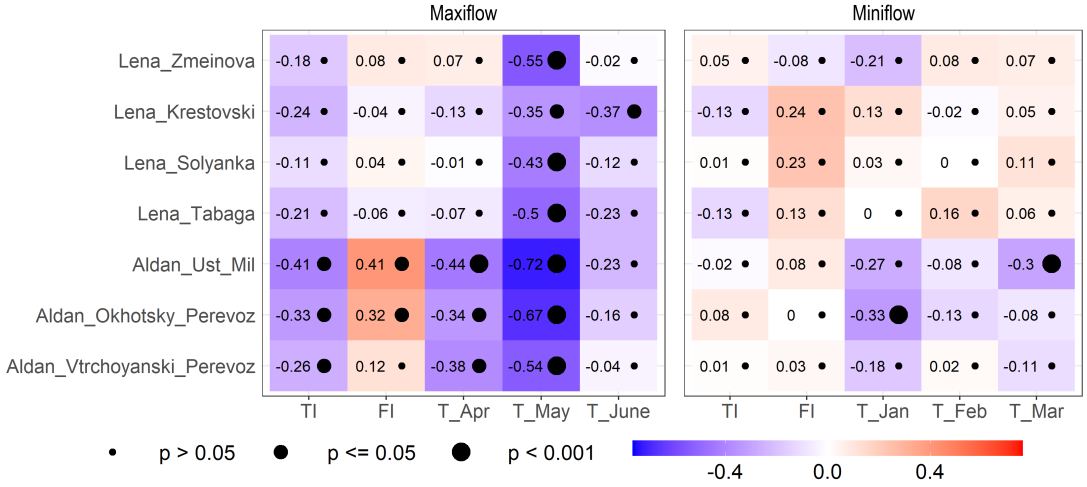

Figure 7.5: Correlations of timing of maxiflow and miniflow against TI, FI, and associated monthly temperature based on the occurrence timing of maxiflow and miniflow. The colors and numbers represent the magnitude of the correlation, whereas the size of the dots denotes the p-value significance of the correlation. Blue colors indicate negative correlations, red colors indicate positive correlations. Large dots show highly significant correlations (p <0.001), medium dots indicate significant correlations ($p \leq 0.05$), and small dots correspond with non-significant correlations (p >0.05).

degradation of permafrost can significantly affect the subsurface condition during the snowmelt season. This could eventually affect the occurring timing of spring runoff peaks. Elevated temperature can increase infiltration during the snowmelt period. As the thawing process continues in spring, more water will infiltrate to the subsurface and enables less water for surface runoff generation. This can eventually lead to an earlier onset of the maxiflow. Nonetheless, the timing of maxiflow in the Lena subbasins shows a lack of such a close relationship with both TI and FI. This can be attributable to the large variability in the timing of maxiflow caused by some abnormalities. In these cases, the occurrence of maxiflow is governed by heavy summer rainfall that is totally independent of the change in temperature.

Differently, the timing of miniflow shows no prevalent correlations with those factors considered (Fig. 7.5, right panel). One of the reasons might be that the timing of miniflow frequently jumps between the two baseflow dips in early and late winter. Another reason is that the miniflow might be more sensitive to the daily temperature, which is not available for this research yet. One may need to design a finer analysis between daily climatic variables and miniflow to capture the underlying mechanism.

7.5 Discussion and conclusion

Our results show a significant increase in the miniflow during 1950-2011 over most of the subbasins of Lena and Aldan Rivers. However, the maxiflow shows a non-significant change during this period of record. These long-term trends on the extreme events are in line with previous studies based on different periods in the Siberian region (Evans et al., 2020; Shiklomanov et al., 2007; L. C. Smith et al., 2007; Tananaev et al., 2016). Furthermore, by using multi-factor-correlation analysis, we relate these extreme events

to the multiple factors that represent the changes in climate and landscape. Our analysis suggests that the inter-annual variability of maxiflow is primarily controlled by the cold season precipitation (snow accumulation). While the magnitude of miniflow is mainly dominated by the warm season precipitation for most of the subbasins, which is driven by the lagged runoff-precipitation response as we discussed in Sec. 4.2.

Based on the daily river flow record, we use the hydrograph to manifest both the general condition and historical evolution in the seasonality of river runoff. The visualization differences among subbasins indicate significant regional patterns in the seasonality of river flow. It is a simple but effective indicator that can reveal the alterations in the magnitude, timing, and duration of river flow events, especially for the runoff peaks. Compared to the other studies on detecting the seasonality of river flow in cold region (Déry et al., 2011; Groisman & Gutman, 2012; L. C. Smith et al., 2007; Spence et al., 2015; Ye et al., 2009), our additional analysis of the maximum and minimum range of flow regime provide clear and direct visualization on the distribution pattern of the river flow events. These results show that all the subbasins have experienced an advanced onset of maxiflow that is greatly influenced by the temperature in May. The occurrence time of miniflow, showing non-significant long-term change over all the subbasins, can not be well explained by any temperature-related factors. Nevertheless, there is an abrupt shift in the timing of miniflow in Lena (gauged at Tabaga) during the middle 1970s, which might be a signal of permafrost-degradation-triggered complex water dynamics over this region.

Our results on the seasonality in river runoff show that the RMMF has decreased from 1950 to 2011 across all the subbasins of the Aldan and Lena Rivers. Given the non-significant change in maxiflow, these substantial reductions in RMMF are primarily caused by the substantial increase in miniflow. Accordingly, RMMF is negatively related to TI but positively correlates to FI, with more vital linkage being registered in the region with a more extensive permafrost distribution. These substantial variations and relationships are indicative of the hydrological consequence of permafrost degradation in this permafrost-affected region. This finding agrees with the analysis done by Ye et al. (2009) for the earlier period (1936-1999), indicating a continued permafrost degradation in southern Siberia.

A vast of climate modeling suggests that, in addition to the warming climate, there is also an increased frequency of extreme rainfall in the future (Allan & Soden, 2008; Min et al., 2011; Trenberth et al., 2003). As thus, one can expect an associated change in the hydrologic extremes under such a changeable climate. A further understanding of the hydrological response to climate variability at a finer scale is needed. Therefore, in the future work, the variability of extreme hydrologic events can be further related to the daily climatic factors by using hydrological modeling, which can reflect the role of daily-scale runoff-rainfall and runoff-temperature response dynamics. This will improve our current understanding of the maxiflow and miniflow generation mechanism under a changing climate in southern Siberia.

Chapter 8

Summary and outlook

8.1 Key findings

In this thesis, we investigated the hydro-climatic dynamics across three southern Siberian catchments with varying permafrost conditions. The multiple-temporal-scale investigations would help to better understand the physical mechanism in hydrological response to changing climate under different permafrost degradations, and to expose permafrost-driven consequences on terrestrial water availability in the southern Siberian region. The main work and key results are:

In Chapter 4, we explore the hydro-climatic dynamics over the entire 60-year period at both annual and intra-annual states to capture the temporal patterns in hydrological processes and potential drivers of these changes from a long-term perspective. These examinations reveal contrast hydrological change patterns between northern and southern catchments over both long-term and decadal scales under changing climate and permafrost degradation. First, due to the larger-scale atmospheric circulation, the precipitation and runoff in Selenga and Aldan (Lena) exhibit "seesaw-like" periodical oscillation. Second, although precipitation shows negligible long-term trends in the three catchments, permafrost degradation has indeed induced significant long-term trends in river runoff. However, the basins covered by different permafrost types have different directions of long-term runoff trends: increased trend in Lena and Aldan underlain by discontinuous and continuous permafrost, while declined trend in Selenga covered by less permafrost extent.

Regarding the periodical oscillations of hydro-climatic variables, in Chapter 5, we focus on one complete cycle of the decadal oscillation (1984-2013) between dry and wet states. By conducting the spatial distribution of the correlations between runoff and precipitation and between runoff and TWS, we further highlight that the lateral permafrost degradation in Selenga triggers surface water loss and leads to a water-deficit condition in this region. Whereas in the Aldan and Lena catchments, the vertical degradation sustains a water-rich surface moisture condition and yields higher runoff during the rainy season. These permafrost-degradation-induced surface water states could further affect the overlying atmospheric condition, which may result in a potential transformation in the hydro-climatic system in southern Siberia.

In order to explore the intensified drying condition in the semi-arid Selenga basin, in Chapter 6, we characterize the propagation of the hydrological drying events in combination with climatic conditions and permafrost thawing index. Our results expose that precipitation deficits in Selenga are likely to propagate to severer hydrological deficits when

they co-occur with higher temperature conditions. What is worse, the warming-induced lateral permafrost degradation in this region may also reinforce the runoff deficits, leading to an abrupt reduction in runoff efficiency and a potentially irreversible shift in the semi-arid water availability.

In Chapter 7, we focus on the two Boreal catchments, i.e., Lena and Aldan, with a special focus on the dynamics of extreme events and their potential relevance to the warming climate and associated permafrost degradation. Our investigation indicates that there are two peaks in the runoff regime for all the tributaries in Lena and Aldan. The first peak, occurring during the late spring or early summer, is strongly controlled by the snowmelt, and has been advanced by 10-15 days due to warming-induced earlier spring melt. The secondary runoff peak, emerging during summer or early autumn, is mainly driven by regime shifts in heavy rainfall and shows a delayed occurrence in autumn. In the case of lowflow, its timing also has no apparent change, but its magnitude exhibits a remarkable increase due to enhanced lagged response between winter runoff and summer precipitation. This emphasizes the importance of permafrost degradation on lowflow generating processes in southern Siberia.

8.2 Implications

► **Gain insights into hydrological consequences of permafrost degradation.**

By investigating the hydro-climatic dynamics from various aspects, our research emphasizes the increasing influence of permafrost degradation on regional water availability in southern Siberia under the rapid warming climate. From a seasonal perspective, it is well-known that permafrost degradation can modulate the intra-annual distribution of river runoff by transferring more fractions of summer precipitation to river runoff in the subsequent seasons (Frampton et al., 2011; L. C. Smith et al., 2007). However, a basin-scale implication of this seasonal response dynamics on the long-term wetting and drying conditions is still a relevant question for the research community on permafrost hydrology (Walvoord & Kurylyk, 2016). Our study addressed this question through the following three investigations.

Firstly, by employing cross-correlation analysis, we have examined the lagged runoff-precipitation response between summer and subsequent cold seasons (Sec. 4.2). This method is a useful tool to detect the possibly changed cross-season relationship between earlier and later periods with different hydro-climatic states. As thus, it could provide valuable information for characterizing the potentially enhanced surface-subsurface connections induced by permafrost degradation. The investigations based on cross-correlation have given insight into the potential wetting and drying dynamics in the hydro-climatic system under different permafrost degradation dynamics in southern Siberia (Chap. 5). Our findings of the permafrost degradation role on hydrological processes are consistent with previous evidence obtained from *in situ* observations over these three catchments (Iijima et al., 2014; Ishikawa et al., 2005; Kopp et al., 2014; V. E. Romanovsky et al., 2010). This agreement indicates that our research has generalized the filed-scale understandings to a large basin-scale, which is of great importance in improving our physical understanding of the integrated hydrological systems and providing fundamental information for the water resource management in the southern

Siberian region.

Furthermore, our investigation has revealed a more pronounced correlation between runoff and TWS than that between runoff and precipitation in the Selenga basin (Fig. 5.5), which indicates a potentially increased importance of groundwater on runoff generating processes. This insight into an increasing partition of groundwater on surface runoff has also been suggested by studies in other permafrost region (St. Jacques & Sauchyn, 2009; Walvoord & Striegl, 2007) as well as by modeling application (Lamontagne-Hallé et al., 2018), which implicates a possible shift to a groundwater dominated hydrological system under enhanced permafrost degradation (Walvoord & Kurylyk, 2016). Driven by this shift, the hydrological system in Selenga has experienced a severer and long-lasting dry condition during 1996-2012 (Chap. 6). Our investigations further suggest that, as warming continues, there could be more permafrost-free areas in this transition region located in the southern boundaries of the permafrost domain (Fig. 3.4). Consequently, we can expect a potentially irreversible evolution in the hydro-climatic system in this vulnerable area under such a continued loss of permafrost.

Additionally, we found an increasing lowflow during the cold season in two Boreal catchments, namely, Lena and Aldan (Chap. 7), which is consistent with the previous findings on change patterns in lowflow in the grand Siberian region (Evans et al., 2020; L. C. Smith et al., 2007). By relating the magnitude of lowflow with climate variables in the warm season (Fig. 7.4, middle panel), our investigations further point out the dominant role of warming-related permafrost degradation on the increasing of lowflow. These cross-seasonal connections indicate that the lagged response mechanism at the seasonal scale (Sec. 4.2) can be used to understand the hydrological dynamics at the event scale.

► Understanding hydro-climatic dynamics from multiple-temporal-scale perspective

Since regional hydro-climatic processes and landscape dynamics vary across multiple time scales (Berghuijs et al., 2014), the associated hydrological change, therefore, substantially depends on the temporal period of focus. In particular, our investigation in Chap. 4 over a 60-year-long period shows that the river runoff in the three southern Siberian catchments underlain by different permafrost distributions exhibits different long-term trends. On top of these trends, there are decadal oscillations between dry and wet states. These periodical oscillations are primarily controlled by the large-scale atmospheric circulations, and they may greatly affect the short-term variations as we detected in Chap. 5. As thus, one should carefully interpret and attribute the hydrological change and their potential causes, especially for the trend in short records. For the region where is highly influenced by large-scale atmosphere circulation, the trend detection and attribution should be conducted during a period of at least one complete cycle of the circulation (Pekárová et al., 2003), for instance, the 30-year-period cycle for the southern Siberian region employed by our study.

The multiple-temporal-scale investigations also bring insight to the prediction of future changes in terrestrial water availability. Driven by "seesaw-like" atmospheric circulation between the Northeast Asia and Siberia (Iwao & Takahashi, 2006), the oscillations of wet and dry states in these three catchments exhibit clear contrast, i.e., the wet-dry-wet-dry oscillation pattern in the south (Selenga) against the dry-wet-dry-wet pattern

experienced in the north (Aldan and Lena). As thus, one can expect a wet and dry state in the south (Selenga) and north (Aldan and Lena), respectively, for the 15-year period after 2013. Nevertheless, given the long-term decreasing (drying) and increasing (wetting) trends in the Selenga (Aldan/Lena) basin, the potential coming up short-term wetting (drying) states in Selenga (Aldan/Lena) might be suppressed.

Overall, our research shows the potential of using multi-source data, including hydrological simulations, hydrometric, and meteorological datasets, for investigating climate, hydrology, and landscape interactions in sparsely monitored regions with limited empirical observations, in particular for using the cross-correlation analysis to reflect the long-term permafrost degradation under a warming climate. Our findings will improve the knowledge on the hydrologic responses mechanisms under the ongoing warming climate in the coupled land-hydrology-atmosphere system in southern Siberia, and will provide useful information for the regional water resource and ecosystem management in the semi-arid mid-latitudes and boreal ecotone.

8.3 Outlook

On the basis of the outcome of this research, there are still some open questions that remain to be solved:

► **Comparative investigation in other mid-latitude catchments.**

It would be of great scientific importance to test whether the results and implications of this research can be extended to other areas with similar climatic or landscape characteristics. In particular, our study has highlighted the importance of both the atmospheric circulation and permafrost degradation on the hydrological processes in the Siberian region. Since the atmospheric circulation in mid-latitude is mainly a result of the quasi-stationary Rossby wave (Coumou et al., 2014), the regions located in different longitude are likely to exhibit similar hydro-climatic regimes. Therefore, a comparative investigation between catchments with and without permafrost at mid-latitude could help to clarify whether there is an irreversible hydrological change in response to warming-induced permafrost degradation.

► **Potentially occurrence of the compound heatwave, drought, and wildfire.**

Based on our investigation in Chap. 6, the Selenga River basin has experienced co-occurrence of dry and hot conditions during 1996-2012 with severer and long-lasting water deficits. Since the physical processes and dynamics in the earth system are tightly coupled, the co-occurring droughts and heatwaves might increase the possibility of wildfire (Williams et al., 2019). As thus, in the future work, it would be interesting to clarify the potential processes causing these compound events, and to provide risk assessment in this vulnerable semi-arid region.

► **Better understanding daily hydro-climatic dynamics.**

A follow-up modeling research on predicting the daily hydrological change in response to climate variability and permafrost disturbance is suggested. Under a warming climate, both mean annual runoff and runoff extremes are expected to experience more significant

change, especially for the transition region like Selenga, where hydrological processes are highly vulnerable to the ongoing climate change (Bates et al., 2008). This region may even experience abrupt shifts in their general conditions (regimes), as we suggested in Chap. 6. However, our investigations on hydrological extremes are only focused on the Lena and Aldan River basins (in Chap. 7), as the daily monitoring discharge data in the outlet of the Selenga River is only available during 1954-1997, thus it is not investigated. Therefore, in future work based on hydrological modeling application, one can extend the length of river runoff data and further conduct sensitivity analysis by relating the variability of hydrological processes to the daily climatic variations. This could provide insights into the daily-scale mechanism of runoff-rainfall and runoff-temperature response dynamics. These scientific contributions will further advance our current understanding of the river runoff generation mechanism under a changing climate in southern Siberia.

► **Teleconnections of hydro-climatic change.**

The hydro-climatic system in the mid-latitude is tightly linked to the atmospheric or oceanic circulations in the Arctic region (J. Cohen et al., 2020; Coumou et al., 2018). It is therefore interesting to estimate the potential teleconnections between Arctic climate and river runoff variability in the southern Siberian catchments, which can be done by analyzing the intra-annual and inter-annual relationship between timeseries of the climatic index (e.g., Arctic Oscillation (AO) or North Atlantic Oscillation (NAO)) and hydro-climatic variables.

► **Potentially enhanced subsurface connections between Selenga River and the Lake Baikal due to permafrost degradation.**

As we noticed in Chap. 6, there is a significant decline in runoff efficiency in the Selenga River (one of the largest tributaries for the Lake Baikal). Given that evapotranspiration in this region shows no considerable change, one may expect that the decreased runoff might be induced by the enhanced water loss from the subsurface system to the Lake Baikal. It would be interesting to test this potential enhanced relationship, and to provide valuable information for regional water resource management.

Appendices

Appendix A

Appendix

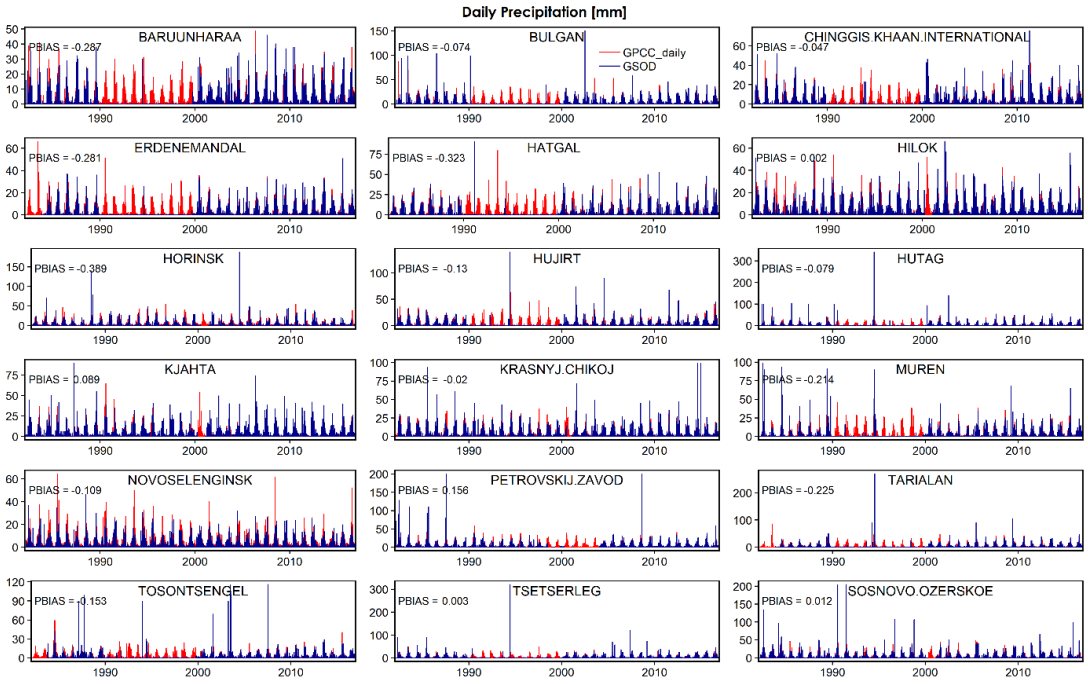

Figure A.1: Daily precipitation time series of GSOD (blue) and GPCC (red) datasets for 18 meteorological stations in the Selenga basin. Large discontinuities in the GSOD dataset occur during the 1990s. The GSOD data come from the National Climatic Data Center, NESDIS, NOAA, U.S. The GPCC data are published by Germany National Meteorological Service.

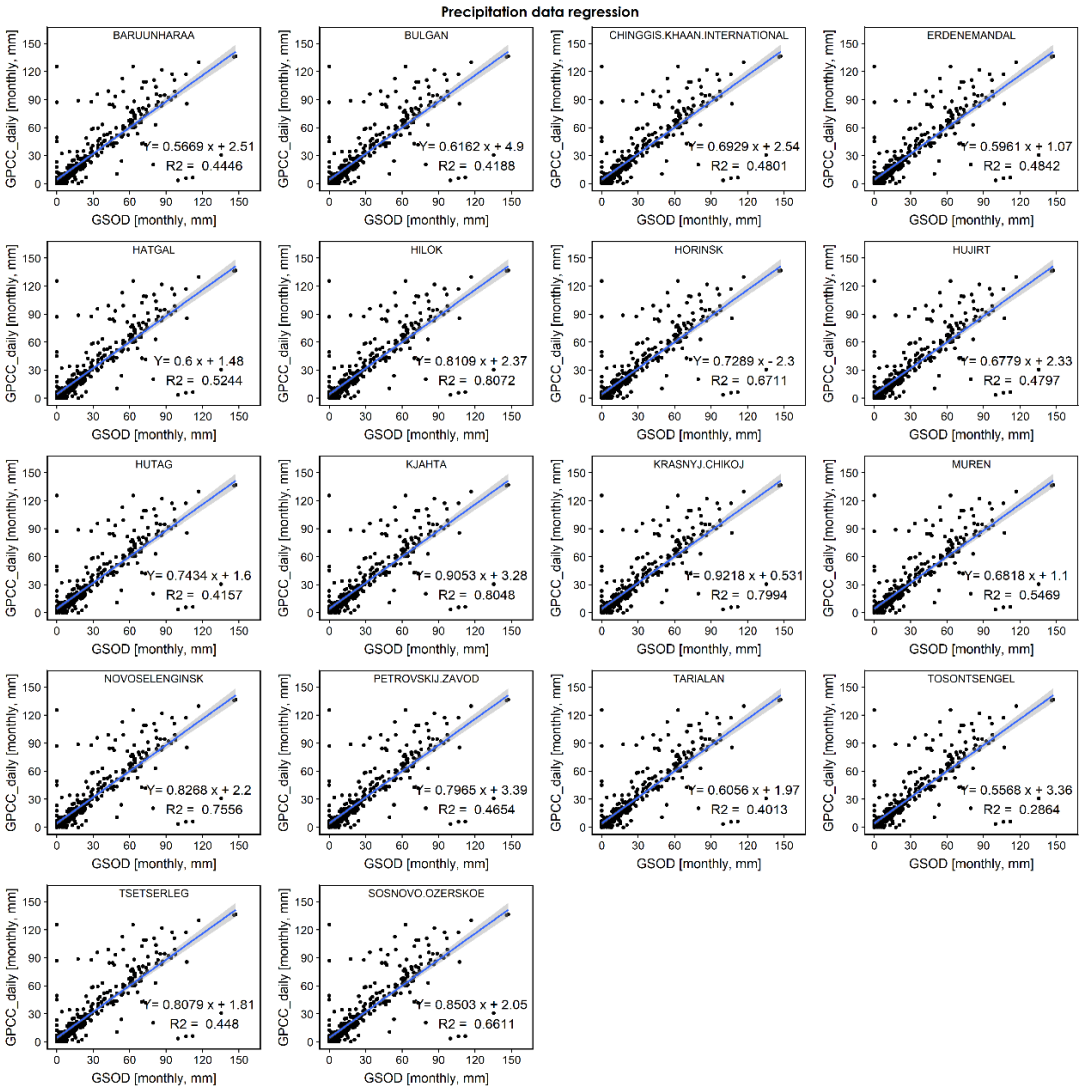

Figure A.2: Regressions of monthly precipitation between the gridded daily GPCC data and GSOD observations.

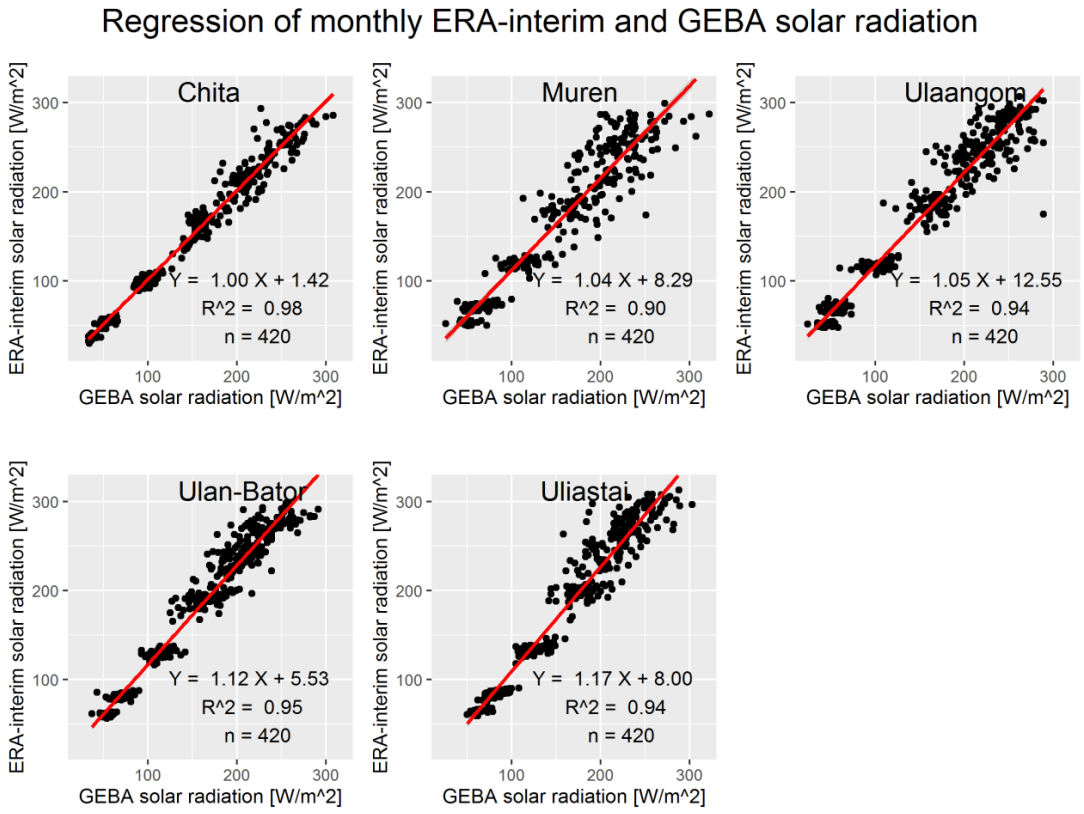

Figure A.3: Regressions of monthly radiation between ERA-Interim reanalysis data and GEBA observations.

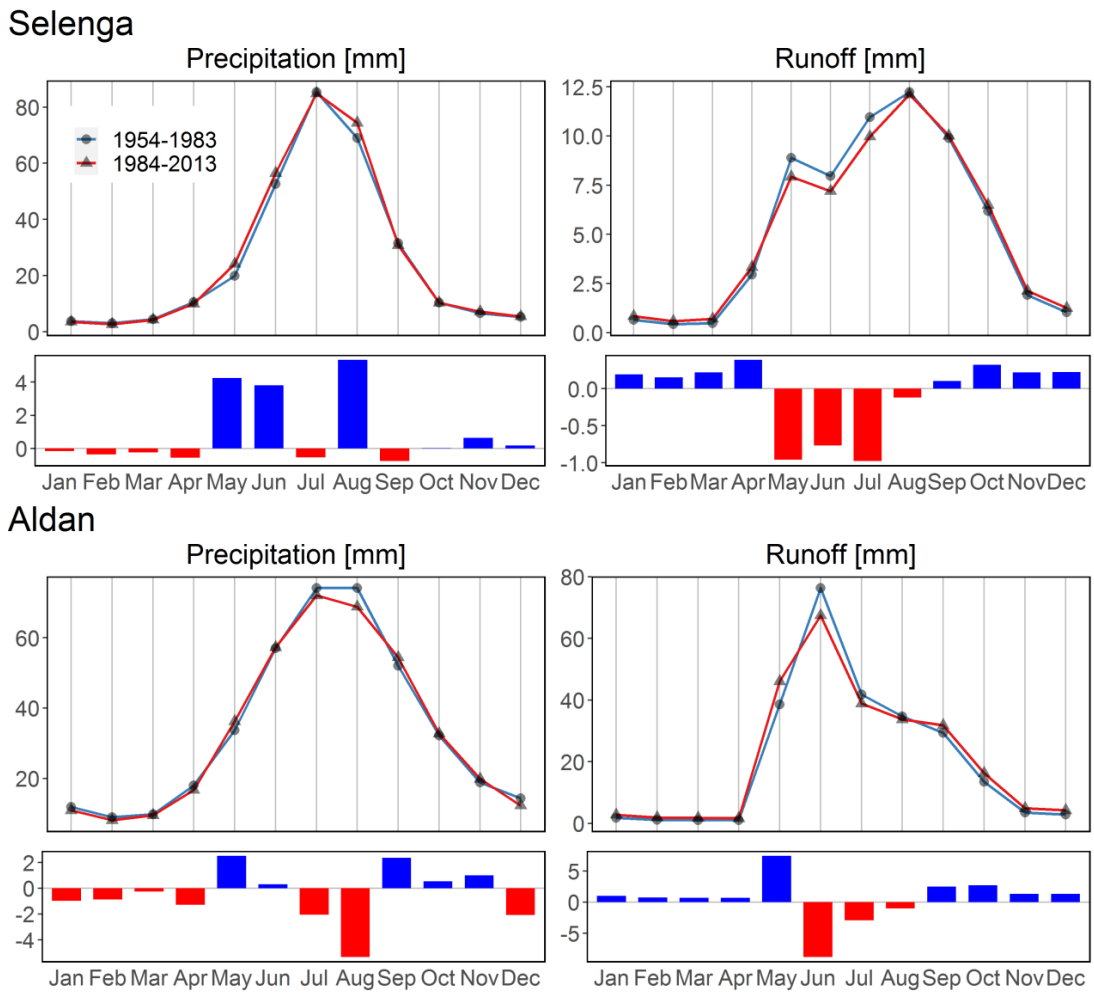

Figure A.4: Regressions of monthly radiation between ERA-Interim reanalysis data and GEBA observations.

Table A.1: Water balance under different ETa data in the Selenga and Aldan basins over the period 1984-2013.

			with TRAIN-ET		
	Precipitation [mm]	Runoff [mm]	ET-TRAIN [mm]	NA	$(ETa + R - P)/P$ [%]
Selenga	314	63	239	NA	3.8
Aldan	399	251	310	NA	40
			with ERA-ET		
	Precipitation [mm]	Runoff [mm]	ET-ERA [mm]	NA	$(ETa + R - P)/P$ [%]
Selenga	314	63	397	NA	46
Aldan	399	251	288	NA	35
			with ERA-ET		
	Precipitation [mm]	Runoff [mm]	ET-TRAIN [mm]	GRACE TWS [mm]	$(ETa + R - P \pm TWS)/P$ [%]
Selenga	314	63	239	63	16
Aldan	399	251	310	44	30

Table A.2: Comparison of ET between the TRAIN simulations, ERA-Interim and observations from Ohta et al., 2008.

		Value range 1998-2006 [mm]	Average of of 1998-2006 [mm]	Absolute Difference with Ohta, 2008 [mm]	Relative Difference with Ohta, 2008 [%]
Ohta 2008	ET	169-220	196	NA	NA
	P	111-347	259	NA	NA
station Curapca	TRAIN ET	140-282	221.16	25.16	12.83%
	ERA ET	231-281	261.26	65.26	33.30%
	GPCC P	198-331	262.11	3.11	1.20%
station Amga	TRAIN ET	187-344	266.12	70.12	35.78%
	ERA ET	254-292	275.41	79.41	40.52%
	GPCC P	222-386	295.98	36.98	14.28%

Table A.3: Correlation between annual runoff and annual precipitation, temperature and PET (** for P<0.001; * for P<0.05).

Basin	Period	Runoff vs Precipitation	Runoff vs Temperature	Runoff vs PET
Selenga	Annual	0.76**	-0.18	-0.72**
	Winter	0.07	0.36*	0.24
	Spring	0.21	-0.19	-0.32*
	Summer	0.77**	-0.56**	-0.80**
	Autumn	0.46**	-0.09	-0.41*
Lena	Annual	0.80**	0.28*	-0.35**
	Winter	-0.05	0.12	-0.38**
	Spring	0.63**	0.46*	0.50**
	Summer	0.58**	-0.19	-0.54**
	Autumn	0.40**	0.20	-0.14
Aldan	Annual	0.68**	0.15	-0.37*
	Winter	-0.24	0.35*	-0.51**
	Spring	0.31*	0.55**	0.44**
	Summer	0.51**	-0.19	-0.46**
	Autumn	0.34*	0.30*	-0.26*

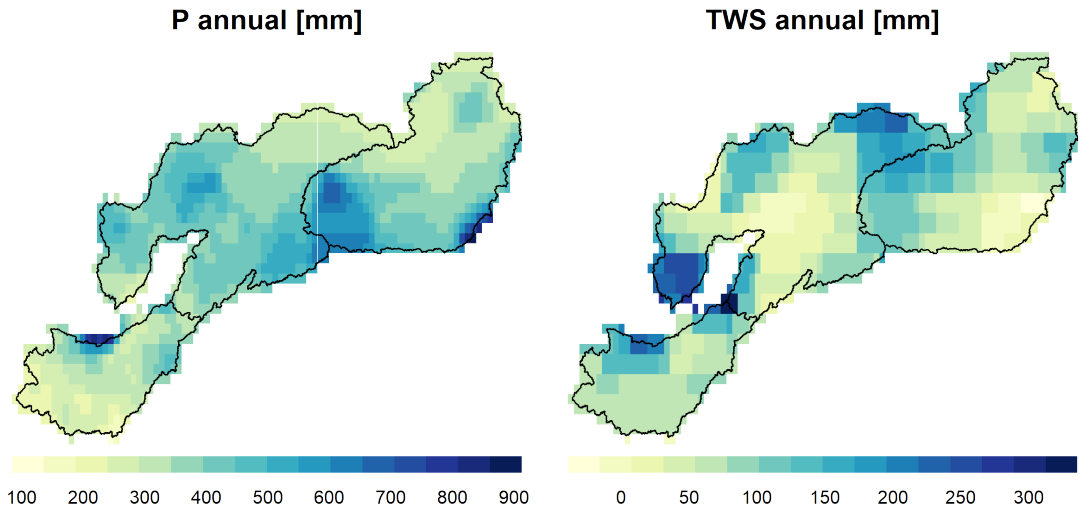

Figure A.5: Multi-year average of precipitation and TWS anomalies during 1984-2013. TWS anomalies are almost equal to 0 in most parts of the study area due to the cancellation between yearly anomalies.

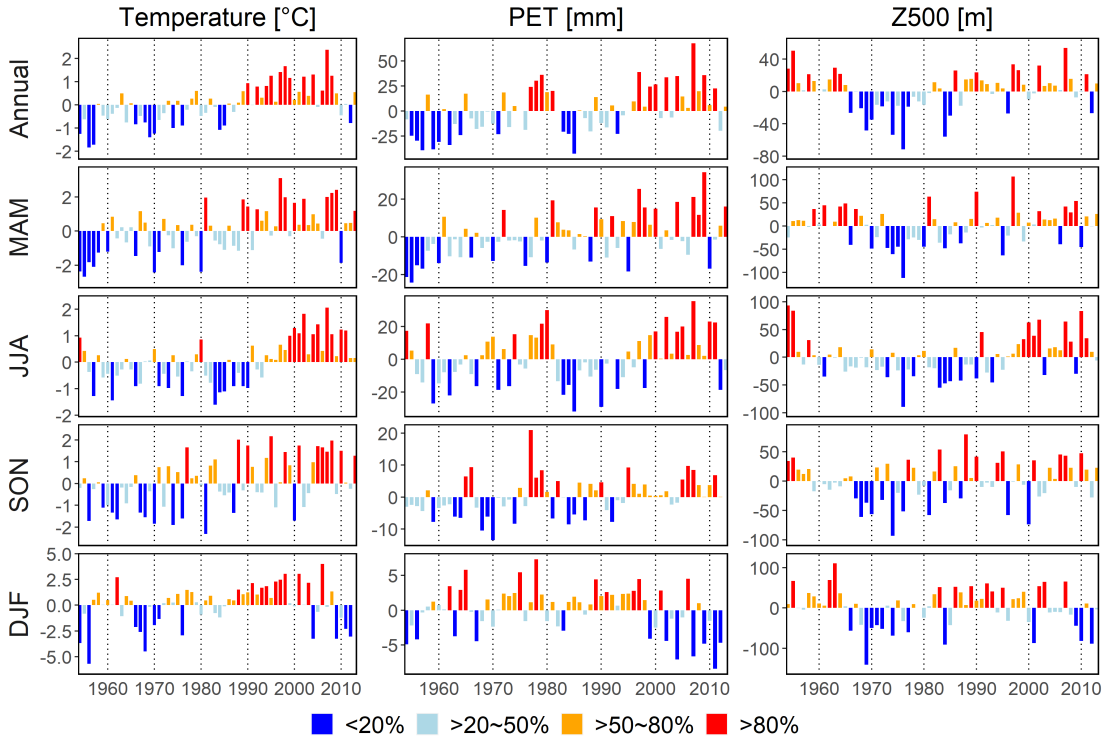

Figure A.6: The standardized anomaly for the temperature, PET and Z500 at annual and seasonal scale in the Selenga river basin, the red (and orange) color indicates extreme events above long-term average, and blue color denotes extreme events below long-term average for these three variables.

Bibliography

Adam, J. C., & Lettenmaier, D. P. (2008). Application of new precipitation and reconstructed streamflow products to streamflow trend attribution in northern eurasia. *Journal of Climate*, *21*(8), 1807–1828.

Allan, R. P., & Soden, B. J. (2008). Atmospheric warming and the amplification of precipitation extremes. *Science*, *321*(5895), 1481–1484.

Bao, G., Qin, Z., Bao, Y., Zhou, Y., Li, W., & Sanjjav, A. (2014). Ndvi-based long-term vegetation dynamics and its response to climatic change in the mongolian plateau. *Remote Sensing*, *6*(9), 8337–8358.

Barstad, I., Grabowski, W. W., & Smolarkiewicz, P. K. (2007). Characteristics of large-scale orographic precipitation: Evaluation of linear model in idealized problems. *Journal of Hydrology*, *340*(1-2), 78–90.

Bartsch, A., Balzter, H., & George, C. (2009). The influence of regional surface soil moisture anomalies on forest fires in siberia observed from satellites. *Environmental Research Letters*, *4*(4), 045021.

Bates, B., Kundzewicz, Z., & Wu, S. (2008). *Climate change and water*. Intergovernmental Panel on Climate Change Secretariat.

Berezovskaya, S., Yang, D., & Kane, D. L. (2004). Compatibility analysis of precipitation and runoff trends over the large siberian watersheds. *Geophysical Research Letters*, *31*(21).

Berghuijs, W. R., Sivapalan, M., Woods, R. A., & Savenije, H. H. (2014). Patterns of similarity of seasonal water balances: A window into streamflow variability over a range of time scales. *Water Resources Research*, *50*(7), 5638–5661.

Bergström, S., et al. (1995). The hbv model. *Computer models of watershed hydrology.*, 443–476.

Bindoff, N. L., Cheung, W. W., Kairo, J. G., Arístegui, J., Guinder, V. A., Hallberg, R., ... others (2019). Changing ocean, marine ecosystems, and dependent communities. *IPCC special report on the ocean and cryosphere in a changing climate*, 477–587.

Biskaborn, B. K., Smith, S. L., Noetzli, J., Matthes, H., Vieira, G., Streletskiy, D. A., ... others (2019). Permafrost is warming at a global scale. *Nature communications*, *10*(1), 1–11.

Blöschl, G., Bierkens, M. F., Chambel, A., Cudennec, C., Destouni, G., Fiori, A., ... others (2019). Twenty-three unsolved problems in hydrology (uph)–a community perspective. *Hydrological sciences journal*, *64*(10), 1141–1158.

Blöschl, G., Hall, J., Parajka, J., Perdigão, R. A., Merz, B., Arheimer, B., ... others (2017). Changing climate shifts timing of european floods. *Science*, *357*(6351), 588–590.

Boike, J., Grau, T., Heim, B., Günther, F., Langer, M., Muster, S., ... Lange, S. (2016). Satellite-derived changes in the permafrost landscape of central yakutia, 2000–2011: Wetting, drying, and fires. *Global and Planetary Change*, *139*, 116–127.

Bonfils, C. J., Santer, B. D., Fyfe, J. C., Marvel, K., Phillips, T. J., & Zimmerman, S. R. (2020). Human influence on joint changes in temperature, rainfall and continental aridity. *Nature Climate Change*, *10*(8), 726–731.

Bring, A., Fedorova, I., Dibike, Y., Hinzman, L., Mård, J., Mernild, S., ... Woo, M.-K. (2016). Arctic terrestrial hydrology: A synthesis of processes, regional effects, and research challenges. *Journal of Geophysical Research: Biogeosciences*, *121*(3), 621–649.

Brown, J., Ferrians Jr, O., Heginbottom, J. A., & Melnikov, E. (1997). *Circum-arctic map of permafrost and ground-ice conditions*. US Geological Survey Reston, VA.

Brutsaert, W., & Hiyama, T. (2012). The determination of permafrost thawing trends from long-term streamflow measurements with an application in eastern siberia. *Journal of Geophysical Research: Atmospheres*, *117*(D22).

Brutsaert, W., et al. (2005). *Hydrology: an introduction*. Cambridge University Press.

Chasmer, L., & Hopkinson, C. (2017). Threshold loss of discontinuous permafrost and landscape evolution. *Global Change Biology*, *23*(7), 2672–2686.

Chen, A., Guan, H., & Batelaan, O. (2021). Seesaw terrestrial wetting and drying between eastern and western australia. *Earth's Future*, *9*(5), e2020EF001893.

Chen, Z., & Grasby, S. E. (2009). Impact of decadal and century-scale oscillations on hydroclimate trend analyses. *journal of Hydrology*, *365*(1-2), 122–133.

Ciavarella, A., Cotterill, D., Stott, P., Kew, S., Philip, S., van Oldenborgh, G. J., ... others (2021). Prolonged siberian heat of 2020 almost impossible without human influence. *Climatic Change*, *166*(1), 1–18.

Cohen, J., Zhang, X., Francis, J., Jung, T., Kwok, R., Overland, J., ... others (2020). Divergent consensuses on arctic amplification influence on midlatitude severe winter weather. *Nature Climate Change*, *10*(1), 20–29.

Cohen, J. L., Furtado, J. C., Barlow, M. A., Alexeev, V. A., & Cherry, J. E. (2012). Arctic warming, increasing snow cover and widespread boreal winter cooling. *Environmental Research Letters*, *7*(1), 014007.

Cook, B. I., Smerdon, J. E., Seager, R., & Coats, S. (2014). Global warming and 21 st century drying. *Climate Dynamics*, *43*(9), 2607–2627.

Coumou, D., Di Capua, G., Vavrus, S., Wang, L., & Wang, S. (2018). The influence of arctic amplification on mid-latitude summer circulation. *Nature Communications*, *9*(1), 1–12.

Coumou, D., Petoukhov, V., Rahmstorf, S., Petri, S., & Schellnhuber, H. J. (2014). Quasi-resonant circulation regimes and hemispheric synchronization of extreme weather in boreal summer. *Proceedings of the National Academy of Sciences*, *111*(34), 12331–12336.

Dai, A. (2011). Drought under global warming: a review. *Wiley Interdisciplinary Reviews: Climate Change*, *2*(1), 45–65.

Davaa, G., & Jambaljav, Y. (2014). Water resources, glacier and permafrost. *Mongolia Second Assessment Report on Climate Change*, *2014*, 109–126.

Dee, D. P., Uppala, S., Simmons, A., Berrisford, P., Poli, P., Kobayashi, S., ... others (2011). The era-interim reanalysis: Configuration and performance of the data assimilation system. *Quarterly Journal of the royal meteorological society*, *137*(656), 553–597.

Déry, S. J., Mlynowski, T. J., Hernández-Henríquez, M. A., & Straneo, F. (2011). Interannual variability and interdecadal trends in hudson bay streamflow. *Journal of Marine Systems*, *88*(3), 341–351.

Déry, S. J., & Wood, E. F. (2005). Decreasing river discharge in northern canada.

Geophysical research letters, *32*(10).

Devoie, É. G., Craig, J. R., Connon, R. F., & Quinton, W. L. (2019). Taliks: A tipping point in discontinuous permafrost degradation in peatlands. *Water Resources Research*, *55*(11), 9838–9857.

Diffenbaugh, N. S., Scherer, M., & Ashfaq, M. (2013). Response of snow-dependent hydrologic extremes to continued global warming. *Nature climate change*, *3*(4), 379–384.

Diffenbaugh, N. S., Swain, D. L., & Touma, D. (2015). Anthropogenic warming has increased drought risk in california. *Proceedings of the National Academy of Sciences*, *112*(13), 3931–3936.

Ding, Y., Wang, Z., & Sun, Y. (2008). Inter-decadal variation of the summer precipitation in east china and its association with decreasing asian summer monsoon. part i: Observed evidences. *International Journal of Climatology: A Journal of the Royal Meteorological Society*, *28*(9), 1139–1161.

Disher, B. S., Connon, R. F., Haynes, K. M., Hopkinson, C., & Quinton, W. L. (2021). The hydrology of treed wetlands in thawing discontinuous permafrost regions. *Ecohydrology*, e2296.

Djebou, D. C. S., Singh, V. P., & Frauenfeld, O. W. (2015). Vegetation response to precipitation across the aridity gradient of the southwestern united states. *Journal of Arid Environments*, *115*, 35–43.

Dobinski, W. (2011). Permafrost. *Earth-Science Reviews*, *108*(3-4), 158–169.

Erdenebat, E., & Sato, T. (2016). Recent increase in heat wave frequency around mongolia: role of atmospheric forcing and possible influence of soil moisture deficit. *Atmospheric science letters*, *17*(2), 135–140.

Evans, S. G., & Ge, S. (2017). Contrasting hydrogeologic responses to warming in permafrost and seasonally frozen ground hillslopes. *Geophysical Research Letters*, *44*(4), 1803–1813.

Evans, S. G., Yokeley, B., Stephens, C., & Brewer, B. (2020). Potential mechanistic causes of increased baseflow across northern eurasia catchments underlain by permafrost. *Hydrological Processes*, *34*(11), 2676–2690.

Fedorov, A., Gavriliev, P., Konstantinov, P. Y., Hiyama, T., Iijima, Y., & Iwahana, G. (2014). Estimating the water balance of a thermokarst lake in the middle of the lena river basin, eastern siberia. *Ecohydrology*, *7*(2), 188–196.

Ford, T. W., & Frauenfeld, O. W. (2016). Surface–atmosphere moisture interactions in the frozen ground regions of eurasia. *Scientific reports*, *6*(1), 1–9.

Frampton, A., Painter, S., Lyon, S. W., & Destouni, G. (2011). Non-isothermal, three-phase simulations of near-surface flows in a model permafrost system under seasonal variability and climate change. *Journal of Hydrology*, *403*(3-4), 352–359.

Frauenfeld, O. W., & Zhang, T. (2011). An observational 71-year history of seasonally frozen ground changes in the eurasian high latitudes. *Environmental Research Letters*, *6*(4), 044024.

Frauenfeld, O. W., Zhang, T., & Mccreight, J. L. (2007). Northern hemisphere freezing/thawing index variations over the twentieth century. *International Journal of Climatology: A Journal of the Royal Meteorological Society*, *27*(1), 47–63.

Fujinami, H., Yasunari, T., & Watanabe, T. (2016). Trend and interannual variation in summer precipitation in eastern siberia in recent decades. *International Journal of Climatology*, *36*(1), 355–368.

Fukutomi, Y., Igarashi, H., Masuda, K., & Yasunari, T. (2003). Interannual variability of summer water balance components in three major river basins of northern eurasia.

Journal of Hydrometeorology, *4*(2), 283–296.

Gautier, E., Dépret, T., Costard, F., Virmoux, C., Fedorov, A., Grancher, D., ... Brunstein, D. (2018). Going with the flow: Hydrologic response of middle lena river (siberia) to the climate variability and change. *Journal of Hydrology*, *557*, 475–488.

Goodison, B. E., Louie, P. Y., & Yang, D. (1998). Wmo solid precipitation measurement intercomparison.

Gouttevin, I., Krinner, G., Ciais, P., Polcher, J., & Legout, C. (2012). Multi-scale validation of a new soil freezing scheme for a land-surface model with physically-based hydrology. *The Cryosphere*, *6*(2), 407–430.

GRDC. (2019). Grdc, in koblenz, germany. *http://www.bafg.de/GRDC/*.

Greve, P., Orlowsky, B., Mueller, B., Sheffield, J., Reichstein, M., & Seneviratne, S. I. (2014). Global assessment of trends in wetting and drying over land. *Nature geoscience*, *7*(10), 716–721.

Groisman, P. Y., & Gutman, G. (2012). *Regional environmental changes in siberia and their global consequences*. Springer Science & Business Media.

Grosse, G., Bartsch, A., Boike, J., Brauchle, J., Fuchs, M., Jones, B. M., ... others (2020). Progress and gaps regarding quantifying and monitoring permafrost thaw dynamics with multi-decadal optical timeseries data..

Gruber, S. (2012). Derivation and analysis of a high-resolution estimate of global permafrost zonation. *The Cryosphere*, *6*(1), 221–233.

Hannaford, J., & Buys, G. (2012). Trends in seasonal river flow regimes in the uk. *Journal of Hydrology*, *475*, 158–174.

Hannaford, J., Buys, G., Stahl, K., & Tallaksen, L. (2013). The influence of decadal-scale variability on trends in long european streamflow records. *Hydrology and Earth System Sciences*, *17*(7), 2717–2733.

Harris, I., Jones, P. D., Osborn, T. J., & Lister, D. H. (2014). Updated high-resolution grids of monthly climatic observations–the cru ts3. 10 dataset. *International journal of climatology*, *34*(3), 623–642.

Hessl, A., Pederson, N., Baatarbileg, N., & Anchukaitis, K. (2013). Pluvials, droughts, the mongol empire, and modern mongolia. In *Agu fall meeting abstracts* (Vol. 2013, pp. PP42A–06).

Hessl, A. E., Anchukaitis, K. J., Jelsema, C., Cook, B., Byambasuren, O., Leland, C., ... Hayles, L. A. (2018). Past and future drought in mongolia. *Science Advances*, *4*(3), e1701832.

Hinzman, L. D., Viereck, L. A., Adams, P. C., Romanovsky, V. E., & Yoshikawa, K. (2006). Climate and permafrost dynamics of the alaskan boreal forest. *Alaska's changing boreal forest*, 39–61.

Hiyama, T., Asai, K., Kolesnikov, A. B., Gagarin, L. A., & Shepelev, V. V. (2013). Estimation of the residence time of permafrost groundwater in the middle of the lena river basin, eastern siberia. *Environmental Research Letters*, *8*(3), 035040.

Hiyama, T., Fujinami, H., Kanamori, H., Ishige, T., & Oshima, K. (2016). Recent interdecadal changes in the interannual variability of precipitation and atmospheric circulation over northern eurasia. *Environmental Research Letters*, *11*(6), 065001.

Hrachowitz, M., Savenije, H., Blöschl, G., McDonnell, J., Sivapalan, M., Pomeroy, J., ... others (2013). A decade of predictions in ungauged basins (pub)-a review. *Hydrological sciences journal*, *58*(6), 1198–1255.

Huang, J., Ji, M., Xie, Y., Wang, S., He, Y., & Ran, J. (2016). Global semi-arid climate change over last 60 years. *Climate Dynamics*, *46*(3-4), 1131–1150.

Humphrey, V., & Gudmundsson, L. (2019). Grace-rec: a reconstruction of climate-driven water storage changes over the last century. *Earth System Science Data*, *11*(3), 1153–1170.

Iijima, Y., Fedorov, A. N., Park, H., Suzuki, K., Yabuki, H., Maximov, T. C., & Ohata, T. (2010). Abrupt increases in soil temperatures following increased precipitation in a permafrost region, central lena river basin, russia. *Permafrost and Periglacial Processes*, *21*(1), 30–41.

Iijima, Y., Ohta, T., Kotani, A., Fedorov, A. N., Kodama, Y., & Maximov, T. C. (2014). Sap flow changes in relation to permafrost degradation under increasing precipitation in an eastern siberian larch forest. *Ecohydrology*, *7*(2), 177–187.

Ishikawa, M., Sharkhuu, N., Zhang, Y., Kadota, T., & Ohata, T. (2005). Ground thermal and moisture conditions at the southern boundary of discontinuous permafrost, mongolia. *Permafrost and Periglacial Processes*, *16*(2), 209–216.

Iwao, K., & Takahashi, M. (2006). Interannual change in summertime precipitation over northeast asia. *Geophysical research letters*, *33*(16).

Jung, M., Reichstein, M., Ciais, P., Seneviratne, S. I., Sheffield, J., Goulden, M. L., ... others (2010). Recent decline in the global land evapotranspiration trend due to limited moisture supply. *Nature*, *467*(7318), 951–954.

Kalnay, E., Kanamitsu, M., Kistler, R., Collins, W., Deaven, D., Gandin, L., ... others (1996). The ncep/ncar 40-year reanalysis project. *Bulletin of the American meteorological Society*, *77*(3), 437–472.

Karthe, D., Chalov, S., Moreido, V., Pashkina, M., Romanchenko, A., Batbayar, G., ... Flörke, M. (2017). Assessment of runoff, water and sediment quality in the selenga river basin aided by a web-based geoservice. *Water Resources*, *44*(3), 399–416.

Kasimov, N., Shinkareva, G., Lychagin, M., Kosheleva, N., Chalov, S., Pashkina, M., ... Jarsjö, J. (2020). River water quality of the selenga-baikal basin: Part i-spatio-temporal patterns of dissolved and suspended metals. *Water*, *12*(8), 2137.

Keener, V., Feyereisen, G., Lall, U., Jones, J., Bosch, D., & Lowrance, R. (2010). El-niño/southern oscillation (enso) influences on monthly no3 load and concentration, stream flow and precipitation in the little river watershed, tifton, georgia (ga). *Journal of hydrology*, *381*(3-4), 352–363.

Kendall, M. G., & Gibbons, J. (1975). Rank correlation methods, 1970. *Griffin, London*.

Kim, J.-S., Kug, J.-S., Jeong, S.-J., Park, H., & Schaepman-Strub, G. (2020). Extensive fires in southeastern siberian permafrost linked to preceding arctic oscillation. *Science advances*, *6*(2), eaax3308.

Klinge, M., Dulamsuren, C., Erasmi, S., Karger, D. N., & Hauck, M. (2018). Climate effects on vegetation vitality at the treeline of boreal forests of mongolia. *Biogeosciences*, *15*(5), 1319–1333.

Kopp, B. J., Lange, J., & Menzel, L. (2017). Effects of wildfire on runoff generating processes in northern mongolia. *Regional Environmental Change*, *17*(7), 1951–1963.

Kopp, B. J., Minderlein, S., & Menzel, L. (2014). Soil moisture dynamics in a mountainous headwater area in the discontinuous permafrost zone of northern mongolia. *Arctic, antarctic, and alpine research*, *46*(2), 459–470.

Korres, W., Koyama, C., Fiener, P., & Schneider, K. (2010). Analysis of surface soil moisture patterns in agricultural landscapes using empirical orthogonal functions. *Hydrology and Earth System Sciences*, *14*(5), 751–764.

Kundzewicz, Z. W., & Robson, A. J. (2004). Change detection in hydrological records-a review of the methodology/revue méthodologique de la détection de changements

dans les chroniques hydrologiques. *Hydrological sciences journal*, *49*(1), 7–19.

Kurylyk, B. L., MacQuarrie, K. T., & McKenzie, J. M. (2014). Climate change impacts on groundwater and soil temperatures in cold and temperate regions: Implications, mathematical theory, and emerging simulation tools. *Earth-Science Reviews*, *138*, 313–334.

Lamontagne-Hallé, P., McKenzie, J. M., Kurylyk, B. L., & Zipper, S. C. (2018). Changing groundwater discharge dynamics in permafrost regions. *Environmental Research Letters*, *13*(8), 084017.

Lenton, T. M. (2012). Arctic climate tipping points. *Ambio*, *41*(1), 10–22.

Lin, J., & Qian, T. (2019). A new picture of the global impacts of el nino-southern oscillation. *Scientific reports*, *9*(1), 1–7.

Lyon, S., Destouni, G., Giesler, R., Humborg, C., Mörth, M., Seibert, J., ... Troch, P. (2009). Estimation of permafrost thawing rates in a sub-arctic catchment using recession flow analysis. *Hydrology and Earth System Sciences*, *13*(5), 595–604.

Lyon, S. W., & Destouni, G. (2010). Changes in catchment-scale recession flow properties in response to permafrost thawing in the yukon river basin. *International Journal of Climatology*, *30*(14), 2138–2145.

MacDougall, A. H., Avis, C. A., & Weaver, A. J. (2012). Significant contribution to climate warming from the permafrost carbon feedback. *Nature Geoscience*, *5*(10), 719–721.

Malsy, M., Flörke, M., & Borchardt, D. (2017). What drives the water quality changes in the selenga basin: climate change or socio-economic development? *Regional environmental change*, *17*(7), 1977–1989.

Mann, H. B. (1945). Nonparametric tests against trend. *Econometrica: Journal of the econometric society*, 245–259.

Mann, M. E., & Gleick, P. H. (2015). Climate change and california drought in the 21st century. *Proceedings of the National Academy of Sciences*, *112*(13), 3858–3859.

Martin, J. T., Pederson, G. T., Woodhouse, C. A., Cook, E. R., McCabe, G. J., Anchukaitis, K. J., ... others (2020). Increased drought severity tracks warming in the united states' largest river basin. *Proceedings of the National Academy of Sciences*, *117*(21), 11328–11336.

McClelland, J. W., Holmes, R. M., Peterson, B. J., & Stieglitz, M. (2004). Increasing river discharge in the eurasian arctic: Consideration of dams, permafrost thaw, and fires as potential agents of change. *Journal of Geophysical Research: Atmospheres*, *109*(D18).

McDonnell, J., Sivapalan, M., Vaché, K., Dunn, S., Grant, G., Haggerty, R., ... others (2007). Moving beyond heterogeneity and process complexity: A new vision for watershed hydrology. *Water Resources Research*, *43*(7).

Meehl, G. A., & Tebaldi, C. (2004). More intense, more frequent, and longer lasting heat waves in the 21st century. *Science*, *305*(5686), 994–997.

Menzel, L. (1996a). *Modellierung der evapotranspiration im system boden-pflanze-atmosphäre* (Unpublished doctoral dissertation). ETH Zurich.

Menzel, L. (1996b). Modelling canopy resistances and transpiration of grassland. *Physics and Chemistry of the Earth*, *21*(3), 123–129.

Min, S.-K., Zhang, X., Zwiers, F. W., & Hegerl, G. C. (2011). Human contribution to more-intense precipitation extremes. *Nature*, *470*(7334), 378–381.

Monteith, J. L. (1965). Evaporation and environment. In *Symposia of the society for experimental biology* (Vol. 19, pp. 205–234).

Mori, M., Kosaka, Y., Watanabe, M., Nakamura, H., & Kimoto, M. (2019). A reconciled

estimate of the influence of arctic sea-ice loss on recent eurasian cooling. *Nature Climate Change*, *9*(2), 123–129.

Mori, M., Watanabe, M., Shiogama, H., Inoue, J., & Kimoto, M. (2014). Robust arctic sea-ice influence on the frequent eurasian cold winters in past decades. *Nature Geoscience*, *7*(12), 869–873.

Munkhjargal, M., Yadamsuren, G., Yamkhin, J., & Menzel, L. (2020). Ground surface temperature variability and permafrost distribution over mountainous terrain in northern mongolia. *Arctic, Antarctic, and Alpine Research*, *52*(1), 13–26.

Muskett, R. R., & Romanovsky, V. E. (2009). Groundwater storage changes in arctic permafrost watersheds from grace and in situ measurements. *Environmental Research Letters*, *4*(4), 045009.

Nelson, F. E., & Outcalt, S. I. (1987). A computational method for prediction and regionalization of permafrost. *Arctic and alpine research*, *19*(3), 279–288.

NESDIS, N. (2019). National climatic data center, nesdis, noaa, u.s. department of commerce. *https://www.ncei.noaa.gov/access/metadata/landing-page/bin/iso?id=gov.noaa.ncdc:C00516*.

Nicolì, D., Bellucci, A., Iovino, D., Ruggieri, P., & Gualdi, S. (2020). The impact of the amv on eurasian summer hydrological cycle. *Scientific reports*, *10*(1), 1–11.

Nitzbon, J., Westermann, S., Langer, M., Martin, L. C., Strauss, J., Laboor, S., & Boike, J. (2020). Fast response of cold ice-rich permafrost in northeast siberia to a warming climate. *Nature communications*, *11*(1), 1–11.

O'Donnell, J. A., Jorgenson, M. T., Harden, J. W., McGuire, A. D., Kanevskiy, M. Z., & Wickland, K. P. (2012). The effects of permafrost thaw on soil hydrologic, thermal, and carbon dynamics in an alaskan peatland. *Ecosystems*, *15*(2), 213–229.

Ohta, T., Hiyama, T., Iijima, Y., Kotani, A., & Maximov, T. C. (2019). *Water-carbon dynamics in eastern siberia*. Springer.

Ohta, T., Maximov, T. C., Dolman, A. J., Nakai, T., van der Molen, M. K., Kononov, A. V., ... others (2008). Interannual variation of water balance and summer evapotranspiration in an eastern siberian larch forest over a 7-year period (1998–2006). *Agricultural and Forest Meteorology*, *148*(12), 1941–1953.

Oshima, K., Ogata, K., Park, H., & Tachibana, Y. (2018). Influence of atmospheric internal variability on the long-term siberian water cycle during the past 2 centuries. *Earth System Dynamics*, *9*(2), 497–506.

Oshima, K., Tachibana, Y., & Hiyama, T. (2015). Climate and year-to-year variability of atmospheric and terrestrial water cycles in the three great siberian rivers. *Journal of Geophysical Research: Atmospheres*, *120*(8), 3043–3062.

Overland, J. E., & Wang, M. (2021). The 2020 siberian heat wave. *International Journal of Climatology*, *41*, E2341–E2346.

Pavelsky, T. M., & Smith, L. C. (2006). Intercomparison of four global precipitation data sets and their correlation with increased eurasian river discharge to the arctic ocean. *Journal of Geophysical Research: Atmospheres*, *111*(D21).

Pekárová, P., Miklánek, P., & Pekár, J. (2003). Spatial and temporal runoff oscillation analysis of the main rivers of the world during the 19th–20th centuries. *Journal of Hydrology*, *274*(1-4), 62–79.

Peng, X., Zhang, T., Frauenfeld, O. W., Wang, K., Luo, D., Cao, B., ... Wu, Q. (2018). Spatiotemporal changes in active layer thickness under contemporary and projected climate in the northern hemisphere. *Journal of Climate*, *31*(1), 251–266.

Peterson, B. J., Holmes, R. M., McClelland, J. W., Vörösmarty, C. J., Lammers, R. B., Shiklomanov, A. I., ... Rahmstorf, S. (2002). Increasing river discharge to the

arctic ocean. *science*, *298*(5601), 2171–2173.

Priess, J. A., Schweitzer, C., Wimmer, F., Batkhishig, O., & Mimler, M. (2011). The consequences of land-use change and water demands in central mongolia. *Land Use Policy*, *28*(1), 4–10.

Rachold, V., Alabyan, A., Hubberten, H.-W., Korotaev, V., & Zaitsev, A. (1996). Sediment transport to the laptev sea–hydrology and geochemistry of the lena river. *Polar Research*, *15*(2), 183–196.

Rawlins, M. A., Serreze, M. C., Schroeder, R., Zhang, X., & McDonald, K. C. (2009). Diagnosis of the record discharge of arctic-draining eurasian rivers in 2007. *Environmental Research Letters*, *4*(4), 045011.

Rawlins, M. A., Steele, M., Holland, M. M., Adam, J. C., Cherry, J. E., Francis, J. A., ... others (2010). Analysis of the arctic system for freshwater cycle intensification: Observations and expectations. *Journal of Climate*, *23*(21), 5715–5737.

Riseborough, D., Shiklomanov, N., Etzelmüller, B., Gruber, S., & Marchenko, S. (2008). Recent advances in permafrost modelling. *Permafrost and Periglacial Processes*, *19*(2), 137–156.

Romanovsky, V., Sazonova, T., Balobaev, V., Shender, N., & Sergueev, D. (2007). Past and recent changes in air and permafrost temperatures in eastern siberia. *Global and Planetary Change*, *56*(3-4), 399–413.

Romanovsky, V. E., Smith, S. L., & Christiansen, H. H. (2010). Permafrost thermal state in the polar northern hemisphere during the international polar year 2007–2009: a synthesis. *Permafrost and Periglacial processes*, *21*(2), 106–116.

Rowland, J., Jones, C., Altmann, G., Bryan, R., Crosby, B., Hinzman, L., ... others (2010). Arctic landscapes in transition: responses to thawing permafrost. *Eos, Transactions American Geophysical Union*, *91*(26), 229–230.

Rubel, F., & Kottek, M. (2010). Observed and projected climate shifts 1901-2100 depicted by world maps of the köppen-geiger climate classification. *Meteorologische Zeitschrift*, *19*(2), 135.

Sato, M., Morimoto, K., Kajihara, S., Tateishi, R., Shiina, S., Koike, K., & Yatomi, Y. (2019). Machine-learning approach for the development of a novel predictive model for the diagnosis of hepatocellular carcinoma. *Scientific reports*, *9*(1), 1–7.

Schneider, U., Becker, A., Finger, P., Meyer-Christoffer, A., & Ziese, M. (2018). Gpcc full data monthly product at 0.58: Monthly land-surface precipitation from rain-gauges built on gts-based and historical data, version 2018. *Deutscher Wetterdienst*, accessed 13 March 2018.

Schubert, S. D., Wang, H., Koster, R. D., Suarez, M. J., & Groisman, P. Y. (2014). Northern eurasian heat waves and droughts. *Journal of Climate*, *27*(9), 3169–3207.

Schuur, E. A., McGuire, A. D., Schädel, C., Grosse, G., Harden, J. W., Hayes, D. J., ... others (2015). Climate change and the permafrost carbon feedback. *Nature*, *520*(7546), 171–179.

Séjourné, A., Costard, F., Fedorov, A., Gargani, J., Skorve, J., Massé, M., & Mège, D. (2015). Evolution of the banks of thermokarst lakes in central yakutia (central siberia) due to retrogressive thaw slump activity controlled by insolation. *Geomorphology*, *241*, 31–40.

Sen, P. K. (1968). Estimates of the regression coefficient based on kendall's tau. *Journal of the American statistical association*, *63*(324), 1379–1389.

Seneviratne, S. I., Corti, T., Davin, E. L., Hirschi, M., Jaeger, E. B., Lehner, I., ... Teuling, A. J. (2010). Investigating soil moisture–climate interactions in a changing climate: A review. *Earth-Science Reviews*, *99*(3-4), 125–161.

Seneviratne, S. I., Lüthi, D., Litschi, M., & Schär, C. (2006). Land–atmosphere coupling and climate change in europe. *Nature*, *443*(7108), 205–209.

Serreze, M. C., Barrett, A. P., Slater, A. G., Woodgate, R. A., Aagaard, K., Lammers, R. B., ... Lee, C. M. (2006). The large-scale freshwater cycle of the arctic. *Journal of Geophysical Research: Oceans*, *111*(C11).

Serreze, M. C., & Etringer, A. J. (2003). Precipitation characteristics of the eurasian arctic drainage system. *International Journal of Climatology: A Journal of the Royal Meteorological Society*, *23*(11), 1267–1291.

Sheffield, J., Wood, E. F., & Roderick, M. L. (2012). Little change in global drought over the past 60 years. *Nature*, *491*(7424), 435–438.

Shiklomanov, A. I., & Lammers, R. B. (2014). River ice responses to a warming arctic-recent evidence from russian rivers. *Environmental Research Letters*, *9*(3), 035008.

Shiklomanov, A. I., Lammers, R. B., Rawlins, M. A., Smith, L. C., & Pavelsky, T. M. (2007). Temporal and spatial variations in maximum river discharge from a new russian data set. *Journal of Geophysical Research: Biogeosciences*, *112*(G4).

Shiklomanov, A. I., Lammers, R. B., & Vörösmarty, C. J. (2002). Widespread decline in hydrological monitoring threatens pan-arctic research. *Eos, Transactions American Geophysical Union*, *83*(2), 13–17.

Shiklomanov, A. I., Yakovleva, T. I., Lammers, R. B., Karasev, I. P., Vörösmarty, C. J., & Linder, E. (2006). Cold region river discharge uncertainty-estimates from large russian rivers. *Journal of Hydrology*, *326*(1-4), 231–256.

Sjöberg, Y., Frampton, A., & Lyon, S. W. (2013). Using streamflow characteristics to explore permafrost thawing in northern swedish catchments. *Hydrogeology Journal*, *21*(1), 121–131.

Slater, L. J., Anderson, B., Buechel, M., Dadson, S., Han, S., Harrigan, S., ... others (2021). Nonstationary weather and water extremes: a review of methods for their detection, attribution, and management. *Hydrology and Earth System Sciences*, *25*(7), 3897–3935.

Smith, L., Sheng, Y., MacDonald, G., & Hinzman, L. (2005). Disappearing arctic lakes. *Science*, *308*(5727), 1429–1429.

Smith, L. C., Pavelsky, T. M., MacDonald, G. M., Shiklomanov, A. I., & Lammers, R. B. (2007). Rising minimum daily flows in northern eurasian rivers: A growing influence of groundwater in the high-latitude hydrologic cycle. *Journal of Geophysical Research: Biogeosciences*, *112*(G4).

Spence, C., Kokelj, S., Kokelj, S., McCluskie, M., & Hedstrom, N. (2015). Evidence of a change in water chemistry in canada's subarctic associated with enhanced winter streamflow. *Journal of Geophysical Research: Biogeosciences*, *120*(1), 113–127.

Stahl, K., Hisdal, H., Hannaford, J., Tallaksen, L., Van Lanen, H., Sauquet, E., ... Jódar, J. (2010). Streamflow trends in europe: evidence from a dataset of near-natural catchments. *Hydrology and Earth System Sciences*, *14*(12), 2367–2382.

Stefan, J. (1891). Über die theorie der eisbildung, insbesondere über die eisbildung im polarmeere. *Ann. Phys*, *278*(2), 269–286.

St. Jacques, J.-M., & Sauchyn, D. J. (2009). Increasing winter baseflow and mean annual streamflow from possible permafrost thawing in the northwest territories, canada. *Geophysical Research Letters*, *36*(1).

Stork, M., & Menzel, L. (2016). Analysis and simulation of the water and energy balance of intense agriculture in the upper rhine valley, south-west germany. *Environmental Earth Sciences*, *75*(16), 1–14.

Streletskiy, D. A., Sherstiukov, A. B., Frauenfeld, O. W., & Nelson, F. E. (2015).

Changes in the 1963–2013 shallow ground thermal regime in russian permafrost regions. *Environmental Research Letters*, *10*(12), 125005.

Sun, C., Li, J., & Zhao, S. (2015). Remote influence of atlantic multidecadal variability on siberian warm season precipitation. *Scientific reports*, *5*(1), 1–9.

Sun, Q., Miao, C., Duan, Q., Ashouri, H., Sorooshian, S., & Hsu, K.-L. (2018). A review of global precipitation data sets: Data sources, estimation, and intercomparisons. *Reviews of Geophysics*, *56*(1), 79–107.

Tananaev, N., Makarieva, O., & Lebedeva, L. (2016). Trends in annual and extreme flows in the lena river basin, northern eurasia. *Geophysical Research Letters*, *43*(20), 10–764.

Tapley, B. D., Bettadpur, S., Ries, J. C., Thompson, P. F., & Watkins, M. M. (2004). Grace measurements of mass variability in the earth system. *Science*, *305*(5683), 503–505.

Teuling, A. J., De Badts, E. A., Jansen, F. A., Fuchs, R., Buitink, J., Hoek van Dijke, A. J., & Sterling, S. M. (2019). Climate change, reforestation/afforestation, and urbanization impacts on evapotranspiration and streamflow in europe. *Hydrology and Earth System Sciences*, *23*(9), 3631–3652.

Tijdeman, E., & Menzel, L. (2021). The development and persistence of soil moisture stress during drought across southwestern germany. *Hydrology and Earth System Sciences*, *25*(4), 2009–2025.

Tijdeman, E., Stahl, K., & Tallaksen, L. M. (2020). Drought characteristics derived based on the standardized streamflow index: A large sample comparison for parametric and nonparametric methods. *Water Resources Research*, *56*(10), e2019WR026315.

Törnqvist, R., Jarsjö, J., Pietroń, J., Bring, A., Rogberg, P., Asokan, S. M., & Destouni, G. (2014). Evolution of the hydro-climate system in the lake baikal basin. *Journal of Hydrology*, *519*, 1953–1962.

Törnros, T., & Menzel, L. (2010). Heading for knowledge in a data scarce river basin: Kharaa, mongolia. *Status and Perspectives of Hydrology in Small Basins*, 270–275.

Törnros, T., & Menzel, L. (2014). Addressing drought conditions under current and future climates in the jordan river region. *Hydrology and Earth System Sciences*, *18*(1), 305–318.

Trenberth, K. E., Dai, A., Rasmussen, R. M., & Parsons, D. B. (2003). The changing character of precipitation. *Bulletin of the American Meteorological Society*, *84*(9), 1205–1218.

Trenberth, K. E., Dai, A., Van Der Schrier, G., Jones, P. D., Barichivich, J., Briffa, K. R., & Sheffield, J. (2014). Global warming and changes in drought. *Nature Climate Change*, *4*(1), 17–22.

Trenberth, K. E., Fasullo, J. T., & Shepherd, T. G. (2015). Attribution of climate extreme events. *Nature Climate Change*, *5*(8), 725–730.

Troy, T. J., Sheffield, J., & Wood, E. F. (2012). The role of winter precipitation and temperature on northern eurasian streamflow trends. *Journal of Geophysical Research: Atmospheres*, *117*(D5).

UNEP, N. M., & Thomas, D. (1992). World atlas of desertification. *Edward Arnold, London*, 15–45.

van Loon, A. F. (2013). On the propagation of drought: how climate and catchment characteristics influence hydrological drought development and recovery.

Vecellio, D. J., Nowotarski, C. J., & Frauenfeld, O. W. (2019). The role of permafrost in eurasian land-atmosphere interactions. *Journal of Geophysical Research: Atmo-*

spheres, *124*(22), 11644–11660.

Velicogna, I., Tong, J., Zhang, T., & Kimball, J. S. (2012). Increasing subsurface water storage in discontinuous permafrost areas of the lena river basin, eurasia, detected from grace. *Geophysical research letters*, *39*(9).

Wagener, T., Sivapalan, M., Troch, P. A., McGlynn, B. L., Harman, C. J., Gupta, H. V., ... Wilson, J. S. (2010). The future of hydrology: An evolving science for a changing world. *Water Resources Research*, *46*(5).

Walvoord, M. A., & Kurylyk, B. L. (2016). Hydrologic impacts of thawing permafrost–a review. *Vadose Zone Journal*, *15*(6).

Walvoord, M. A., & Striegl, R. G. (2007). Increased groundwater to stream discharge from permafrost thawing in the yukon river basin: Potential impacts on lateral export of carbon and nitrogen. *Geophysical Research Letters*, *34*(12).

Walvoord, M. A., Voss, C. I., Ebel, B. A., & Minsley, B. J. (2019). Development of perennial thaw zones in boreal hillslopes enhances potential mobilization of permafrost carbon. *Environmental Research Letters*, *14*(1), 015003.

Wang, G., Wang, P., Wang, T.-Y., Zhang, Y.-C., Yu, J.-J., Ma, N., ... Liu, C.-M. (2019). Contrasting changes in vegetation growth due to different climate forcings over the last three decades in the selenga-baikal basin. *Remote Sensing*, *11*(4), 426.

Wild, M., Ohmura, A., Schär, C., Müller, G., Folini, D., Schwarz, M., ... Sanchez-Lorenzo, A. (2017). The global energy balance archive (geba) version 2017: A database for worldwide measured surface energy fluxes. *Earth System Science Data*, *9*(2), 601–613.

Williams, A. P., Abatzoglou, J. T., Gershunov, A., Guzman-Morales, J., Bishop, D. A., Balch, J. K., & Lettenmaier, D. P. (2019). Observed impacts of anthropogenic climate change on wildfire in california. *Earth's Future*, *7*(8), 892–910.

Woo, M.-k. (2012). *Permafrost hydrology*. Springer Science & Business Media.

Wouters, B., & Schrama, E. J. (2007). Improved accuracy of grace gravity solutions through empirical orthogonal function filtering of spherical harmonics. *Geophysical Research Letters*, *34*(23).

Yang, D., & Kane, D. L. (2020). *Arctic hydrology, permafrost and ecosystems*. Springer Nature.

Yang, D., Kane, D. L., Hinzman, L. D., Zhang, X., Zhang, T., & Ye, H. (2002). Siberian lena river hydrologic regime and recent change. *Journal of Geophysical Research: Atmospheres*, *107*(D23), ACL–14.

Yasunari, T. J., Nakamura, H., Kim, K.-M., Choi, N., Lee, M.-I., Tachibana, Y., & da Silva, A. M. (2021). Relationship between circum-arctic atmospheric wave patterns and large-scale wildfires in boreal summer. *Environmental Research Letters*, *16*(6), 064009.

Ye, B., Yang, D., & Kane, D. L. (2003). Changes in lena river streamflow hydrology: Human impacts versus natural variations. *Water resources research*, *39*(7).

Ye, B., Yang, D., Zhang, Z., & Kane, D. L. (2009). Variation of hydrological regime with permafrost coverage over lena basin in siberia. *Journal of Geophysical Research: Atmospheres*, *114*(D7).

Yue, S., & Wang, C. Y. (2002). Applicability of prewhitening to eliminate the influence of serial correlation on the mann-kendall test. *Water resources research*, *38*(6), 4–1.

Zhang, P., Jeong, J.-H., Yoon, J.-H., Kim, H., Wang, S.-Y. S., Linderholm, H. W., ... Chen, D. (2020). Abrupt shift to hotter and drier climate over inner east asia

beyond the tipping point. *Science*, *370*(6520), 1095–1099.

Zhang, T., Frauenfeld, O. W., Serreze, M. C., Etringer, A., Oelke, C., McCreight, J., ... others (2005). Spatial and temporal variability in active layer thickness over the russian arctic drainage basin. *Journal of Geophysical Research: Atmospheres*, *110*(D16).

Zhang, Y., Cheng, G., Li, X., Han, X., Wang, L., Li, H., ... Flerchinger, G. (2013). Coupling of a simultaneous heat and water model with a distributed hydrological model and evaluation of the combined model in a cold region watershed. *Hydrological Processes*, *27*(25), 3762–3776.

Acknowledgements

I would like to thank everyone that has helped and supported me through this memorable journey to a PhD here at Heidelberg University. This journey would not have been possible without the financial support from CSC (China Scholarship Council) and DAAD-STIBET.

I would like to express my sincere gratitude to my supervisor Prof. Dr. Lucas Menzel for giving me the opportunity to work in his research group of Hydrology and Climatology. I am grateful for his insightful guidance, generous support, and inspiring discussion during my PhD study. His passion and knowledge on permafrost hydrology have been very refreshing. I have gained, and will continue to gain, countless benefits from the folder he shared with me, which contains numerous literatures of landmark studies on permafrost hydrology. These literatures helped me to develop a systematic understanding of the study status in this field. I am also grateful that Lucas has provided me his TRAIN model, valuable data, and datasets, all of which are the foundation of this research. Furthermore, I also appreciated very much that Lucas has supported me to attend so many international conferences, which provided me the opportunity to extend my view on various fields of hydrological science. These experiences and his encouragement have always kept me motivated.

I am sincerely grateful to Dr. Erik Tijdeman for his refreshing ideas in research, his countless assistance with R-coding, and his enlightening discussion on droughts. His enthusiasm and humor provided me a joyful and relax time during my PhD study. I would also like to thank Dr. Munkhdavaa Munkhjargal for giving me his advice and sharing his knowledge in permafrost. I appreciated very much that he translated the name of gauge stations, from Mongolian to English, in the Selenga River basin. Moreover, I would like now to thank Dr. Hotaek Park (a senior Scientist at JAMSTEC, Japan) for sharing the river discharge data of the Lena and Aldan River basins.

I would like to thank all my current and former colleagues in the group for their help and supports, and for the nice time we spend together: Dr. Erik Tijdeman, Dr. Munkhdavaa Munkhjargal, Michael Kraft, Verena Maurer, Guyen Battuvshin, Wenyu Zhao (赵文宇), Theresa Keller, Julian Weier, Leonard Kurtz, Dr. Matthias Stork, Dr. Arnab Muhuri, Prof. Dr. Gang Li (李钢), Dr. Caleb Pan, Michal Spitalniak. I especially thank Theresa Keller for running the TRAIN model, thank Julian Weier for his support in making the nice map for the study area, and thank Prof. Dr. Lucas Menzel and Michael Kraft for proofreading the German abstract. Special thanks also to Mrs. Irmgard Barnes for her work on office documents and delicious cakes.

Finally, I am indebted to my parents Yanju Li (李彦菊) and Yuke Han (韩玉科), my grandparents Shulan Wang (王淑兰) and Yonghua Li (李永华), and my brother Guoqiang Han (韩国强) and his wife (赖芹平) for their endless supports and encouragements. Special thanks to Chunhai Lyu (吕纯海), for his utmost support.